ELECTROHYDRAULIC COMMINUTION STUDIES

by

ERDOGAN   YIGIT

A THESIS SUBMITTED FOR THE DEGREE OF

DOCTOR OF PHILOSOPHY

IN THE

FACULTY OF ENGINEERING

OF THE

UNIVERSITY OF LONDON

DEPARTMENT OF MINING AND MINERAL TECHNOLOGY

ROYAL SCHOOL OF MINES

IMPERIAL COLLEGE OF SCIENCE AND TECHNOLOGY

LONDON

JULY 1967

ABSTRACT

Electrohydraulic comminution was studied both theore-
tically and experimentally. Factors studied were the under-
water spark path, the resultant shock waves, fracture me-
chanism, and shape factor and size distribution of the pro-
ducts. The electrical parameters of an underwater discharge
from a capacitor were studied theoretically.

It was shown that the underwater spark path preferen-
tially follows any solid surface between two electrodes.

It has been found that the main fracture mechanism in
electrohydraulic comminution is caused by tensile forces
due to both hoop and reflected stresses.

The importance of more intense shock wave reflections,
which would produce Hopkinson spalling, is demonstrated
with single and multiple spark crushing experiments.

Dependance of energy consumption on the feed size and
physical properties of the rock was investigated.

It has been proved that the electrohydraulic comminu-
tion products have better cubic shape and sharper size
distribution than those of conventional methods.

Some preliminary tests have been performed concerning
selective crushing and liberation. Although the studies on
these subjects are not complete, the test results on selec-
tive comminution with an annular electrode system are

promising. In addition, a small but significant increase in liberation compared with conventional methods has been observed using a pointed electrode system.

Metal wear on the electrodes was determined for ordinary and stainless "silver" tool steel, and compared with that of conventional comminution.

AKNOWLEDGEMENTS

CONTENTS

INTRODUCTION

It is well known that electrical energy can be stored in a capacitor and then rapidly discharged. The electrohydraulic effect is the name given to the production of a shock wave of high intensity by the underwater discharge from a capacitor.

The earlist recorded use of the electrohydraulic effect[1] was by Svedberg. He produced colloidal metal suspensions by means of a capacitor discharge through a liquid as early as 1905. The possible use of the electrohydraulic effect as potential use of power was pointed out by Pokrovsky and Stanyukovic[2] in 1944. In 1949 Schaaffs[3] studied the spark discharges in liquid dielectrics. He determined the resulting dynamic pressures and showed that a dynamic pressure between 10,000 and 100,000 kg/cm^2 (140,000 to 1,400,000 p.s.i.) is possible, and strongly suggested that the energy of the spark could be used ,for instance in metal forming.

In 1957 Früngel and Keller[4] showed that the efficiency of conversion of electrical energy into mechanical energy can be as high as 50% in the bursting of a container of water by an underwater spark.

Fracture of brittle solids by electrohydraulic effect appears to have originated with Russian workers, although some experiments were done in the Research Laboratories

of the Allis-Chalmers Manufacturing Corp. [5] as early as

1952. In 1955 Yutkin [6] published his book " The Electro-

hydraulic Effect" in which he described how electrohydrau-

lic impulses were used to break, cut, and drill rock, to

pump and atomise liquids, and to hammer metals.

In 1962, at the U.K. Atomic Energy Research Establishment,

at   Harwell, Maroudas [7,8,9,10] obtained crushing efficien-

cies lower than those of conventional crushers, but higher

than those obtained with previous electrohydraulic crushers,

by reducing the inductance of the spark circuit to 0.1

microhenries. Further attempts at increasing the efficiency

of electrohydraulic comminution via the electrical para-

meters seems to have led to diminishing returns [10] . Hence

a new approach was needed; accordingly it was decided that

a study of the mechanism of rock fracture by electrohydrau-

lic comminution might be fruitful.

CHAPTER I   THEORETICAL CONSIDERATIONS

1.1   ELECTRICAL PARAMETERS

Electrohydraulic comminution is the method of crushing in which the rock particles are fractured by shock waves produced by underwater electric discharges. The underwater spark is produced by the rapid discharge of a capacitor across external underwater electrodes, resulting in a highly ionized, high pressure, high temperature plasma.

When a spark is produced across underwater electrodes, the resultant spark plasma tends to expand. The mechanical inertia of the surrounding water resists this expansion, resulting in the development of high pressures, i.e. shock waves of high intensity. The objective therefore is to supply the maximum possible power to the spark channel in the shortest possible time, i.e. while the volume of plasma is still small. This implies a short rise time of current or short time constant of the discharge circuit.

As was observed experimentally by Martin[13], the pressure of the spark channel is of the order of 10,000 atmospheres and the temperature of the spark channel is of the order of 10,000 $^{\circ}$K. (Martin measured nearly 30,000 $^{\circ}$K at the moment of peak current and 8,300 atmospheres with 5.8 μF , 25 kV as discharge parameters.)

In electrohydraulic crushers the underwater sparks are

generated by a circuit whose basic elements are shown in Fig. 1. The equivalent analytical circuit diagram of the above electrohydraulic crusher is shown in Fig. 2, where A represents the electrical values within the capacitor and charging circuit and B represents the electrical values of the discharge circuit. The symbols are as follows:

V_E =Charging voltage of power supply

E =Power supply

$R_{Charging}$=Charging resistance

V =Charging voltage of capacitor

$R_{Leakage}$ =Leakage resistance

R_C =Effective total resistance between terminals

L_C =Effective total inductance between terminals

S =Switching means (Air gap)

C_L =Total capacitance of internal conductors in the discharge circuit

L_L =Total inductance of internal conductors in the discharge circuit

$R_{Water}(t)$ =Effective resistance of the water gap which is a function of the time

The following treatment is based on that of Früngel [14].

General definition of the efficiency of a capacitor discharge is given as follows:
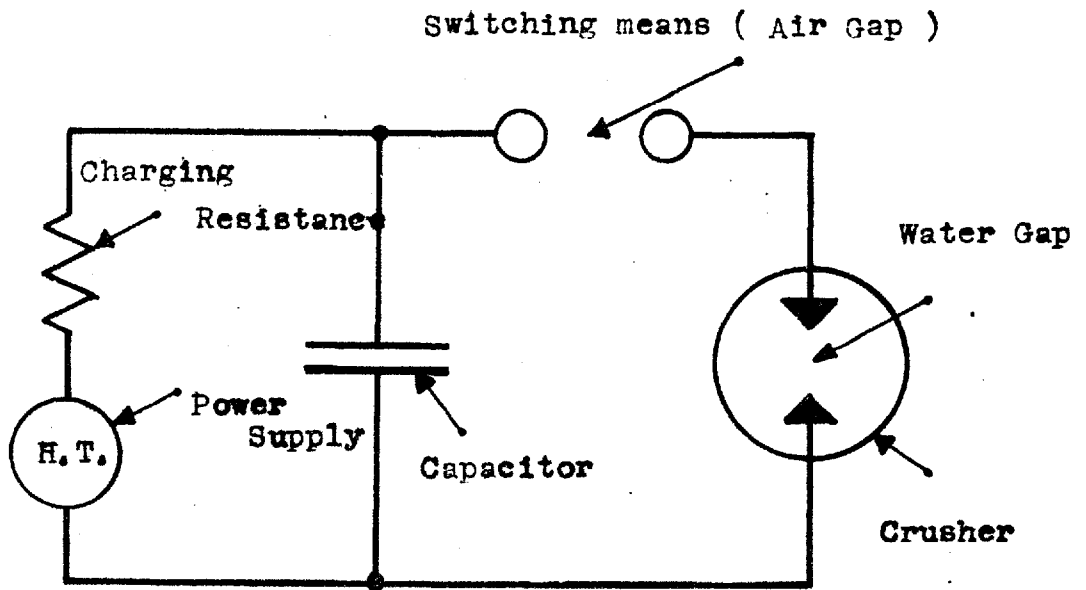
Fig. 1   Basic electrical circuit of an electrohyd-
raulic crusher.
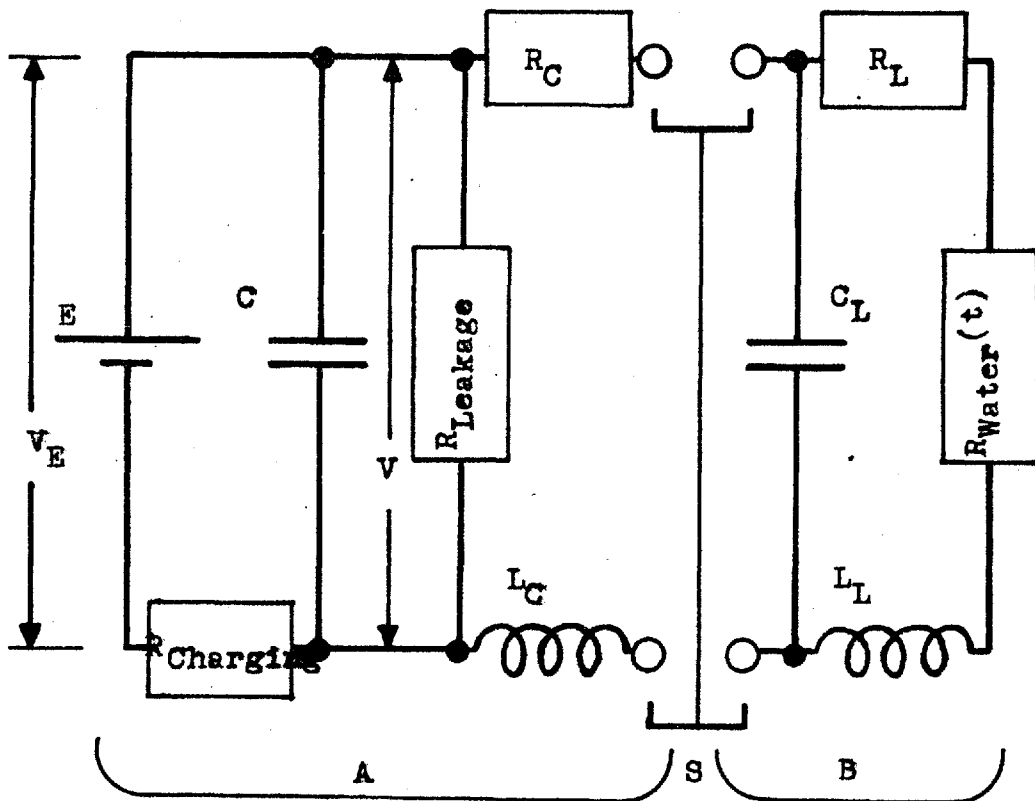
Fig. 2   Equivalent analytical electrical circuit of
an electrohydraulic crusher.

$$\eta = \frac{\int_o^t I^2 . R_{Load}(t).dt}{\sum_o^t \frac{1}{2}.C.V^2} \qquad \begin{array}{l} \text{(Joules)} \\[6pt] \text{(Joules)} \end{array} \qquad (1)$$

where I   =average effective current during during the

discharge cycle

$R_{Load}(t) \cong R_{Water}(t)$ in case of underwater discharge

For the highest efficiency the following points are important.
As long as $C_L \ll C$, the $R_{Leakage}$ and C_L have no influence.
R_C, L_C, R_L, and L_L are of great influence and these values
should be made as near as possible to zero by proper design,
i.e. such as coaxial arrangements for low inductances and
broad thick conductors for low resistances.

It is very important to withdraw the stored energy in
the capacitor as a power impulse of extremely short dura-
tion. The discharge time (T) and energy of the capacitor
$(\frac{1}{2}.C.V^2)$ give a power impulse as follows:

$$N = \frac{\frac{1}{2}.C.V^2}{T} \qquad \text{(Watts)} \qquad (2)$$

when a rectangular discharge wave form is assumed.

The total discharge time (T) depends only on (C) and
the inductance of the whole discharge circuit (L), "if an
eventual time-extending influence of impulse object is
disregarded, which , in extremely intense sparks, can be

assumed to be zero.

$$T = \pi \sqrt{L.C} \tag{3}$$

where $L = L_C + L_L$

Substituting (T) in equation (2)

$$N = \frac{1}{2\pi} . V^2 . \sqrt{\frac{C}{L}} \tag{4}$$

It is clear from above formula, if C is predetermined that the achievable power is proportional to $\frac{1}{\sqrt{\frac{L}{}}}$

Maroudas et al.[10], assuming that $R_{Water}(t)$ is constant throughout the discharge, have found that the current discharge has the form of a damped sine wave of time constant $\frac{1}{w_o} = \sqrt{L.C}$. The damping factor ξ of this discharge has the following form:

$$\xi = \frac{1}{2} . R . \sqrt{\frac{C}{L}} \tag{5}$$

where $R = R_{Water}(t) + R_L + R_C$

Critical damping is achieved when $\xi = 1$. As illustrated theoretically in Fig.3 of ref. (10) the power release in the discharge circuit is a function of damping factor ξ . It is clear from the Fig.3 that the most concentrated release in the initial peak occurs for values of damping factor ξ in the range of 0.5 to 1.0 .

Maroudas et al.[7,8,9,10] also came to the conclusion, that the high rate of energy release which would result in high shock pressures, can be obtained by low values of the time constant $\sqrt{L.C}$. Since the capacitance is a factor
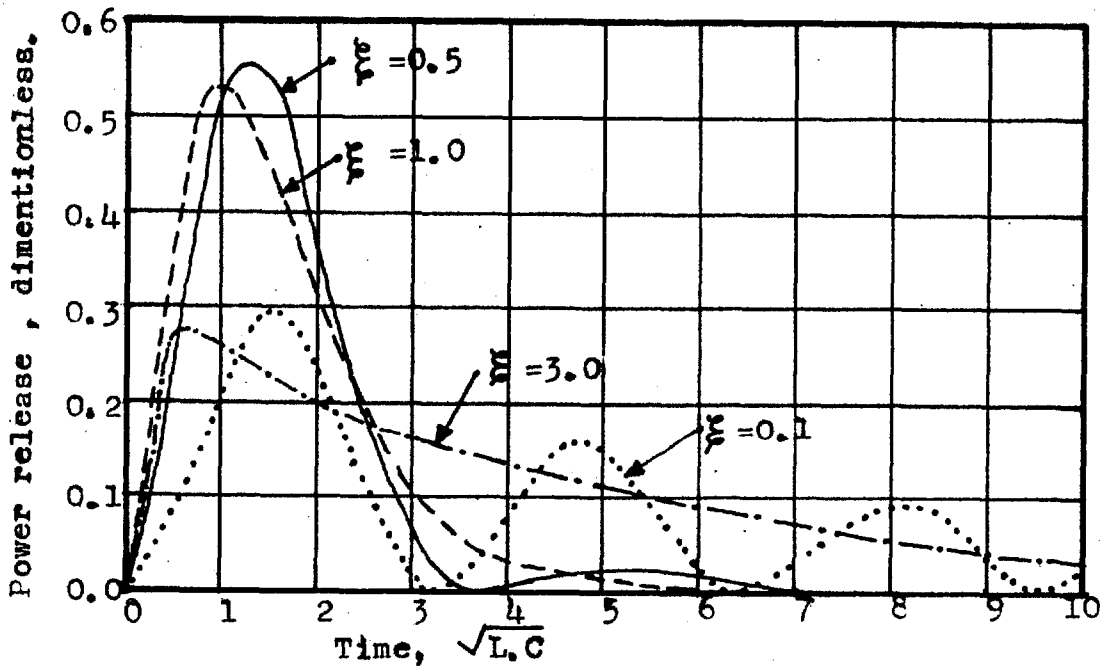
Fig. 3 Power release as a function of damping factor ξ
(after Maroudas et al.)
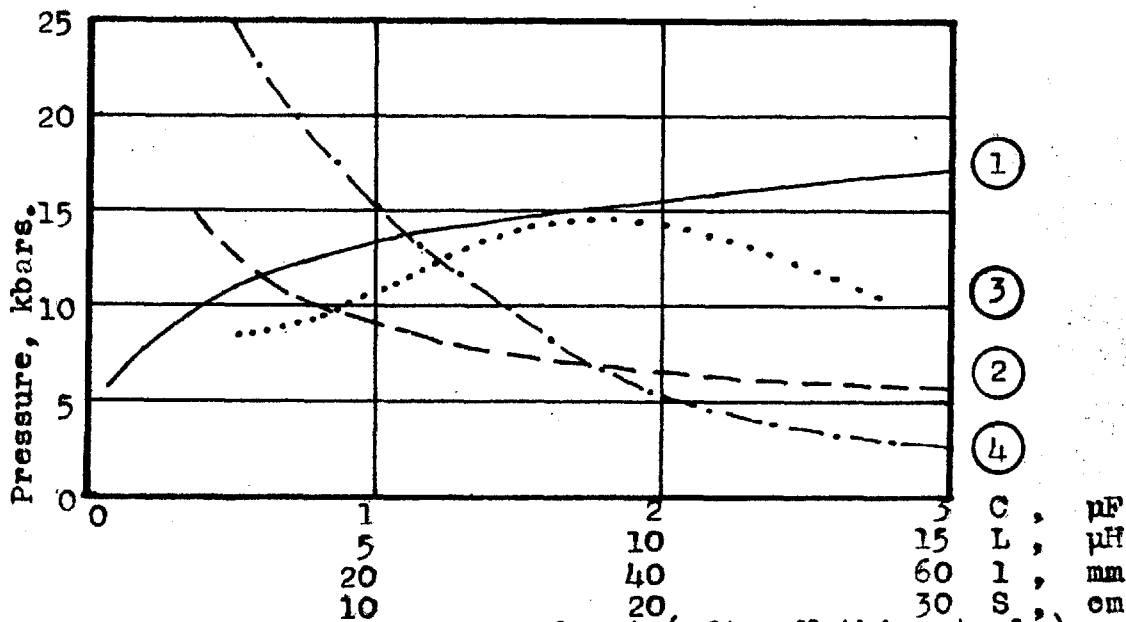
Fig. 4 Pressure at shock wave front.(after Yutkin et al.)

① f(C) at V=42 kV, L=9 μH, l=30 mm.

② f(L) at V=30 kV, C=0.56 μF, l=30 mm.

③ f(l) at V=30 kV, C=0.56 μF, L=2.08 μH.

④ f(S) at V=30 kV, C=0.19 μF, L=2.9 μH, l=30 mm.

in the total energy, efforts were directed to obtaining low values of inductance. Maroudas [8] calculated the maximum pressure generated on the discharge channel boundary using a formula which was developed by Zingermann [15] assuming the curve of power release versus time has triangular form instead of exponential form.

$$P = A. \sqrt{\frac{\rho. W}{\theta. T}} \qquad \text{(Kilobars)} \qquad (6)$$

where A = dimensionless complex integral function ,

approximately equal to 0.7

ρ = density of the liquid

W = energy deposited per unit length of the, gap, joules/cm

θ = duration of the front

T = duration of the first cycle

By substituing

$$W = \frac{C. V^2}{2. l}$$

where l = length of the water gap

and optimum values of

$$\theta = 1.2 \sqrt{L. C} \qquad \text{and}$$
$$T = 3 \sqrt{L. C}$$

which are corresponding to a nearly damped discharge, an estimate of P is obtained.

$$P = 0.82 \frac{V}{\sqrt{L. l}} \qquad \text{(Kilobars)} \qquad (7)$$
where V (kV)

$$L \quad (\mu H)$$

$$l \quad (cm)$$

The importance of low inductance in obtaining high
pressures from underwater discharges is made clear from the
above equation.

Yutkin et al. (16) calculated the pressure on the dis-
charge channel using experimental values in the Zingermann
formula. The pressure, as derived functions of capacitance
(C), inductance (L), length of the spark gap (l), and dis-
tance to the axis of spark channel (S) is shown in Fig. 4
of ref. (16). From the Fig. 4 the importance of low inductance
in obtaining high pressures is again clear.

1.2 UNDERWATER SPARK PATH

During the past ten years almost all workers on electro-
hydraulic comminution have used pointed electrodes for ini-
tiating the underwater sparks. The path of the sparks was
either not considered or assumed to be a straight line,
possibly with branches. It was not described precisely, es-
pecially in presence of solid particles. Martin (13) in his
research on high pressure arc plasma , made some observa-
tions on the spark path using an 11 μF capacitor for his
circuit. At low voltages, 4 to 10 kV, and low water tempe-
ratures - up to 15°C - before the breakdown, spherical

structures were formed on the tips of the electrodes. The sphere on the positive electrode was always larger. There was no detectable mechanical disturbance in water indicating that the spheres did not represent an appreciable change in the water density. If a dielectric barrier was inserted between electrodes the spheres grew very large, whilst doing so they refused to contact a solid surface. The breakdown path always appeared to terminate at the center of spheres. He interpreted the spheres as regions of spontaneous electrical polarization. At higher voltages – 20 kV or more – the spheres were not formed. Both electrodes produced branches. When a conducting path was established, the unsuccesful branches became dormant. He concluded finally that the spark path is unpredictable even in homogenous fluids.

When solid particles are present around the electrodes, as is the case in electrohydraulic comminution, it is clear that a spark path would not be a straight line, since there is a high probability of direct obstruction by solid particles on assumed spark path. Furthermore it is highly probably that the spark would follow any solid surface which contacted two electrodes and provided a certain conductivity between them, provided that the particles to be crushed, and the electrodes, have the right size and shape.

1.3   SHOCK WAVES PRODUCED BY UNDERWATER SPARKS

If the underwater spark path is assumed to be a straight line as an idealized form, initially a cylindrical shock wave front is produced, which becomes more spherical as it expands.

A shock wave can create both dilatational (longitudinal) and distortional (shear) disturbances in an elastic medium. In longitudinal disturbances the particle motion at the front of the disturbance is parallel to the direction of propagation of disturbance, particle motion being in the same direction for compression and in the opposite direction for tension. In distortional (shear) disturbances the particle motion is perpendicular to the direction of propagation.

The velocities of longitudinal and shear waves are given by the following formulae [17].

$$C_L = \left[\frac{3 \cdot K \cdot (1-\gamma)}{\rho \cdot (1+\gamma)} \right]^{1/2} \tag{8}$$

where C_L = velocity of longitudinal wave

K = bulk modulus of medium

ρ = density of medium

γ = Poisson's ratio of medium

$$C_S = \left(\frac{G}{\rho} \right)^{1/2} \tag{9}$$

where C_S = velocity of shear wave

G = rigidity modulus of medium

ρ = density of medium

The velocity of shear waves (C_S) is usually one half of the longitudinal velocity (C_L).

Longitudinal waves are of primary importance in the production of fractures in electrohydraulic comminution, because:

a. They have higher velocities than shear waves.

b. They **are** capable of producing tensile stresses within the bodies.

c. The shock wave is not directly transmitted to most of the solid particles in the vicinity of the spark. i.e. The shear waves could not be transmitted by the water surrounding the rock particles and consequently only longitudinal waves would be transmitted to those solid particles.

A solid particle in water, subjected to a normal longitudinal plane wave, is shown in Fig. 5. The compressive stress of the wave which reaches the solid body from the spark is σ_I. This stress divides into two components at the first interface between water and solid body (interface water/solid). One component is the reflected compressive stress, σ_R, and the other component is the transmitted stress σ_{Tr}. This latter transmitted longitudinal stress wave travels within body and reaches the second interface
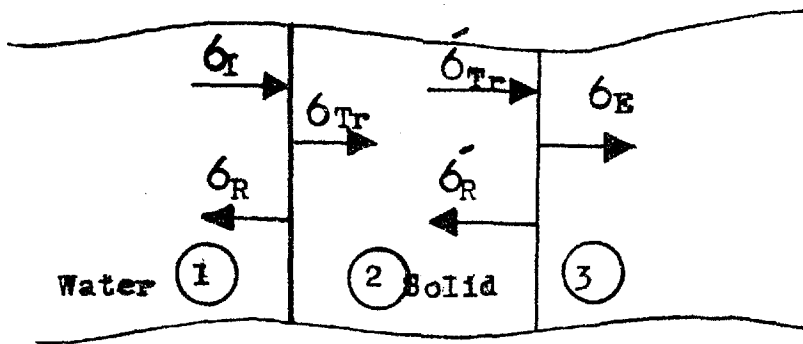
Fig. 5 Partition of the stress for a plane shock
wave striking an immersed body
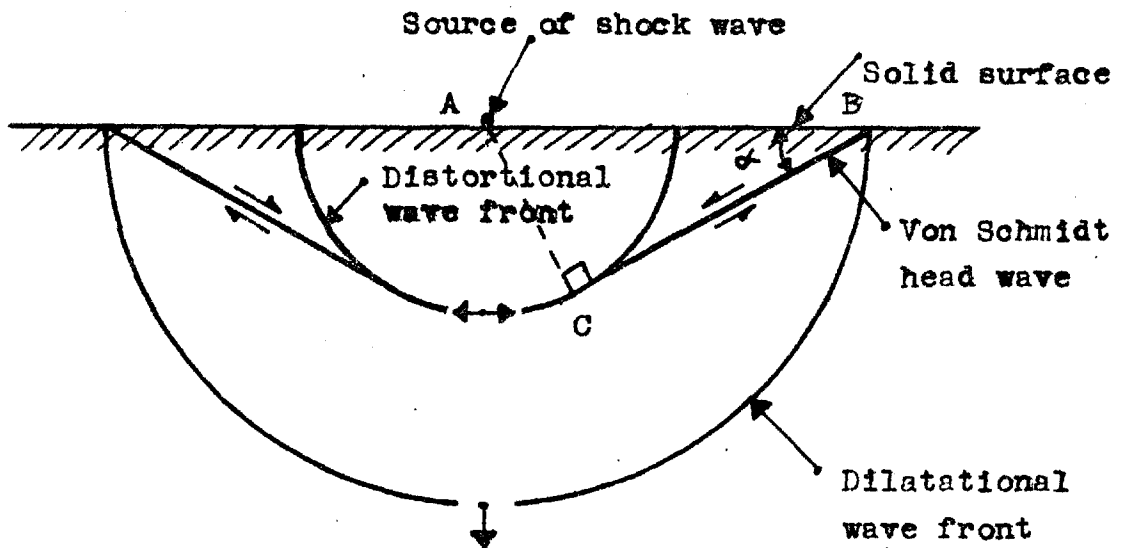
Fig. 6 Von Schmidt head wave and distortional and
dilatational wave front.

(interface solid/water).During transmission σ_{Tr} loses some of its original intensity, depending on the distance which it has travelled and the absorption factor of the body material.Let this attenuated pulse now be called σ'_{Tr}.At the interface solid/water σ'_{Tr} divides into two components.The one component is the reflected tensile stress σ'_{R} and the other is transmitted compressive stress σ_{E}.

The formulae for reflected and transmitted stresses, for normal incidence are as follows [17,18] :

$$\sigma_{R} = \frac{\rho_2 \cdot c_2 - \rho_1 \cdot c_1}{\rho_2 \cdot c_2 + \rho_1 \cdot c_1} \cdot \sigma_{I} \tag{10}$$

The resultant sign in the above formula indicates the type of the reflected stress (+ for compression, - for tension).

$$\sigma_{Tr} = \frac{2 \cdot \rho_2 \cdot c_2}{\rho_2 \cdot c_2 + \rho_1 \cdot c_1} \cdot \sigma_{I} \tag{11}$$

where σ_{I} = intensity of the stress of shock wave

σ_{R} = intensity of the stress of reflected wave

σ_{Tr} = intensity of the stress of transmitted wave

ρ_1, ρ_2, c_1, c_2 are the respective densities and velocities of propagation of elastic disturbances in two materials.

More complex relationships describe the reflection of an elastic wave striking an interface obliquely. In general, either longitudinal or shear waves will generate reflected and transmitted waves of both types, with the original energy being partitioned between them. Additionally, when a longitudinal wave strikes an interface, Rayleigh surface waves might be generated. However the amplitude of a Rayleigh wave is appreciable only near the surface of the body.

When a longitudinal and a shear wave front are generated simultaneously on a solid surface, the so called von Schmidt head waves are produced (Fig. 6). Von Schmidt head waves are plane shear waves and have been observed by several workers [20,21]. A theoretical attempt was made by Sauter [22] to explain their formation.

1.4 FRACTURE MECHANISM IN ELECTROHYDRAULIC COMMINUTION

A solid body can be subjected to the shock wave produced by an underwater spark in two ways:

1. The shock wave would be transmitted to the solid, by a water layer surrounding it. This implies:

a. Attenuation of the longitudinal stress wave reaching the solid particle.

b. Shear stress waves cannot be transmitted to the solid particle.

2. The shock wave would be generated on the immediate surface of the solid body. In this case:

a. No losses due to attenuation in water would occur for longitudinal stress wave.

b. Shear waves are also produced in the solid body resulting in von Schmidt head waves.

Electrohydraulic crushing is a mechanism in which either case could occur.

I. When a solid body is struck by longitudinal wave, it is subjected to four sorts of stresses.

(i)   Normal compressive stress of longitudinal wave front.

(ii) Hoop stress, as in a pressure vessel, due to expanding cylindrical wave front of the compressive stress of longitudinal wave within the body.

(iii) Reflected tensile stress of the longitudinal wave at solid/water interface, which would produce Hopkinson spalling.

(iv) Compound tensile stress concentrations, due to reinforcement of reflections from the corners of the solid and to the interferences among tensile and shear stresses.

Theoretical considerations were taken into account by the author in order to find the most likely mode of fracture (12). In this treatment the shock wave source is

assumed to be on the solid surface and it is assumed further that no shear stress is generated by the source. Briefly, when a cubic shape , i.e. a square section is considered, it is concluded that the most likely mode of fracture is due to hoop stress, on the following grounds:

a. The compressive strength of the rocks is about 20 times higher than their tensile strength, thus discounting initial failure due to comressive stress.

b. In Fig. 7 the total hoop tensile force T_{hoop}, across the unit section, which is produced by the cylindrical compressive wave front, as in pressure vessel, is:

$$T_{hoop}= \frac{1}{2}. a. p \qquad (12)$$

where   a = diameter of wave front

   p = compressive pressure of the wave front at

   distance a/2 from the source

The hoop stress distribution along the section is not uniform, being highest at the source.

In Fig. 8 the tensile force $T_{Hopkinson}$ exerted by a reflected wave across the unit section, which is highest at the half the wave length assuming a triangular wave form, is:

$$T_{Hopkinson}= a. p' \qquad (13)$$

where   a = length of section

   p' = average resultant tensile stress intensity

   of the reflected wave front at half wave length
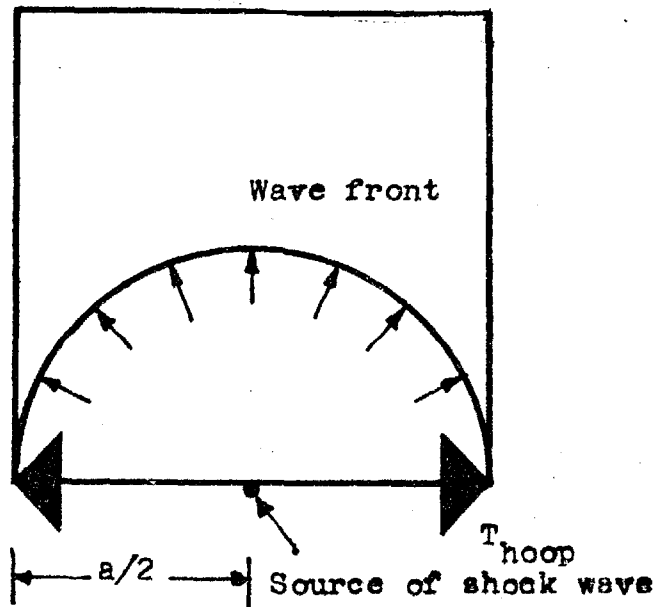
Fig. 7 Hoop tensile force in a square section which is
subjected to a cylindrical shock wave front.
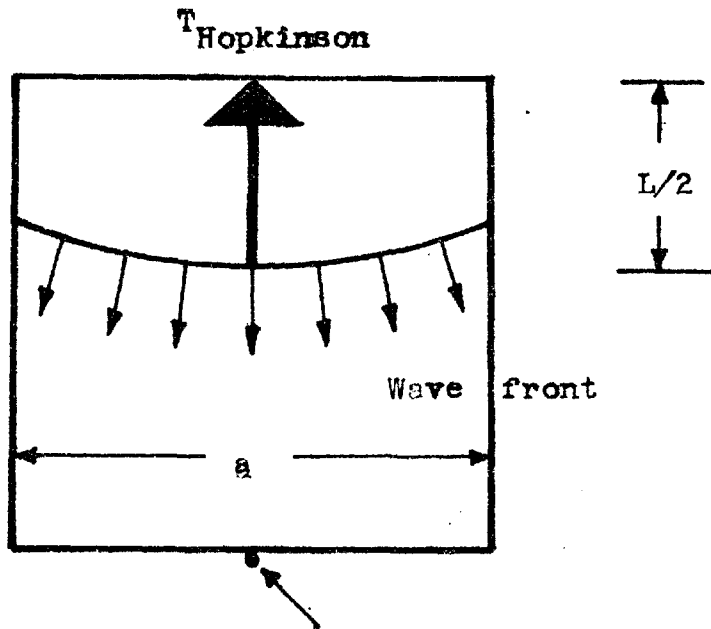
Fig. 8 Reflection of a cylindrical shock wave front at
the opposite face to the source, in a square
section, neglecting the reflections at the sides.

Tensile stress distribution along the section is not u-
niform being highest in the middle, since the reflected wave
front is not planar.

When T_{hoop} and $T_{Hopkinson}$ are compared with each other,
assuming half the wave length is smaller than the size of
specimen it would seem from equations (12) and (13) that
$T_{Hopkinson}$ is **greater than** T_{hoop}. But, even 90° angle
of incidence, for example for glass/water interface, the
coefficient of reflection is 0.5 (for a longitudinal wave
at 20 kbar). For angles other than 90°, shear stresses are
reflected. (For example for a material of Poisson's ratio
0.25, the angle of incidence ranging from 60° to 80°,
practically all the energy goes into shear wave)

Considering also the attenuation of the intensity of
the wave during transmission and the impossibility of ref-
lections developing their peak pressures along a curved
wave front at the same time, because of varying distance
to reflection points, it would appear that the hoop ten-
sile stress is the major source of fracture
of particles.

2. The geometry of the specimen and the type of the
loading are very important parameters influencing the fi-
nal fracture mode. Thus when the shock wave is produced on
the surface of a solid body a shear wave also is generated

within the body, accompanied by von Schmidt head waves.
Von schmidt head waves are plane shear waves, which are
capable of producing shear fractures.(Fig.6) Hence if the
size of specimen is taken semi-infinite, the radial ten-
sile cracks due to hoop stresses would be generated in
combination with shear fractures.The resultant likely
fracture mechanism is seen in Fig.9.

It is clear from Fig.6 that

$$\sin \alpha = \frac{\overline{AC}}{\overline{AB}}$$

Assuming that both longitudinal and shear shock wave
fronts are generated on the surface

$$\overline{AC} = t \cdot C_S$$

$$\overline{AB} = t \cdot C_L$$

where   t   = time

C_S = velocity of shear wave

C_L = velocity of longitudinal wave

Putting these values in the above formula

$$\sin \alpha = \frac{C_S}{C_L}$$

Then substituting the values of C_S and C_L from the
formulae (8) and (9)

$$\sin \alpha = \sqrt{\frac{G/\rho}{3 \cdot K \cdot (1-\nu)/\rho \cdot (1+\nu)}}$$
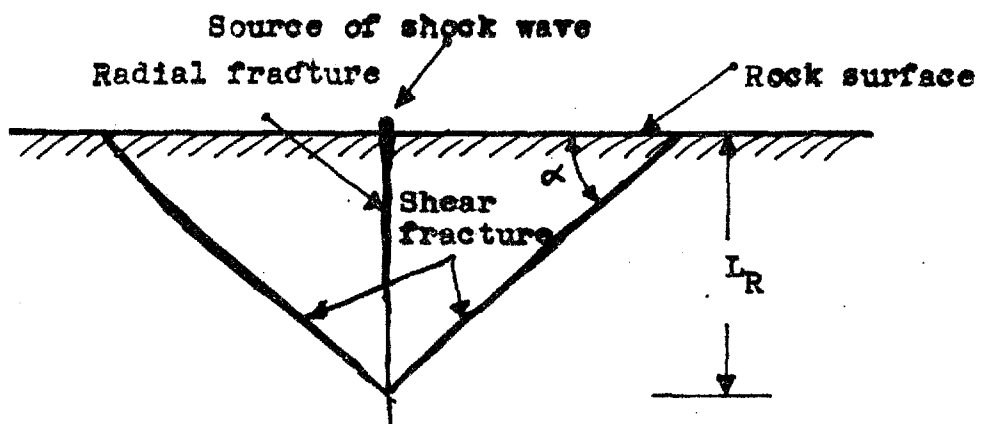
Fig. 9 The combination of shear and radial fracture.

After simplification

$$\sin \alpha = \sqrt{\frac{1-2\cdot y}{2-2\cdot y}}$$ (14)

where y = Poisson's ratio

It is clear from above formula α is a function of Poisson's ratio of material only.

The depth of radial tensile crack L_R would be a function of elastic and sonic properties of material, such as moduli of elasticity and absorption factor among others.

1.5   SHAPE FACTOR IN ELECTROHYDRAULIC
COMMINUTION

It is fairly well established[12] that the chief cause of fracture in electrohydraulic comminution lies in:

a. Radial fractures due to hoop stresses and

b. Hopkinson spallings due to reflected tensile waves.

Since both these phenomena are central to the production of cubic fracture it will be described in more detail.

An elongated rectangular prism (i.e. a "flaky" particle) is taken as a feed particle and loaded by a cylindrical shock wave front from the underwater spark. There are then two extreme positions corresponding to the two possible mechanisms of fracture described below.

a. Radial Fracture

In Fig. 10 the prism loaded such a manner as to give

Shock wave front

Shock wave source
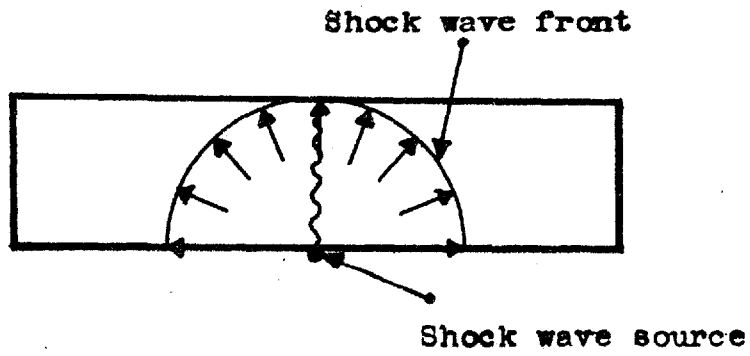
Fig. 10 Radial fracturing due to
hoop stresses.

Reflected
wave front

a

Shock wave
front
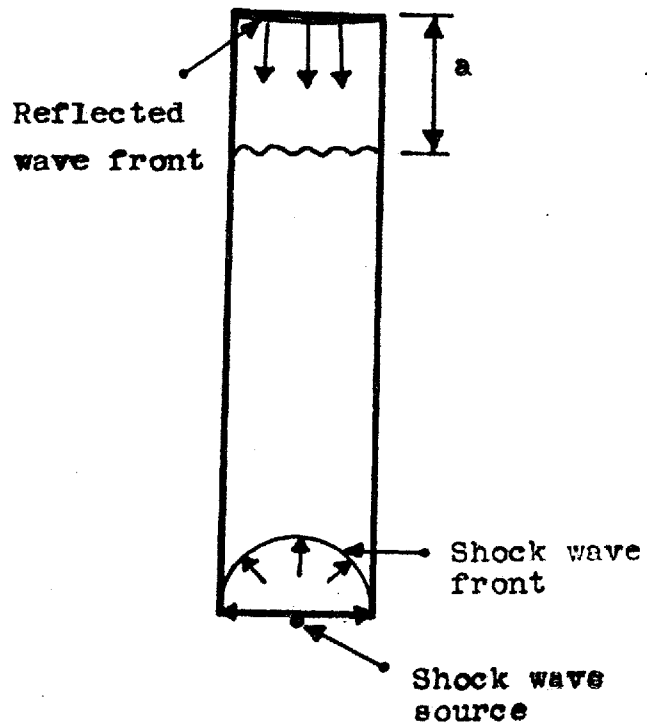
Shock wave
source

Fig. 11   Hopkinson spalling

radial fractures due to hoop stresses. When the pressure in the shock wave front is very intense, additional radial fractures are produced, starting from initial impact point. However, there is a critical threshold intensity of shock pressure in which the hoop stress is just enough to cause one central radial fracture. After this fracture, the prism is divided into two prisms, each one being much less elongated than the feed prism. If the resultant prisms are loaded in a similar fashion then after further fractioning the resultant prisms become more and more cubic.

b. Hopkinson Spalling

In Fig. 11 the prism is loaded in such a manner as to give Hopkinson spalls due to reflected tensile stress. The thickness of the spalls "a" and the number of spalls are a function of the wave shape, wave length, pressure at the shock wave front and dynamic tensile strength of the material. Let us assume that one spall of certain thickness only is produced. After the first spall the resultant prisms are less elongated, and if the main prisms continue to be loaded in the same manner, then after a further one or two stages the products become much more cubic.

These two extreme cases of loading mechanisms, with perfect rectangular shape of feed are, of course, not encountered in the practical crushing of irregular feed

particles. It is probable, however, that experimentally the average crushing mechanism would approximate to either of the above extreme cases, so that eventually the product from an electrohydraulic comminution device would consist of "cubic" grained, i.e. statically isometrical particles. For example Fig.12 shows an irregular elongated specimen of flint, which has been broken into two "equidimensional" fragments by radial fracture.

By contrast, when the mechanism of fracture in conventional compression is examined, it appears that the predominant fracture pattern in this case is caused by shear stresses. A familiar breakage model, for static failure under uniaxial compression loading, is shown in Fig.13. This is known as Smekal's fracture pattern[34]. It is clear from Fig.13 that the resultant fragments are not likely to be cubic, but on the contrary are more likely to be wedge shaped prisms.

1.6   SIZE DISTRIBUTION OF PRODUCTS

It is a familiar observation in rock mechanics that after strength-testing of regular dimensioned rock specimens, the fracture surfaces of tensile specimens are clean cut ; whereas on the contrary, the fracture surfaces of compression rock specimens are powdery due to shear

Fig. 12   Single radial fracture of an irregular
           Flint pebble.
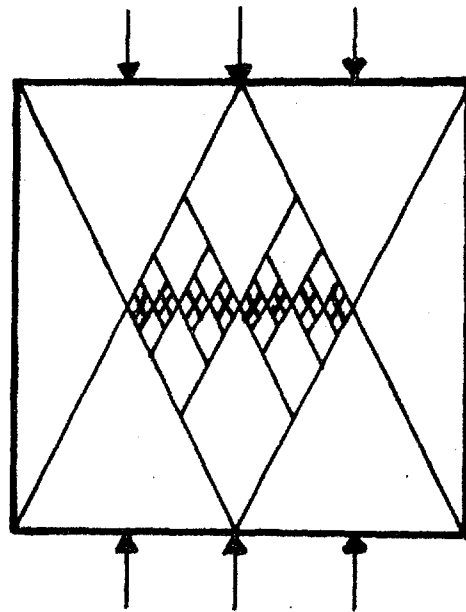
Fig. 13 Compression breakage—
     Idealized fracture pattern

failure. In conventional crushing the particle fracture
is mostly caused by compression and resultant shear stres-
ses, by direct shear forces, and by sliding frictional
forces after primary failure, all of which obviously pro-
duce fine particles. In contrast, in electrohydraulic com-
minution the main fractures were found to be caused by
tensile stresses, either hoop tensile stress or reflec-
ted "Hopkinson" tensile shock waves. Since failure is thus
caused by tensile forces it is reasonable to assume that
in principle electrohydraulic comminution devices should
produce fewer fine particle, i.e. sharper cut-off in the
tail of size distribution curves, than would conventio-
nal crushing.

Furthermore, electrohydraulic comminution can be very
similar to single "free crushing" of particles which would
produce sharper size distributions In the author's design
of electrohydraulic crushers, the particles which are sub-
jected to shock waves always have a high probability of
escaping from the vicinity of the spark before the suc-
ceeding pulse, and consequently only the as yet unbroken
particles are subjected to subsequent pulses.

CHAPTER II EXPERIMENTAL RESULTS

2.1 SPARK PATH IN ELECTROHYDRAULIC COMMINUTION

The electrode arrangement shown in Fig. 14 was used in the experiments ,since in the pointed electrode system there was no possibility of following the spark path with a simple observation system. In Fig. 14 the high tension electrode is a circular plate and the earth electrode is a concentric ring. The sparks occur randomly in the annular space between electrodes, if there are no solid particles present.

The observations on the spark path originated in a series of experiments which were carried out in order to obtain the energy relationship versus average feed size for various rocks, with the above electrode arrangement. The trend showed a decrease in energy consumption (both Bond's index and Joules/cm^2) with a decrease of average feed size. This result was contrary to expectation and was first attributed to a more efficient filling of the vicinity of the electrodes, i.e. an increase in the probability for direct spark impact on the particle. (It had hitherto been assumed that sparks would occur at random in a more or less straight lines between the electrodes, and thus would only occasionally strike a particle directly.) It was decided to eliminate the random occurrence of sparks by choosing the arrangement

High tension electrode

Earth electrode

Plan   Section

Fig. 14   Circular electrode arrangement.

High tension electrode

Earth electrode

Plan   Section
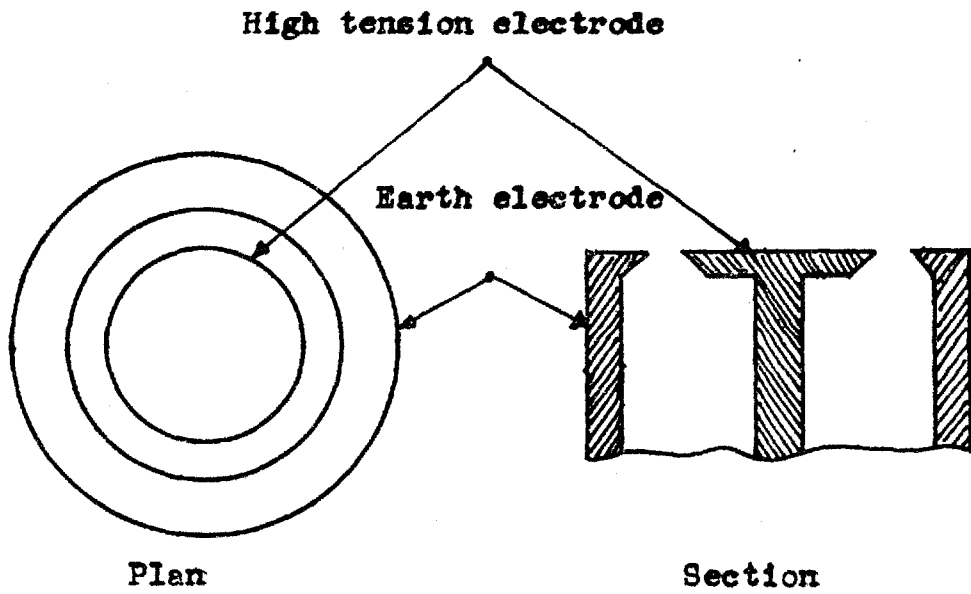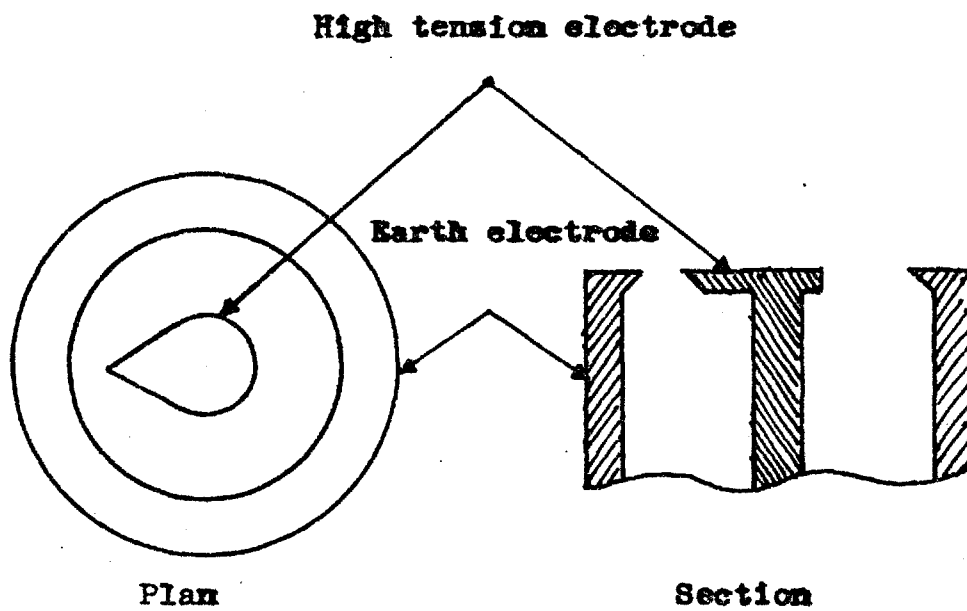
Fig. 15   Pointed-circular electrode arrangement

shown in Fig.15, in an attempt to obtain a further increase in comminution efficiency. Using this arrangement the spark always initiated from the pointed end of the high tension electrode nearest to the earth ring, and single feed particles were manually placed in the electrode gap for each pulse. Surprisingly, the efficiency was not increased, in fact a slight decrease was observed.

Hence it was concluded that the previous assumption of random occurrence of sparks was not correct in the presence of solid particles. On the contrary, for a given number of sparks, each pulse must have been in direct contact with at least one feed particle. To prove this hypothesis only one rock particle was placed in contact with two electrodes shown in Fig.14, on each occasion. The sparks were observed visually and from the damage caused to rock particle, it was seen that the sparks always followed the rock particles. Similarly, using smooth-surfaced synthetic rock specimens, (a mixture of quartz sand and epoxy resin), it was proved further that the sparks were following the immediate surface, since after each spark some mechanical damage was observed on the surfaces of these synthetic rock specimens, with accompanying burning of the resin on the spark track. The same arrangement was again used, this time with a fine copper wire (193 microns in diameter),

which exploded on spark discharge. In each case only slight damage was observed but no burning in the epoxy resin matrix. Similar results are reported in Chapter 2.2.1.6 . These two findings are explained in the following way:

(i.) In the exploding wire case, a very thin layer of water was protecting the epoxy resin surface, resulting in effective absorption of both the distortional (shear) wave and heat wave which are produced by the spark.

(ii.) In the bare underwater spark case however, there was no absorption. i.e. sparks were formed in direct contact with epoxy resin matrix.

A further type of experiment was carried out. Two solid specimens of different conductivities and/or roughnesses, such as chalcopyrite and synthetic rock, were placed across the annular electrodes at the same time and one spark was discharged.

It was found that:

(i.) The spark would follow the more conducting surface.

(ii.) The spark would follow the smoothest surface which would provide the shortest distance, if the other parameters were the same.

Table 1. shows the experimental results.

Table 1. Selectivity of spark occurrence with various

pairs.

0.1 µF, 30 kV discharge voltage,

1 cm. underwater gap length ,

demineralised water discharge medium

Type of pair	Spark occurrence	Diagnosis
Chalcopyrite versus synthetic and natural rocks(Flint,Limestone, Felsite,Sandstone)	Chalcopyrite	Chalcopyrite is conductive
Synthetic rock versus natural rocks (Flint, Limestone,Felsite, Sandstone)	Synthetic rock	Synthetic rock has smoothest surface
Smooth surfaced synthetic rock versus rough surfaced synthetic rock	Smooth surfaced synthetic rock	Smooth surface
Flint pebbles versus natural rocks (Granite, Felsite, Limestone)	Flint	Smooth surface

2.2. FRACTURE MECHANISM IN ELECTROHYDRAULIC COMMINUTION:

Experimental results concerning the fracture mechanism are published in ref. 12. Therefore the previous findings are discussed only briefly. The new findings and some modifications are explained in detail.

2.2.1 EXPLODING WIRE TECHNIQUE

Using this technique, the cylindrical shock wave front was generated by exploding copper wires of 36 s.w.g. (193 microns in diameter) in the experiments.

Although the exploding wire technique is not completely similar to actual electrohydraulic crushing mechanism, it has three main advantages:

(i.) The length of the cylindrical shock wave front is increased up to 4 cm. compared to 1 cm. for the bare spark for the same energy level, which allows the use of specimens of reasonable large sizes.

(ii.) Straight line shock wave source was obtained.

(iii.) The position of the spark on the specimen, i.e. the position of the shock wave source on the specimen, was arranged reasonably accurately.

2.2.1.1 EXPERIMENTAL EQUIPMENT

Briefly, the experiments were designed to study frac-

ture patterns produced in specimens of regular geometry and uniform mechanical properties. A synthetic rocklike material was mainly used, consisting of graded quartz sand and epoxy resin.

The electrical pulse was generated by two capacitors (each of 10 kV, 20 μF) connected in series. The circuit was similar to that shown in Fig.1 . In the experiments, the electrical loop between capacitor and underwater electrodes was kept reasonably small in order to reduce inductance.

The crushing chamber used in experiments is shown in Fig.16 .

2.2.1.2 INTERNAL LOADING OF SPECIMENS

Cylindrical, square, rectangular and triangular prisms of synthetic rock were used in the experiments. The specimens had holes along their axes. The exploding wire was either placed in the hole and confined by water around it, i.e. distortional (shear) wave would not be transmitted, and a part of longitudinal wave would be transmitted through water layer, or else it was tamped inside the specimen during casting to obtain more effective confinement, i.e. longitudinal and distortional (shear) wave would be transmitted to the surrounding specimen completely.

Fracture patterns in square and triangular prisms are
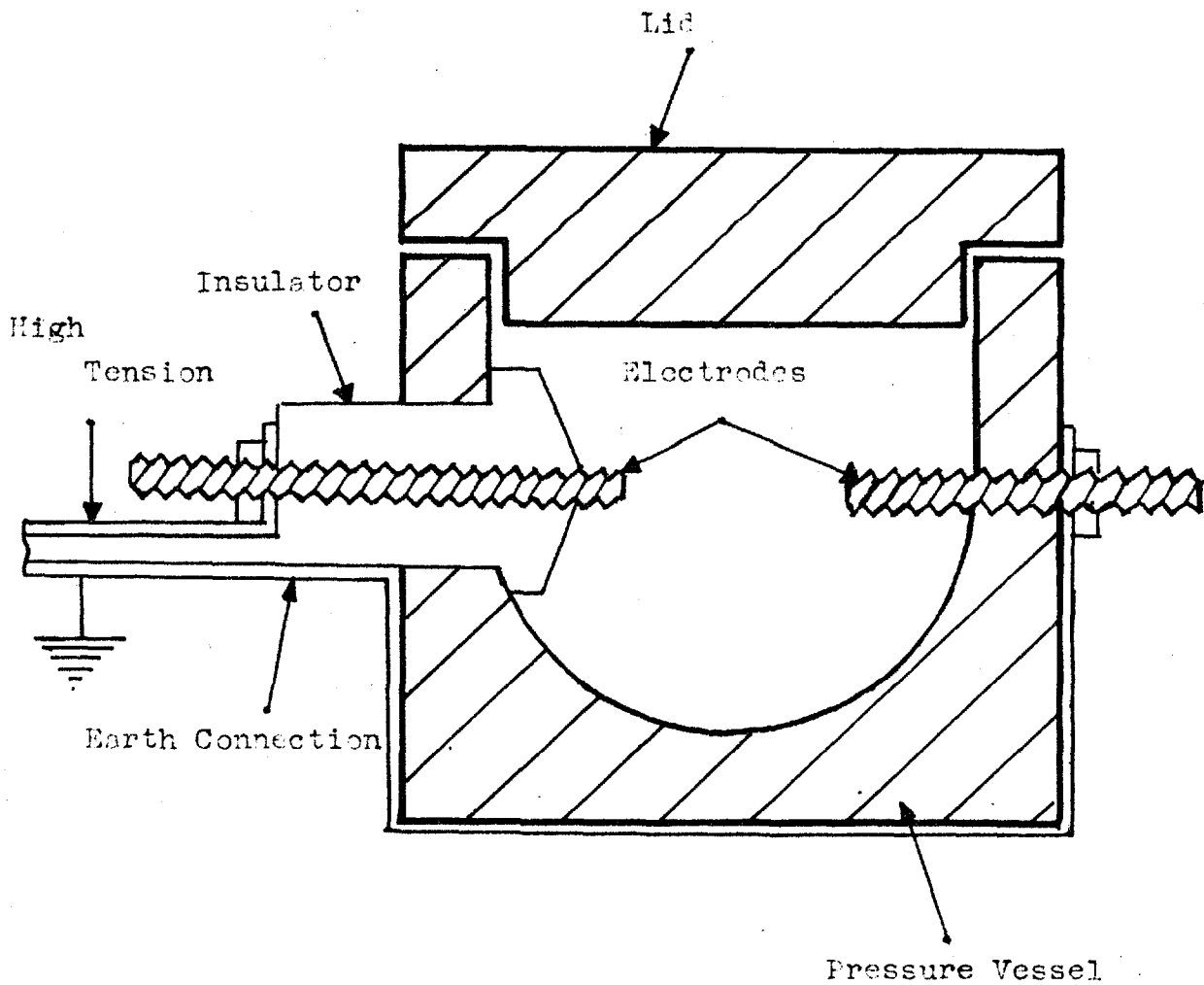
Fig. 16 The electrohydraulic crushing chamber used
in the experiments on fracture mechanism

shown in Fig. 17 .

The findings for internal loading of specimens were as follows:

1. All fracture patterns show a remarkable radial symmetry. The main cracks seem to have traversed the statically weakest radial sections of the specimens. These lines of fracture are analoguus to those caused by hoop stresses in the static loading of a cylindrical pressure vessel. The propagation of the cracks is from the centre. i. e. the highest hoop tensile stress in dynamic loading occurs nearest to the axis of the cylinder, as in the static loading of the pressure vessel.

2. Signs of compression damage i. e. pulverised material, attributable to a purely compressive shock wave or to the shear wave in combination with compressive longitudinal wave, were not detectable.

3. The intensity of shock wave front is a factor in initiating the cracks and determining the number of cracks.

4. The exploding wire technique gives results similar to those obtained in a larger scale in rock-blasting, except that there were no signs of a "crush zone" around the wire. However, both "critical fracture of crater" and "pre-splitting" were reproduced.

Fig. 17 Fracture patterns in square and triangular
prisms due to internal loading.

2.2.1.3 EXTERNAL LOADING OF SPECIMENS

Experiments were performed by placing the exploding wire on the external faces of square , rectangular, cylindrical and triangular prisms. In each case it was assumed that a thin layer of water between exploding wire and specimen existed, i.e. the shear wave would not be transmitted and a part of longitudinal wave would be transmitted through the water layer. Therefore, the formation of plane shear waves (von Schmidt head wave) would not be expected, although a plane surface is provided.

The findings for external loading of specimens were as follows:

1. Radial cracks due to hoop stress and Hopkinson spallings have been observed, varying with loading faces and geometry of specimens.

2. The intensity of shock wave front is a factor in initiating both the radial cracks and the Hopkinson spalls and in determining their number.

3. There were no signs of corner fractures, scabbing or compression damage, hence reflected tensile waves play a minor part in electrohydraulic crushing, unless they can be intensified by proper methods.

Photographs of a radial crack and a Hopkinson spalling are shown in Fig. 18 .
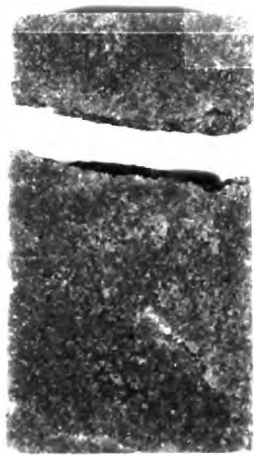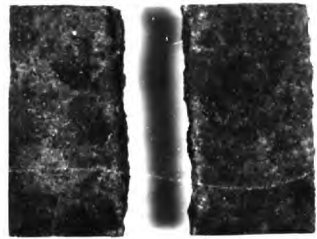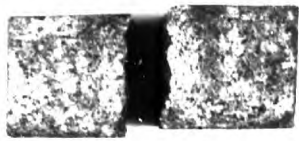
Fig.18   A radial crack (top) and a Hopkinson
spalling (bottom).

2.2.1.4 PRODUCTION OF MORE INTENSE REFLECTED TENSILE WAVES

The efficiency of reflection is an important parameter in the production of higher tensile stresses. For this reason the reflection coefficient should be increased. Thus, referring to Fig.5 in Chapter 1.3 , medium 1 would be water, medium 2 would be rock and 3 air. Because of the very low impedance of air ($\rho.c = 4.10^{-4}$) the reflection coefficient δ_R/δ_I is almost unity, i.e. practically the whole intensity of the wave is reflected.

Briefly, a square prism was subjected to the pulse, while the prism was only half immersed in water. Intense reflected tensile stresses and their concentrations resulted in a product of many fractured fragments. A similar prism was subjected to a similar pulse while completely immersed in water. This time the prism was found to be without any completed fracture.

A rectangular prism was subjected to the pulse in the same way while only half immersed in water. Two Hopkinson spalls were produced compared to one spall when completely immersed in water, thus indicating a doubling of the reflection coefficient. These results are shown in Fig.19 .
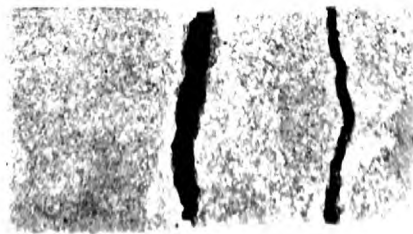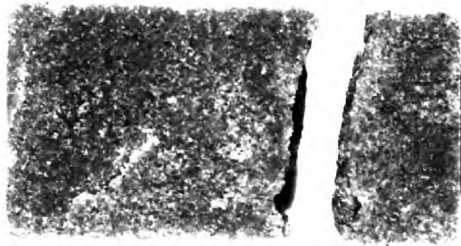
Fig. 19   The effect of reflecting medium in the
          production of Hopkinson spalls.
          Top)   Completely in water
          Bottom) Reflecting surface in air

2.2.1.5 FRACTURE MECHANISM WITH SIMULTANEOUS MULTIPLE SPARKS

It was found that as many as three separate copper wires would explode simultaneously with one capacitor discharge (10 μF, 10 kV discharge voltage).This phenomenon suggested some experiments to observe the result of interacting cylindrical shock waves.

a. Internal loading with simultaneous multiple sparks:

Rectangular prisms of synthetic rock with two symmetric holes parallel to the axes were fractured by placing two exploding wires in the holes, while the specimens were immersed in water.From the fracture patterns it seems that the main fractures occur along the lines of concentration of hoop stresses due to two cylindrical shock wave fronts.

The fracture patterns are shown in Fig.20 .

b. External loading with simultaneous multiple sparks:

Rectangular prisms of synthetic rock were fractured by placing two exploding wires either on one face or on two opposite faces separately.The resultant fracture patterns are shown in Fig.21 .In (a) two shock wave fronts were in the same face.Reinforcement of hoop stresses resulted in radial fracture.In (b) two shock wave fronts were in the opposite faces.Reinforcement of hoop stresses resulted again in radial fracture.In (c) the shock wave fronts were
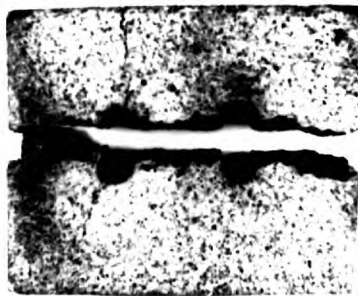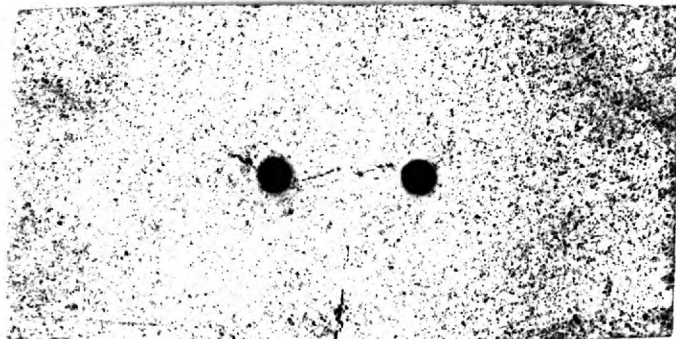
Fig. 20 Fracture patterns due to internal loading of
two simultaneous shock wave fronts.
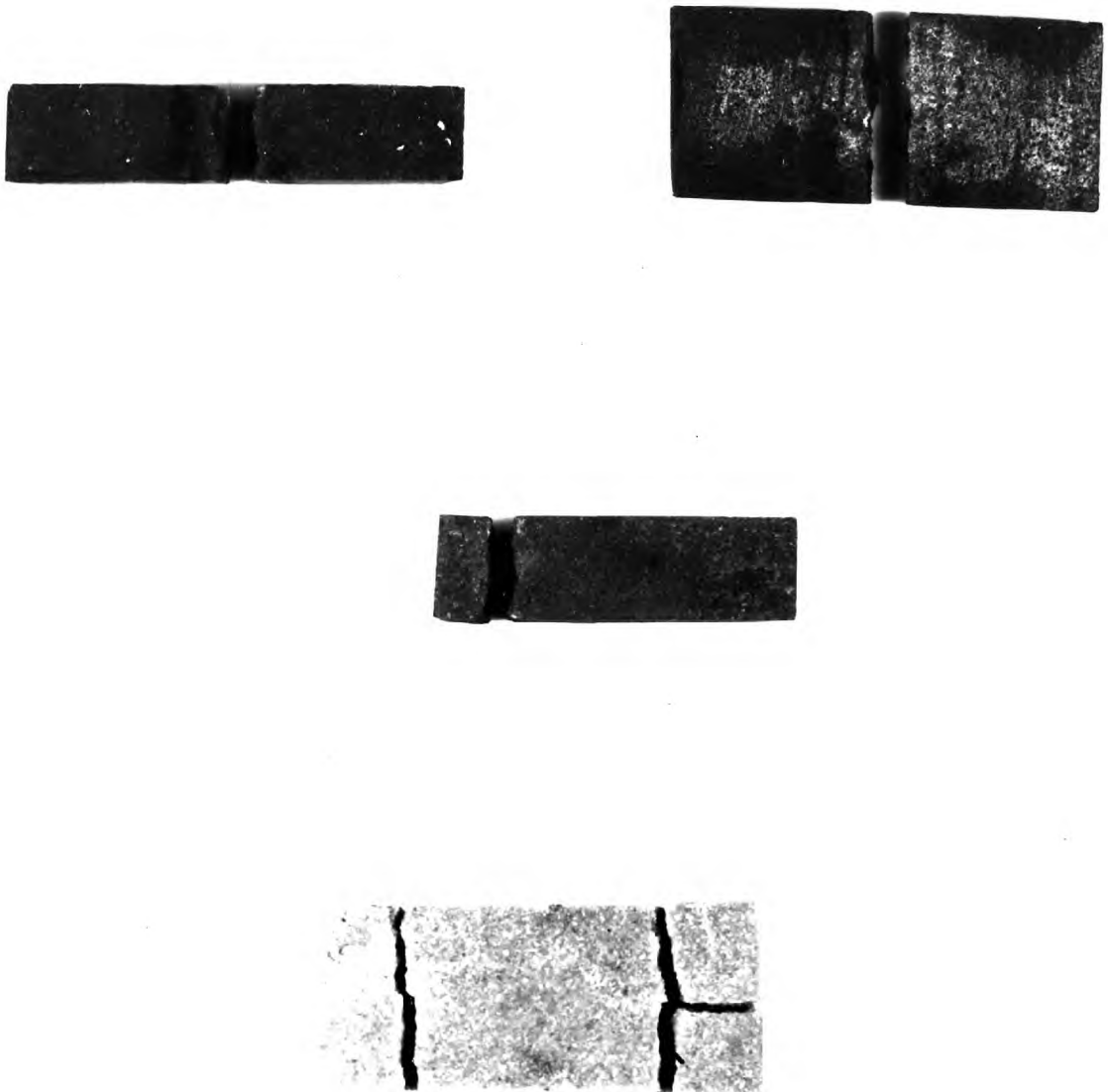
Fig.21 Fracture patterns due to external loading

of two simultaneous shock wave fronts.

Top (a)   Two shock wave front in the same face

Middle (b)Two shock wave front in the opposite faces

Bottom (c)Two shock wave front in the opposite faces

in the opposite faces. Reinforcement of reflected tensile waves produced Hopkinson spalls. Right hand spall was fractured into two due to intense reflections at the solid/air interface.

From these fracture patterns, it seems that both the hoop and Hopkinson stresses due two separate cylindrical shock wave fronts can reinforce each other. Thus, two shock wave fronts of low intensities, which cannot produce fractures alone, might produce fractures after reinforcement.

2.2.1.6 COMPRESSION DAMAGE

The so-called compression damage (Fig.9), which is the combination of radial fractures due to hoop stresses and shear fractures due to von Schmidt head waves, would not be expected, since the generation of von Schmidt head waves was not possible for the following reasons:

a. In most cases a thin layer of water was surrounding the exploding wire, which cannot efficiently transmit shear waves to solid bodies.

b. When the exploding wire was surrounded by solid (epoxy resin, or synthetic rock itself) the shear waves are transmitted to the solid; but the necessary condition, which is the providing of a plane surface for the produced longitudinal and shear waves, was not present.

To investigate compression damage with exploding wires, two types of experiments were performed. In first case the exploding wire was placed on the synthetic rock specimen surface and exploded while the specimen was immersed in water. No practical damage was observed. In the second case the exploding wire was placed on the surface of specimen and exploded while the specimen was in air. A damage channel of 1 mm. diameter along the source was observed. It seems that the above damage might have been caused by heat wave, which is not absorbed fully by surrounding air layer. Presumably explosion gases are cooled and absorbed more rapidly in water (first case) , than in air (second case).

2.2.2   BARE SPARK TECHNIQUE

Bare sparks were used especially to investigate shear fractures, after results of investigations on the spark path. Furthermore, bare sparks are more effective in electrohydraulic comminution than the exploding wire explosions ,due to better coupling of shock waves.

("Bare spark" term is used in the text for defining an underwater spark in which the exploding medium is water.)

2.2.2.1 INTERNAL LOADING OF SPECIMENS

The synthetic rock specimens similar to those used in

exploding wire technique but smaller, were fractured using the same apparatus (Fig.16). The pointed electrodes were placed in the holes in specimens and the spark discharged between them. Similar fracture patterns to those of exploding wires were obtained.

2.2.2.2 EXTERNAL LOADING OF SPECIMENS

The apparatus shown in Fig.25 was used in the experiments with electrode arrangements which are shown in Figs.14 and 15 . The capacitor used in the experiments was of 0.1 μF 35 kV charging voltage. The synthetic and natural rock specimens of small size were fractured. Although not so perfect, the fracture patterns were similar to those obtained with exploding wires. Complete and incomplete radial cracks due to hoop stresses were obtained, as were Hopkinson spalls due to reflected tensile stresses.

2.2.2.3 COMPRESSION DAMAGE

To investigate the compression damage, the bare sparks were discharged on the synthetic and natural rock specimens of semi-infinite size, as explained in previous Chapter 2.2.2.2 with the same experimental equipment. In the rocks of moderate strength (Limestone and weak Sandstone) slight but definite compression damage were observed after one

pulse, as predicted in Chapter 1.4 (Fig.9).The most frequently

encountered form of damage is seen in Fig.22 .The clear cut

radial cracks due to hoop stresses are visible in the so

called craters.Shear fracture was shown by the powdery appea-

rance and material was weakened at the fracture surfaces.

(It would be easily scratched by a knife). In the strong

rocks (Granite, Quartzite, strong Sandstone) no appreciable

damage was observed after one spark.But the material along

the spark track changed its appearance, i.e. its colour.

When it was scratched by a knife a weakening was apparent.

After several sparks, shallow craters were formed, but

without showing apparent radial cracks.

2.3.   ENERGY CONSUMPTION IN ELECTROHYDRAULIC

         COMMINUTION

There are three main so called "laws" of comminution

namely those due to Rittinger[23], Kick[24], and Bond[25,26].

According to these laws, work input should be proportional

to new surface produced , particle volume for a given reduc-

tion ratio , or crack length respectively. In fact, energy

consumption depends, very much on initial feed size[27,28,29,30],

final product size[29], size distribution of products, energy

concentrations[29,30,31] and type of applied forces during

crushing,i.e. type of crushing machine.Among the three laws

Rock surface Radial fracture

Length of spark
or shock wave front

Shear fracture
surfaces

Plan

Rock surface
Shear fracture
surfaces
Radial fracture

Section
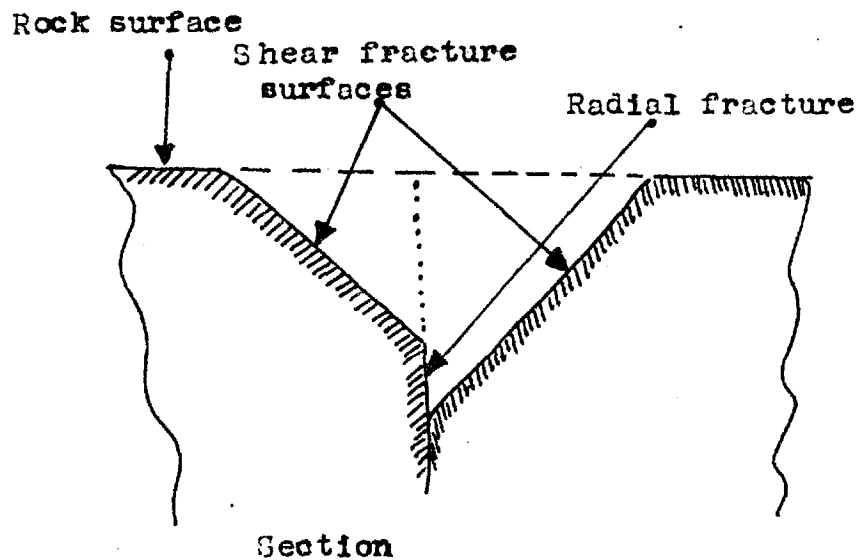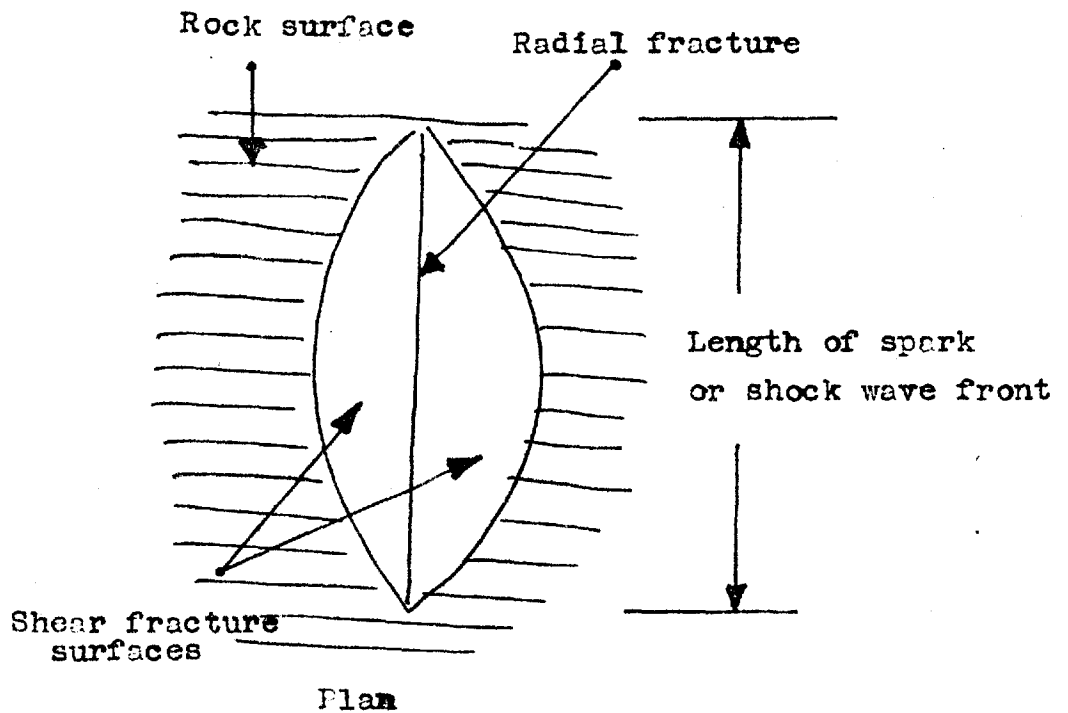
Fig.22 Compression damage (Combination of radial and
shear fractures)

the Bond's law is more practical and gives more constant values of work input for chosen material with a given machine, in constant test conditions, with relatively wide ranges of initial feed size . Therefore the Bond's Index,

$$(B.I. = W. \frac{\sqrt{R}}{\sqrt{R} - 1} . \sqrt{\frac{P}{100}} \qquad (15)$$

where W = energy consumption ,   kWhr/ton

R = reduction ratio, $\frac{F}{P}$

F = 80% passing feed size   microns

P = 80% passing product size   microns)

is chosen mainly for comparisons in different test conditions and with conventional comminution.(In the calculations of Bond's Indexes, R is taken as a ratio between average feed and average product size, since in all experiments scalped feeds were used.)At the same time however, the surface energies which are computed by determining mathematically the new surface area produced from the size distribution graphs, the Kick's constants ,

$$(K = \frac{W}{\log R} \qquad (16)$$

where W = energy consumption   kWhr/ton

R = reduction ratio , $\frac{F}{P}$

F = average feed size

P = average product size   )

feed size, average product size, reduction ratio, energy consumption per ton crushed products, were also quoted

beside Bond's Indexes in the tables.

At present the efficiency of electrohydraulic comminution is low. In general, if Bond's Indexes are considered, electrohydraulic comminution is about 3-10 times less efficient than conventional comminution. In practice, the comparisons with conventional crushing vary videly with these three laws. This is understandable, since all laws have some assumptions (32), such as certain size distribution of crushed product. Even in conventional comminution size distributions of products vary with the nature of rock and also from one type of machine to another (33). In electrohydraulic comminution, as it will be shown later, the slope of size distribution curves of the products in log-log plot are always steeper than those of conventional comminution, i.e. less production of fines. Therefore the energy consumption would be very much in favour of conventional crushing if the Rittinger's law is taken as the basis of comparison, since the fine particles contribute considerably to the surface area production.

On the other hand, for economical reasons, if very fine particles are considered as a waste of material, as it is in very wide range of industrial operations, i.e. in concentration processes of ores, in coarse aggregate production from the quarries, the energy consumed in these particles

shouldbe considered also as a loss of energy.Hence in these applications electrohydraulic comminution could actually be more efficient, since less energy goes into fines.

Briefly, at present , there is no sound comparison basis, not only for scientific but also for economic purposes.Therefore it is suggested that in the last resort, the requirements for certain types of crushed products in various industries , would form the set of bases for comparisons.Thus, the energy consumption in electrohydraulic crushing might represent higher efficiency in one application, than in another.

2.3.1 THE EFFECT OF ELECTRICAL PARAMETERS ON THE EFFICIENCY OF CRUSHING

In the present studies the electrical parameters were not investigated, since:

a. The research on this subject [6,7,8,9] was already available, though not extensive.

b. The necessary equipment for the studies of electrical parameters was not available.

The one well known criterion, as is demonstrated theoretically in Chapter 1.1 ,is to provide low inductance in the discharge circuit for better electrical efficiency.Maroudas et al. [7,8,9] have made crushing experiments using coaxial

arrangements to obtain lower inductances. It was found that the comminution efficiency was increasing with decreasing values of inductances, i.e. with increasing electrical efficiency.

In the discharge circuits used in the present studies, coaxial arrangements for low inductances, broad thick conductors for low resistances, and relatively large under water gaps for good damped discharge, were used in order to obtain as high as possible electrical efficiencies. (Figs. 3 and 4) The inductance of the circuit used with the crushing chamber shown in Fig. 16, was found from oscilloscope measurements to be about 1-2 microhenries. An attempt was also made to determine the inductance of electrohydraulic crushing device shown in Fig. 25 but without success due to heavy interference on the oscilloscope screen. It can be assumed however that the inductance was far lower than above value of 1-2 microhenries, since complete coaxial arrangements and the shortest possible connections were used in the design of the device.

2.3.2   THE EFFECT OF MORE INTENSE REFLECTED
TENSILE WAVES AND THEIR PRODUCTION

As is demonstrated in Chapter 2.2.1.4 the coefficient of reflection is an important factor in the production of

reflected tensile stresses. After providing a solid/air inter-
face for reflections of shock waves, the intensity of reflec-
ted tensile wave is almost doubled, as indicated by the
number of Hopkinson spalls.

In order to investigate the comminution efficiency of
more intense reflected tensile waves two types of experiments
were performed.

2.3.2.1   SINGLE SPECIMEN EXPERIMENTS WITH
EXPLODING WIRE TECHNIQUE

The exploding wire was held between two slices of the
specimen, with either a very thin layer of water and an
elastic band, or else by a thin layer of solidified epoxy
resin. The crushing chamber shown in Fig.16 was used with
two capacitors of 20 μF each connected in series. The speci-
mens of synthetic rock, a sandstone, and a granite, were
fractured in three different ways.

(i.)   Completely submerged in water.

(ii.) With the lower half submerged in water and the
upper half in contact with air.

(iii.) With all the outer surfaces completely in air.

The fracture patterns were observed as follows:

(i.)   With the specimen completely in water the frac-
ture pattern was usually either a single split or a cross,

except with granite which was fractured into coarse fragments.

(ii.) With the specimens half in air, half in water, the slice of specimen in contact with air was crushed into many many small pieces, while the underwater slice of specimen was fractured into two pieces only, except the granite which was fractured into fine fragments.

(iii.) With specimens completely in air, they were all broken into many small pieces, with some fines. The granite produced most fines.

In   Table 2 the energy consumptions for granite, in terms of Bond's Index, Joules/cm^2, and Kick's constants are shown.

It is clear from   Table 2, that the all three laws of comminution indicate increased comminution efficiency with increasing intensity of reflected tensile waves in the solid/air interface.

2.3.2.2 BATCH TYPE COMMINUTION EXPERIMENTS

The crushing chamber shown in Fig.24 was used in the experiments with ordinary tap water. The same two capacitors of each 20 μF were used in series in the discharge circuit. Quartz feed of two sizes were crushed in two different ways:

(i.)   In case A the feed was crushed whilst all the particles were immersed in water.

SECTION

Steel pipe

Earth
Connection

Feed particles

Electrodes

Water level

High tension
Connection

Rubber bung

PLAN

95 mm.
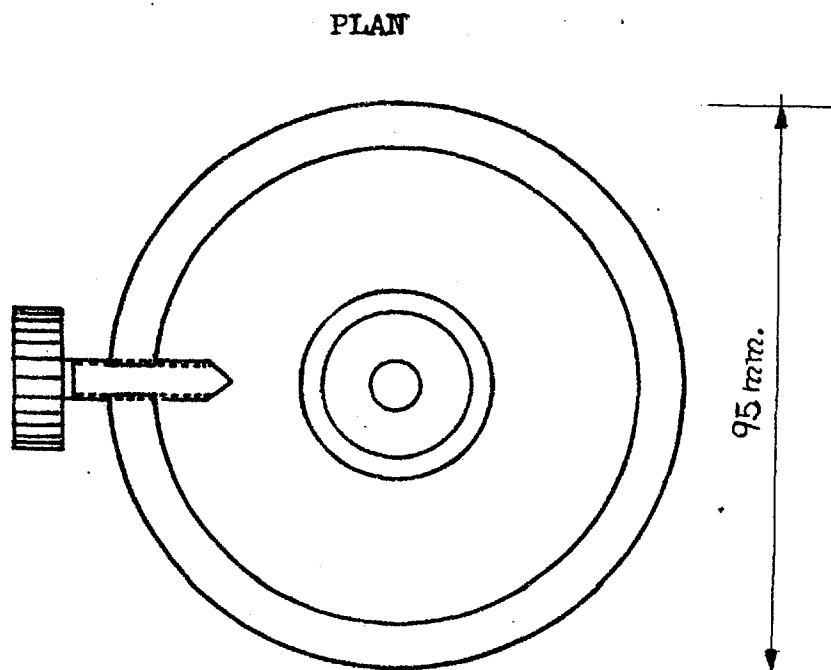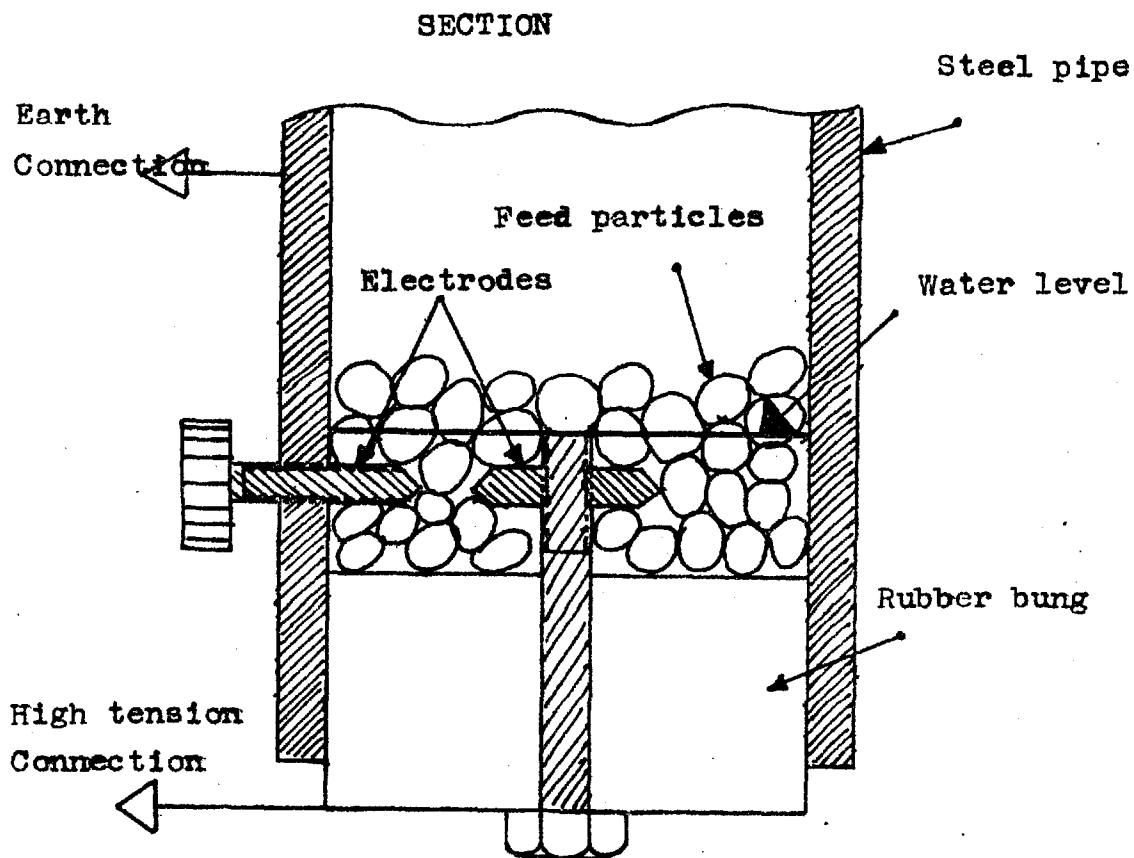
Fig. 24 Crushing chamber for batch type electrohydraulic

comminution

Table 2. Energy consumption of a granite in single electro-
trohydraulic crushing with exploding wire technique
10 µF, length of exploding wire about 4 cm.

	Specimen underwater	Half of the specimen in air	Specimen in air
Disharge voltage kV	10.6	9.6	10.4
Initial size mm.	30.	30.	31.
Average product size mm.	8.07	4.93	2.74
Reduction Ratio	3.7	6.1	11.3
Energy Consumption kWhr/ton	2.1	1.8	1.8
Bond's Index Ratios	47.3 1.0	20.0 0.42	16.6 0.35
Joules/cm^2 Ratios	2.06 1.0	0.65 0.32	0.31 0.15
Kick's Constant Ratios	3.7 1.0	2.3 0.62	1.7 0.46

(ii.) In case B only the electrodes were covered by water, i.e. water level was approximately 0.5 cm. above electrodes. In this case a part of some feed particles were in contact with air, while the other parts of these particles were immersed in water. Thus, the shock wave entered these particles with small losses due to reflections at water/solid interface, but reflected almost completely at the solid/air interface.

The experimental results are shown in Table 3 .

It is clear from Table 3 , that all three laws of comminution indicate increased efficiency for a batch type operation by providing solid/air interfaces for outgoing waves in some of the feed particles.

In a prototype of a developed electrohydraulic comminution device (Fig. 25) which is shown diagramatically, experiments of above type were also performed using a capacitor of 0.1 uF and 35 kV discharge voltage using demineralised water as a discharge medium. There was a gradual increase in energy consumption with decreasing water level. However, this discrepancy may be due to following reasons:

For this energy level (about 50-60 joules per pulse), which is about 10 times lower than the previous case (about 400-500 joules per pulse),

(i.) the crushing was presumably mainly due to radial

Table 3 a. Energy consumption for Quartz in batch type

of electrohydraulic comminution

10 μF , 1 cm. underwater gap length,
ordinary tap water discharge medium,
about one pulse per minute repetition rate

Feed size	8.73 mm. (7/16"-1/4")					
400gr. per test	A	B	A/B	A	B	A/B
Average discharge voltage, kV	8.04	8.01		10.43	10.89	
Average product size, mm.	3.18	2.86		2.88	2.77	
Average reduction ratio	2.75	3.05		3.04	3.17	
Average energy consumption, kWhr/ton	8.65	5.10		10.15	8.11	
Average Bond's Index	164.9	87.7	1.88	180.6	134.8	1.34
Average Joules/cm^2	1.32	0.72	1.86	1.17	0.97	1.20
Average Kick's constant	19.7	10.5	1.87	21.0	16.2	1.30

Table 3 b. Energy consumption for Quartz in batch type

of electrohydraulic comminution

IO μF , 1 cm. underwater gap length,
ordinary tap water discharge medium,
about one pulse per second repetition rate

Feed size	4.76 mm. (1/4"-1/8")					
400 gr. per test	A	B	A/B	A	B	A/B
Average discharge voltage, kV	8.07	8.4		11.20	11.22	
Average product size, mm.	1.42	1.39		1.30	1.27	
Average reduction ratio	3.55	3.41		3.66	3.73	
Average energy consumption, kWhr/ton	19.48	9.83		18.63	12.23	
Average Bond's Index	208.1	107.7	1.93	191.2	122.9	1.56
Average Joules/cm^2	1.30	0.78	1.67	1.16	0.77	1.50
Average Kick's constant	35.4	18.5	1.92	33.1	21.3	1.53

cracks, and there was very little contribution of Hopkinson spallings,

(ii.) the inertia of surrounding water was presumably low due to decrease of water level, which is important in the development of shock waves,

(iii.) in low water levels, so called surface flashes on the water surface between electrodes, are often observed, which are not effective in production of shock waves of high intensity.

2.3.3   THE EFFECT OF FEED SIZE

For Hopkinson spalling , and for the fractures due to concentrations of reflected tensile stresses, the size of the feed particles should be greater than half the wave length of the stress pulse in order to obtain high comminution efficiencies. Therefore, with decreasing feed size, a decrease in comminution efficiency would be expected. On the other hand, with smaller feed particles, the spark gap vicinity can be more effectively filled and shock wave front more effectively used in crushing. In fact, actual comminution efficiency is the combination of these two factors.

In the crushing Chamber shown in Fig. 24, Quartz particles of 7/16"-1/4" and 1/4"-1/8" feed sizes were crushed.

The results are already shown in   Table 3.a and b .
Comminution efficiency decreases with decreasing feed
size according to three laws.This is understandable, since
the Hopkinson spallings, and fractures due to concentration
of reflected tensile stresses, were presumably contri-
buting very much to comminution and the efficient filling of
the spark gap vicinity was not an effective factor in this
high energy level with above range of feed size . Although
feed particle size was smaller than half the wave length,
the intensity of the shock wave front was presumably seve-
ral times higher than the dynamic tensile strength of the
Quartz, so that resultant tensile stresses, high enough
to fracture , were developed within the solid particles.

Further experiments were performed in the electrohyd-
raulic comminution device shown diagrammatically in Fig.25,
which was developed during studies.The capacitor of 0.1 μF,
and 35 kV discharge voltage was used with demineralised
water.In ordinary tap water the underwater spark deve-
lopment after capacitor discharge , was not possible for
reasonable long underwater spark gaps with this low energy
level due to the conductivity of water.

The fairly wide ranges of feeds of Limestone, Flint
and Quartz were crushed.The energy consumptions in terms
of Bond's Index, Joules/cm^2 and Kick's constants are shown
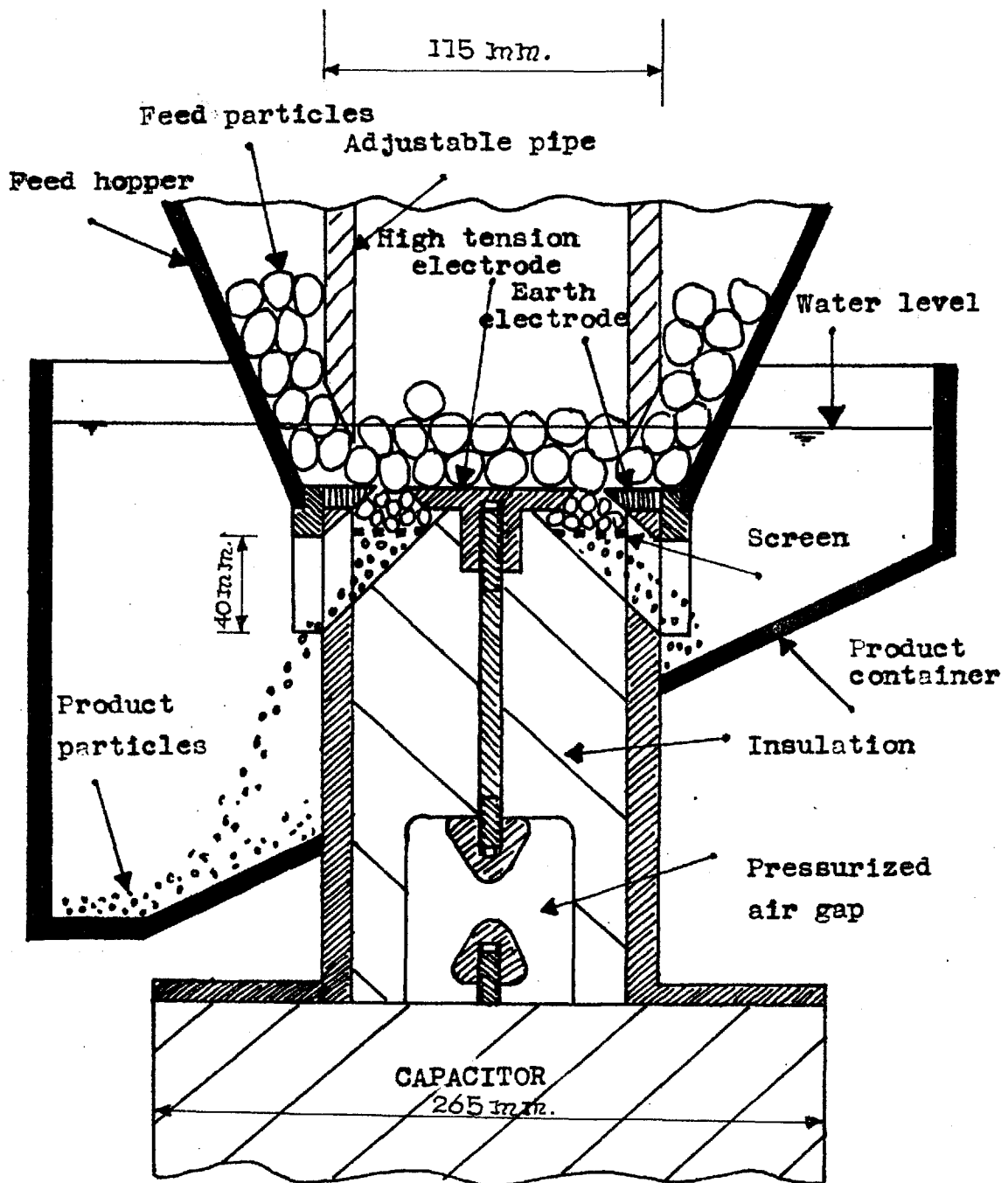
Fig. 25 Electrohydraulic comminution device

in Figs.26,27,28 in log-log plot , respectively.The ener-
gy consumptions and other relevant data for Limestone,
Flint and Quartz, are also shown in   Tables 4,5,6
respectively.

Bond's Indexes and surface energies indicated an
increase in the comminution efficiency with decreasing
feed size.But Kick's constants show an opposite trend.
This observation also shows how these three comminution
laws contradict each other.The trend of an increase in
efficiency was accepted , since it was indicated by more
practical considerations.This trend is understandable,
since the Hopkinson spalling, and fractures due to concen-
tration of reflected tensile stresss were not presumably
contributing very much to comminution at this energy
level, and efficient filling of the spark gap vicinity was
the main factor in the comminution efficiency.This trend
is also in accord with observations made in experiments
with same crushing device, mentioned in Chapter 2.3.2.2,
to investigate the effect of providing solid/air interface
to the feed particles.

2.3.4   THE EFFECT OF PHYSICAL PROPERTIES
          OF ROCK

The fractures in electrohydraulic comminution are

Table 4. Energy consumption for Limestone in electro-
hydraulic comminution for various feed sizes

0.1 µF, 35 kV discharge voltage,
1cm. underwater spark gap length,
demineralised water discharge medium,
about one pulse per two second repetition rate

Feed size (½ kgr. per test)	7-10 mesh	7 mesh - 1/8"	1/8"-1/4"	1/4"-1/2"	1/2"-1"
Product size mm.	1.11	1.74	1.88	3.60	5.65
Reduction ratio	1.84	1.61	2.54	2.65	3.37
Energy consumption kWhr/ton	5.86	4.11	7.80	7.10	7.00
Bond's Index Ratios	89.6 0.58	92.8 0.60	109.1 0.71	133.0 0.86	154.0 1.00
Joules/cm.^{2} Ratios	0.76 0.19	1.46 0.35	1.86 0.44	2.60 0.62	4.20 1.00
Kick's constant Ratios	22.13 1.00	19.87 0.90	19.27 0.87	16.78 0.76	13.27 0.60

Table 5. Energy consumption for Flint in electrohyd-
raulic comminution for various feed sizes

0.1 μF, 35 kV discharge voltage,
1 cm. underwater spark gap length,
demineralised water discharge medium,
about one pulse per two second repetition rate

Feed size (½ kgr per test)	7-10 mesh	7 mesh - 1/8	1/8"-1/4"	1/4"-3/4"	3/4"-1/2"	1/2"-1"
Product size mm,	1.06	1.71	1.72	3.31	4.59	5.11
Reduction ratio	1.92	1.64	2.80	2.40	2.40	3.72
Energy consumption kWhr/ton	4.58	2.40	5.47	4.60	4.40	5.77
Bond's Index Ratios	57.6 0.50	50.3 0.44	69.5 0.61	93.5 0.82	106.7 0.93	114.7 1.00
Joules/cm.^{2} Ratios	0.71 0.26	0.93 0.34	1.14 0.41	1.85 0.67	2.15 0.78	2.75 1.00
Kick's constant Ratios	16.16 1.00	11.17 0.64	12.23 0.76	12.10 0.75	11.57 0.72	10.11 0.63

Table 6. Energy consumption for Quartz in electrohyd-

raulic comminution for various feed sizes

0.1 µF, 35 kV discharge voltage,
1 cm. underwater spark gap length,
demineralised water discharge medium,
about one pulse per two second repetition rate

Feed size (½ kgr. per test)	7-10 mesh	7mesh-1/8"	1/8"-1/4"	1/4"-7/16"
Product size mm.	0.90	1.38	1.36	5.34
Reduction ratio	2.28	2.03	3.49	1.63
Energy consumption kWhr./ton	4.91	3.67	5.80	2.72
Bond's Index Ratios	54.5 0.62	55.9 0.64	60.8 0.69	87.9 1.00
Joules/cm.^{2} Ratios	0.38 0.71	0.39 0.73	0.50 0.94	0.53 1.00
Kick's constant Ratios	13.72 1.00	11.93 0.87	10.67 0.78	12.81 0.93

Fig. 26 Bond's Index-feed size relation
         for various rocks
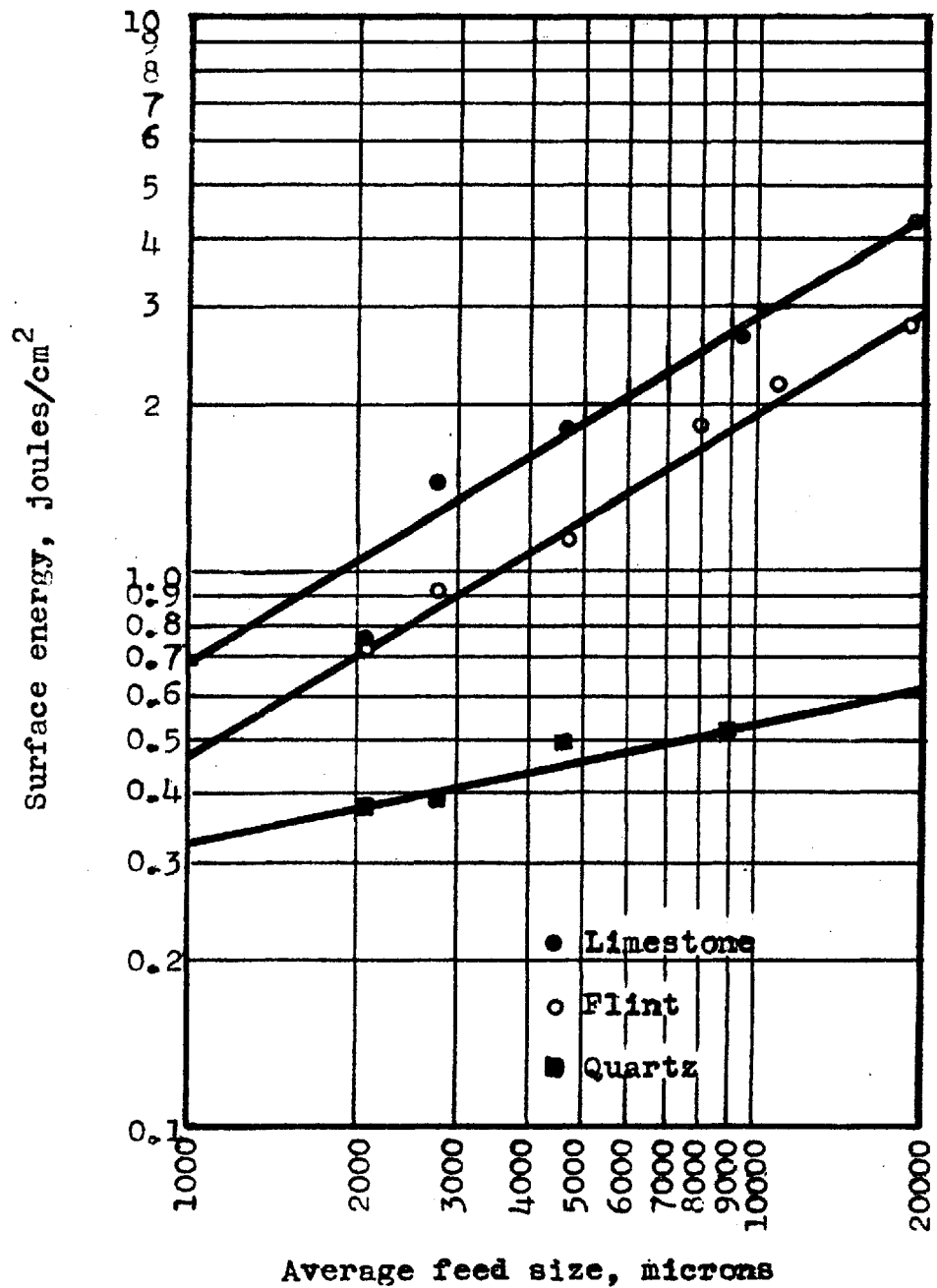
Fig. 27 Surface energy-feed size relation
for various rocks
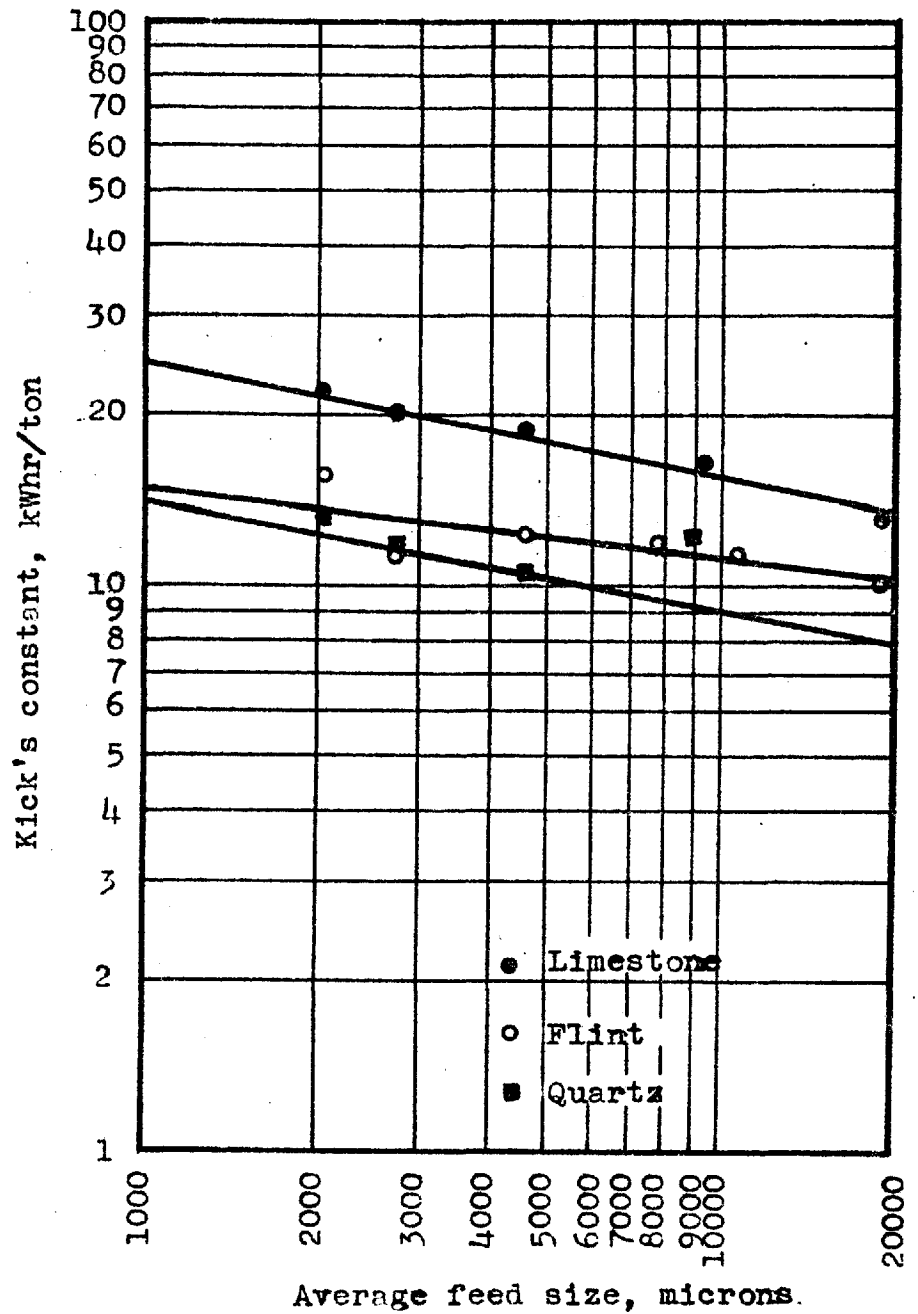
Fig. 28   Kick's constant-feed size relation
for various rocks

mainly due to tensile stresses. Therefore the dynamic
tensile strength of rock is of more importance than its
compressive or shear strength. Furthermore, attenuation of
shock waves in the solid bodies, which is dependant on the
energy absorption factor of rock which is partly due to
plasticity and brittleness of rock particles, is an impor-
tant parameter in electrohydraulic comminution.

On the other hand, the fractures, in conventional
crushing methods are caused generally by compression,
shear and frictional forces. Therefore , compressive
strength and hardness of the rock to be crushed are
major parameters in conventional comminution.

The synthetic rock, sandstone and granite specimens
were crushed by the exploding wire technique, with single
sparks, as previously described in Chapter 2.3.2.1 . The
most effective crushing was obtained with granite. No
attempt was made to determine the tensile strength of the
natural rocks used in the experiments. Although, the tensile
strength of the rocks vary very widely not only with their
chemical compositions, but also with their grain size,
localities, stratification and the direction of the load
applied with respect to their strata and depend very much
on the test method, preparation of specimens, and size of

specimens, usual figures for tensile strength $^{(35 \text{ to } 41)}$

are 700-1,800 p.s.i. for granite, 1,000-1,500 p.s.i.

for sandstone.The tensile strength of synthetic rock was

determined by the Brazilian test and found to be about

1,500 p.s.i. .Granite is also the most brittle of the

three rocks tested and has very likely inherent internal

stresses near to the interfaces between its different

mineral grains, which would be developed during its ori-

ginal cooling.These internal stresses might contribute to

the resultant fractures.The synthetic rock,which presumably

has the highest tensile strength and is most plastic

among the three, due to its epoxy resin matrix,produced

less fines.

Limestone, flint and quartz feeds were crushed elec-

trohydraulically, as explained in Chapter 2.3.3 , with

multiple successive sparks.Energy consumptions are given

in Figs.26,27,28 and in the Tables 4,5,6 .The ascending

order of comminution efficiency is limestone, flint , and

quartz.

Although, the order of tensile strengths of these

rocks is not very much in agreement with the above order

(Usually tensile strengths are 1,000-2,000 p.s.i. for

limestone, 2,000-3,000 p.s.i. for flint and 1,500-2,000

p.s.i. for quartz), it may be significant that limestone

is most plastic of the three and required more energy, and quartz which is most brittle, required the least energy.

The descending order of Bond's Indexes in conventional comminution is flint, quartz, and limestone (namely 26, 14, and 12 respectively (26))This order is in agreement with the order of compressive strength of these rocks, which is flint, quartz, limestone .(namely 50,000-100,000 p.s.i., 20,000-30,000 p.s.i., and 10,000-20,000 p.s.i. respectively) Furthermore, this order is also not contradictory with the order of their hardness, which is flint, quartz, limestone (7, 7, 3 respectively on the Mohr scale).

2.4   THE SHAPE FACTOR IN ELECTROHYDRAULIC COMMINUTION

The shape of products of electrohydraulic comminution was first investigated visually and under a microscope during tests on liberation.The fragments of electrohydraulic crushing products were always more cubic than those of laboratory jaw crusher , hammer or vibration mill. However, these observations were set aside for some time; systematic study of particle shape was only undertaken after the more fundamental studies had thrown light on the mechanism of shaping by hoop and Hopkinson stresses.

2.4.1   CHOICE OF ROCKS

The first tests on the shape factor in electrohydrau-
lic comminution were started with available rocks from the
departments store.(Quartz, Granite, Feldspar)After
obtaining good shape with these rocks, it was decided to
crush an extremely flaky rock, and accordingly flint
pebbles were obtained from Headley Heath, Surrey.It is
well known that flint gives extremely flaky, razor-like
fragments with conventional crushing.These flint pebbles
showed good results also, and so by courtesy of the
British Granite and Whinstone Federation , rock samples
were obtained from some British quarries which were
representative of materials with good strength, but
inclined to be flaky on crushing.

2.4.2   BASIS FOR COMPARISON OF EXPERIMENTAL
            RESULTS
                                            (42,43,44)
    a. There are two British Standard's tests
at present to determine the shape factor of aggregates.

    1. Flakiness index:

        This is the percentage of flaky material in a given
range of particle sizes, flakiness being defined as abi-
lity to pass through a standard slotted test sieve.(A
particle is defined as flaky if its thickness is less

than 0.6 of its "mean size". "Mean size" of particle assumed
to be mean of the aperture sizes of the pair of perforated
plate, square-aperture test sieves.(Table 7)[52])

2. Elongation index:

This is the percentage of elongated particles in
a given range of particle sizes, elongation being defined
as inability to pass between standard test bars.(A particle
is defined as elongated if its length is greater than 1.8
times of its mean size.(Table 7[52])

Table 7. Dimensions of Flakiness and Elongation gauges

Size of aggregate			Width of slot in flakiness gauge, (0.6 M) (in.)	Distance bet-ween pegs on elongation gauge, (1.8 M) (in.)
Passing B.S. sieve of aperture size,(in.)	Retained on B.S. sieve of aperture size,(in.)	"Mean size" (M) (in.)		
2	1 1/2	1.75	1.05	3.15
1 1/2	1	1.25	0.75	2.25
1	3/4	0.88	0.53	1.57
3/4	1/2	0.63	0.38	1.12
1/2	3/8	0.44	0.26	0.79
3/8	1/4	0.31	0.19	0.56

b. Percentage of voids

Percentage of voids in the bulk of particles is also

an indication of shape of grains. In practice, well shaken well packed equi-size spheres settle down to about 38% voids. It is clear that if equi-size cubes were packed perfectly well together, there would be nil percent of voids theoretically. Therefore, it is reasonable to assume that with particles becoming more cubic, percentage of voids would decrease. For this reason it would be expected that a lower percentage of voids would result from electro-hydraulic comminution than from conventional methods.

2.4.3   THE RESULTS

Numerous rock samples were crushed in the electrohyd-raulic comminution device shown in Fig. 25 , the capacitor used was again of 0.1 μF capacity and 35 kV discharge voltage, discharge medium being demineralised water , and in a one H.P. Dodge type Sturtevant laboratory jaw crusher. Feed size of the rocks was generally 1"-2" in the experiments. Comparative crushed products of jaw crusher and the electrohyd-raulic comminution device are shown in Figs. 29 and 30. In Fig. 29 the size of flint fragments is 3/4"-1/2" and in Fig. 30 1/2"-3/8". In these photographs the upper two rows consisting of six particles represent the product of electrohydraulic comminution and the lower two rows, again consisting of six particles, represent the product of the
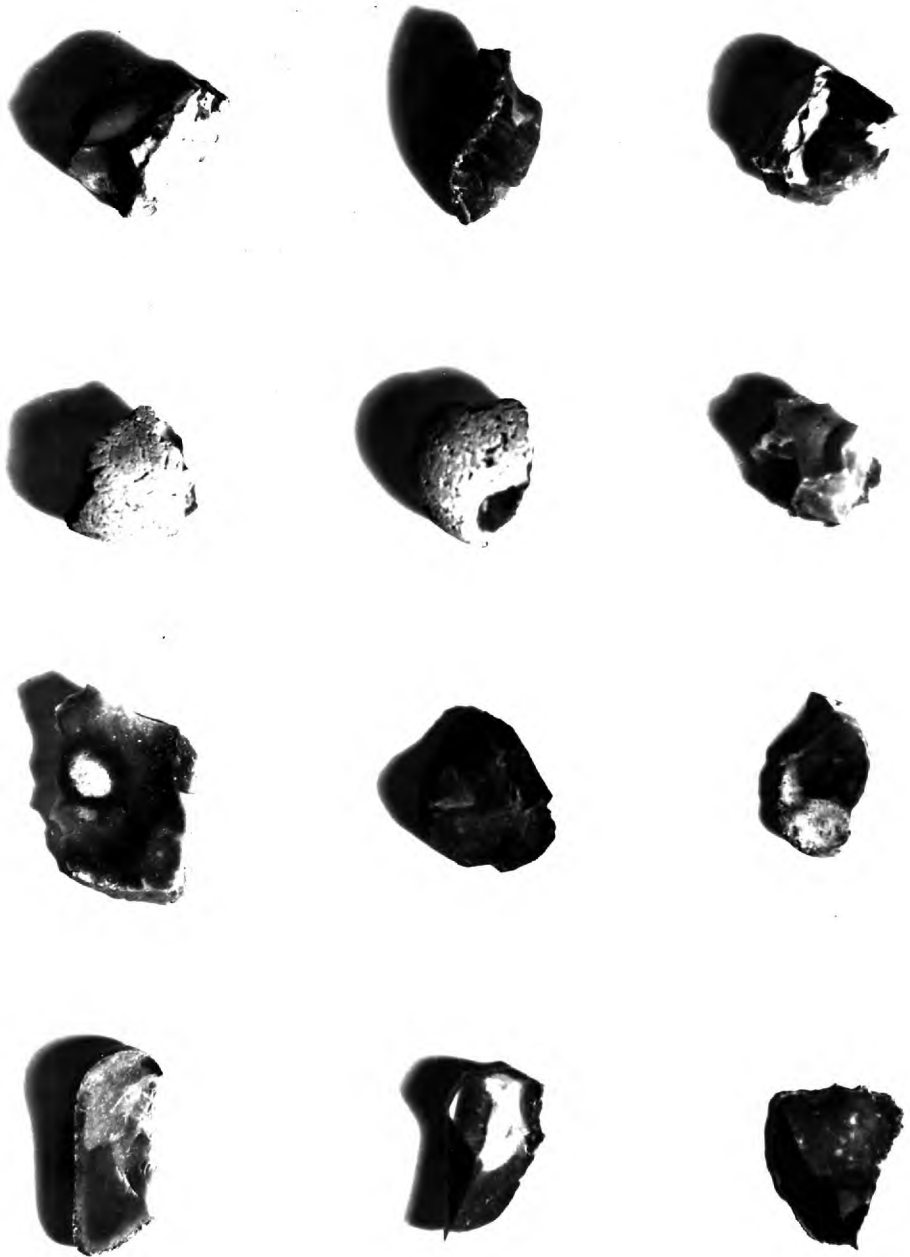
Fig. 29   Comparative 3/4"-1/2" products of electrohydraulic
comminution device and jaw crusher
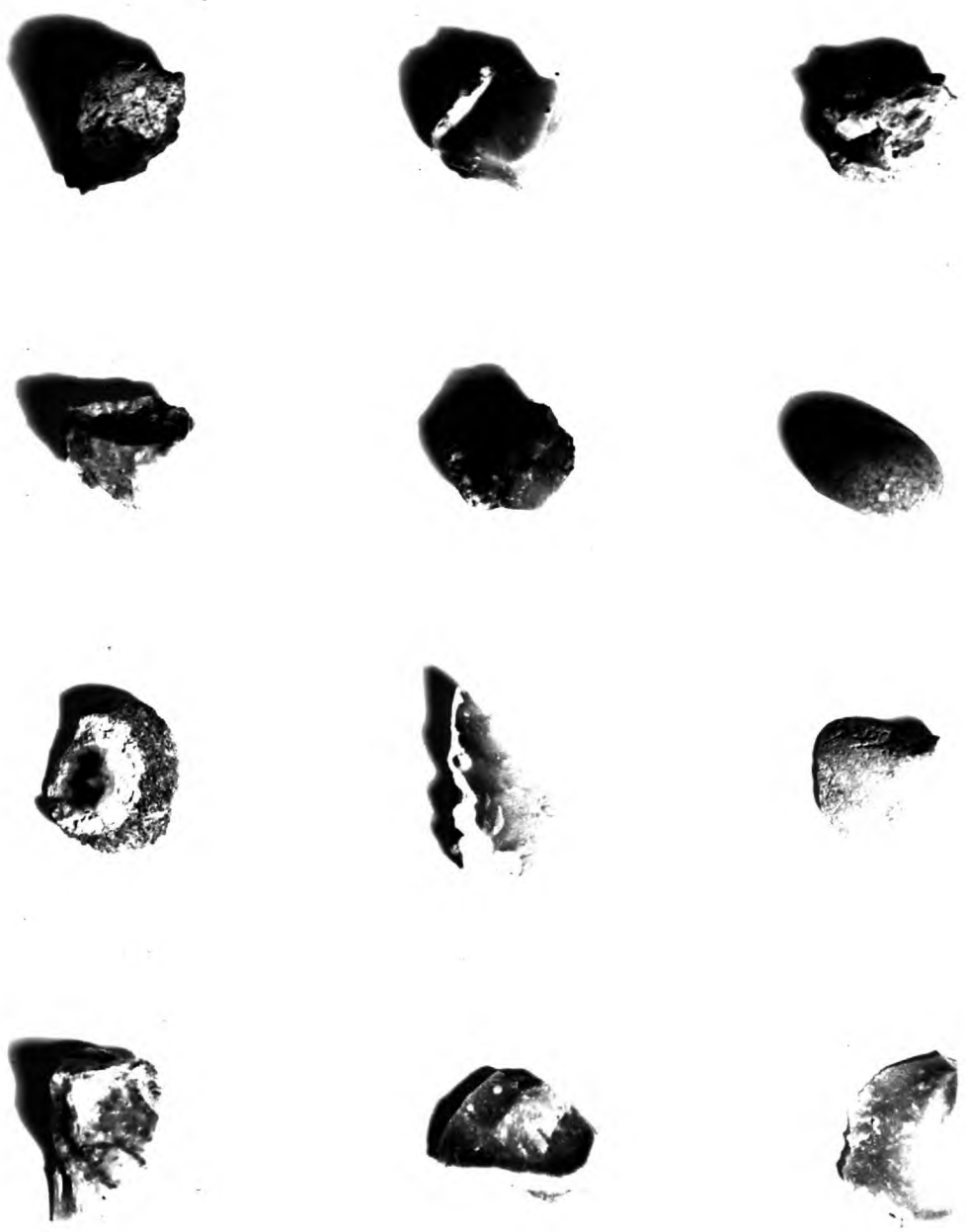
Fig. 30   Comparative 1/2"-3/8" products of electrohydraulic
comminution device and jaw crusher

jaw crusher. In these photographs the third dimension is represented by shadows. It is clear from these figures that the third dimension of grains from the electrohydraulic comminution product is always longer than from the jaw crusher product, i.e. the grains of electrohydraulic comminution product are more cubic.

Flakiness indices:

The Table 8 a and b show the comparative indices of crushed particles. The superiority of electrohydraulic comminution in the production of cubic shapes is clear from the Table , although the jaw crushers produce fairly flaky fragments among conventional crushers [45] . (Table 10) In some cases electrohydraulic comminution produced nil (0.0) percent flakiness.

Elongation indices:

The Table 9. a and b show the comparative elongation indices of crushed particles. The electrohydraulic comminution products are not as good as in elongation index as in flakiness index, but still superior to jaw crushed products.

Percentage of voids:

A quartz feed of 7/16"-1/4" was crushed respectively in the laboratory jaw crusher, a laboratory hammer mill and in the electrohydraulic crusher shown in Fig. 24 .

Table 8 a. Comparison of Flakiness index for products from
electrohydraulic comminution and jaw crusher
respectively

FELSITE   RED QUARTZITE

Size range	Flakiness index	
	E.H.C.	JAW
3/4"-1/2"	2.6	38.5
1/2"-3/8"	2.3	25.0
3/8"-1/4"	1.2	32.0
Mean	2.0	31.8

Size range	Flakiness index	
	E.H.C.	JAW
3/4"-1/2"	0.0	71.4
1/2"-3/8"	5.8	19.1
3/8"-1/4"	0.0	26.2
Mean	2.0	38.9

ALBITIZED OLIVINE DOLERITE   PROXENE ANDESITE

(Criggion Quarry)   (Moon's Hill Quarry)

Size range	Flakiness index	
	E.H.C.	JAW
3/4"-1/2"	0.0	45.3
1/2"-3/8"	1.9	29.5
3/8"-1/4"	10.3	48.5
Mean	4.1	41.1

Size range	Flakiness index	
	E.H.C.	JAW
3/4"-1/2"	2.9	37.0
1/2"-3/8"	2.4	47.9
3/8"-1/4"	15.3	49.4
Mean	6.9	44.7

Table 8 b. Comparison of Flakiness index for products
from electrohydraulic comminution and jaw
crusher respectively

OLIVINE BASALT

FLINT

(Dumbuck Hill Quarry)

Size range	Flakiness index	
	E.H.C.	JAW
3/4"-1/2"	0.0	40.0
1/2"-3/8"	0.0	51.0
3/8"-1/4"	7.0	46.1
Mean	2.3	46.4

Size range	Flakiness index	
	E.H.C.	JAW
3/4"-1/2"	5.0	98.5
1/2"-3/8"	2.5	25.9
3/8"-1/4"	0.0	19.3
Mean	2.5	47.9

LIMESTONE

QUARTZ-DIORITE-PORPYRITE

(Enderby Quarry)

Size range	Flakiness index	
	E.H.C.	JAW
3/4"-1/2"	1.4	95.5
1/2"-3/8"	3.8	19.6
3/8"-1/4"	3.0	40.8
Mean	2.7	51.6

Size range	Flakiness index	
	E.H.C	JAW
3/4"-1/2"	0.0	100.0
1/2"-3/8"	2.8	39.3
3/8"-1/4"	7.7	52.6
Mean	3.5	63.9

Table 9 a. Comparison of Elongation Index for products
from electrohydraulic comminution and jaw
crusher respectively

FELSITE   RED QUARTZITE

Size range	Elongation index	
	E. H. C.	JAW
3/4"-1/2"	0.0	18.8
1/2"-3/8"	6.0	40.1
3/8"-1/4"	8.5	42.6
Mean	4.8	33.8

Size range	Elongation index	
	E. H. C.	JAW
3/4"-1/2	8.6	41.2
1/2"-3/8"	0.0	30.9
3/8"-1/4"	16.4	40.6
Mean	8.3	37.6

ALBITIZED OLIVINE DOLERITE   PYROXENE ANDESITE

(Criggion Quarry)   (Moon's Hill Quarry)

Size range	Elongation index	
	E. H. C.	JAW
3/4"-1/2"	0.0	16.6
1/2"-3/8"	16.8	24.8
3/8"-1/4"	12.3	37.6
Mean	9.7	26.3

Size range	Elongation index	
	E. H. C.	JAW
3/4"-1/2"	18.9	25.0
1/2"-3/8"	0.0	37.8
3/8"-1/2"	3.2	50.0
Mean	7.4	37.6

Table 9 **b.** Comparison of Elongation Index for products
from electrohydraulic comminution and jaw
crusher respectively

OLIVINE BASALT   FLINT

(Dumbuck Hill Quarry)

Size range	Elongation index	
	E.H.C.	JAW
3/4"-1/2"	9.4	57.8
1/2"-3/8"	13.0	36.6
3/8"-1/4"	12.0	38.9
Mean	11.4	44.4

Size range	Elongation index	
	E.H.C.	JAW
3/4"-1/2"	1.5	2.0
1/2"-3/8"	5.0	32.1
3/8"-1/2"	14.3	31.6
Mean	7.0	21.9

LIMESTONE   QUARTZ-DIORITE-PORYRITE

(Enderby Quarry)

Size range	Elongation index	
	E.H.C.	JAW
3/4"-1/2"	11.8	14.6
1/2"-3/8"	0.0	38.2
3/8"-1/4"	18.5	33.7
Mean	10.1	28.8

Size range	Elongation index	
	E.H.C.	JAW
3/4"-1/2"	6.5	27.3
1/2"-3/8"	10.7	25.7
3/8"-1/4"	19.7	39.7
Mean	12.3	20.9

Table 10 Flakiness and Elongation index of Linestone
(45)
With various crushers

Type of crusher	Flakiness index %		Elongation index %	
	3/4"–1/2"	1/2"–3/8"	3/4"–1/2"	1/2"–3/8"
Jaw crusher	26	31	33	30
Cone crusher	32	36	44	39
Rolls	23	32	47	41
Fixed hammer unstricted outlet	17	16	22	19
Swing hammer unstricted outlet	15	19	23	24
Swing hammer with grid in outlet	22	22	27	24
Electrohydraulic comminution	2	4	12	0
Hand breaking	25	26		

The percentage of voids in various size fragments of pproducts was determined in as constant as possible test conditions. The results are shown in Fig.31 .Although the averaging curves are represented with straight lines in log-linear plot, the trend is clear. With decreasing size the percentage of voids increases, while the electrohydraulic comminution product has always a lower percentage of voids than either the jaw or impact crusher product.

The percentage of voids of other rock samples were not determined, since the amount of samples were found unsatisfactory due to side effects$^{(46)}$,i.e. the volume of the container must be large enough in order to ignore the discontinuous contact with the sides of container by the particles, this effect being proportional to the particle size.

2.5 SIZE DISTRIBUTION OF THE PRODUCTS

Size distribution curves of various electrohydraulic comminution products are compared with those of a laboratory jaw crusher, which gives one of the sharpest size distribution curves among conventional crushers, due to unrestricted outlet.The results are shown in log-log plots in Figs. 32 to 46 .

It is clear from these figures that the size distributiom
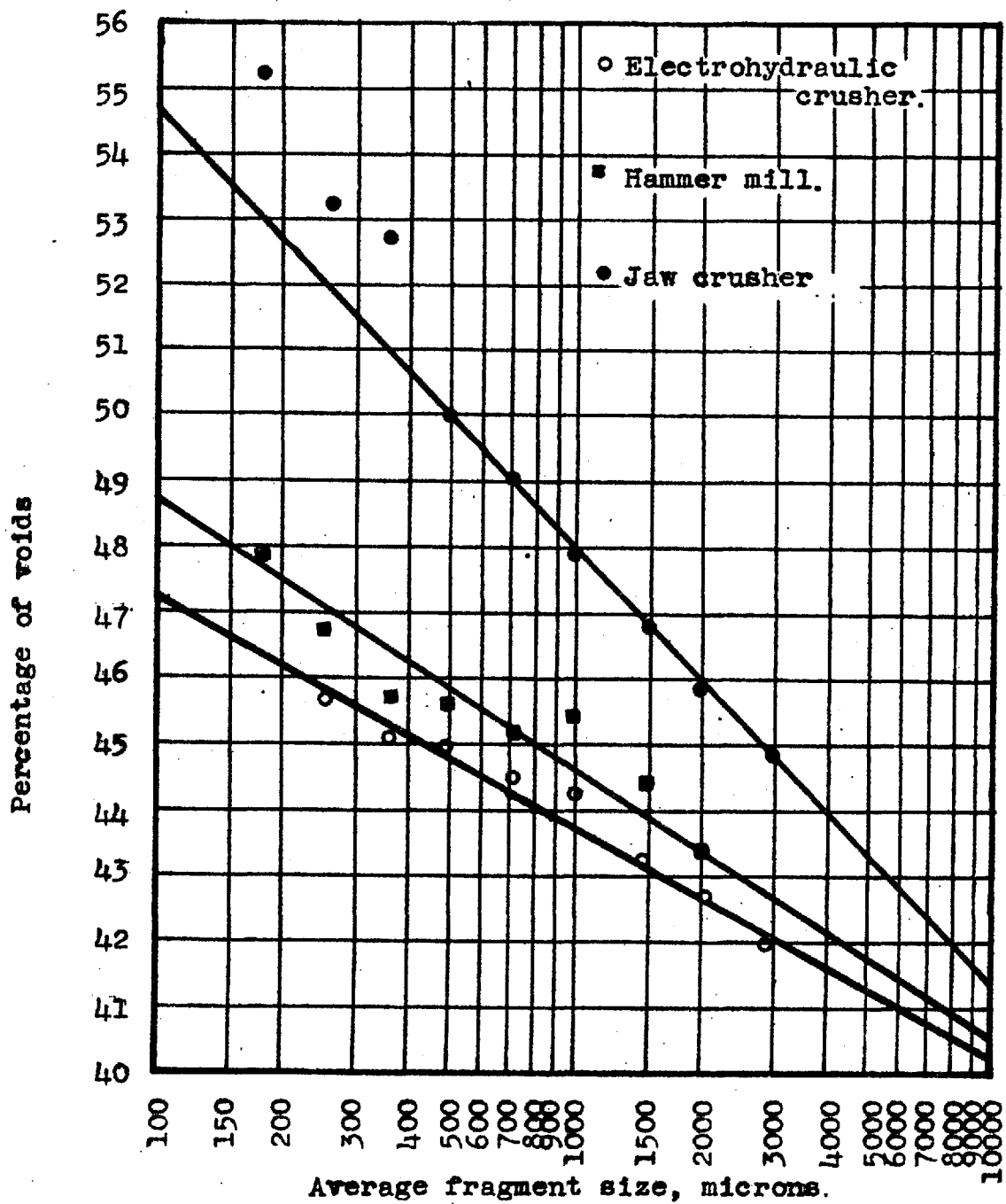
Fig. 31 The comparative percentage of voids of Quartz with various sizes.

Fig. 32 The comparative size distribution curves of Molochite.

Feed size 1/2"-1"

Fig. 33   The comparative size distribution curves
of Flint. Feed size 1"-2"

Fig.34   The comparative size distribution curves

of Quartzite(fine grained). Feed size 1"-2"

Fig. 35   The comparative size distribution curves

of Quartz-Diorite-Porphyrite(Enderby Quarry).

Feed size 1"-2"
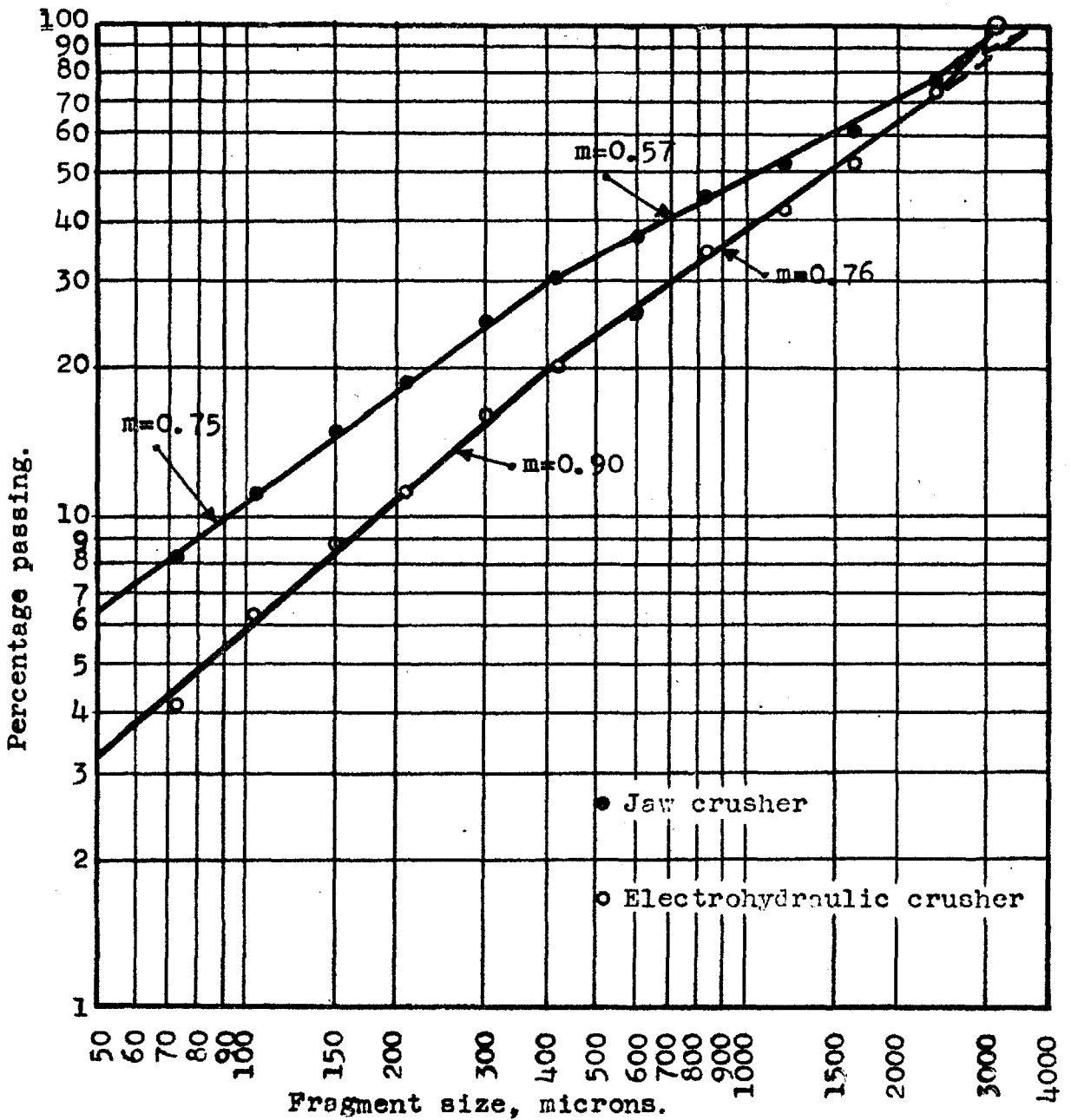
Fig. 36   The comparative size distribution curves

of Albitized Olivine-Dolerite(Criggion

Quarry) Feed size 1"-2"

Fig. 37   The comparative size distribution curves
           of Red Quartzite(coarse grained)
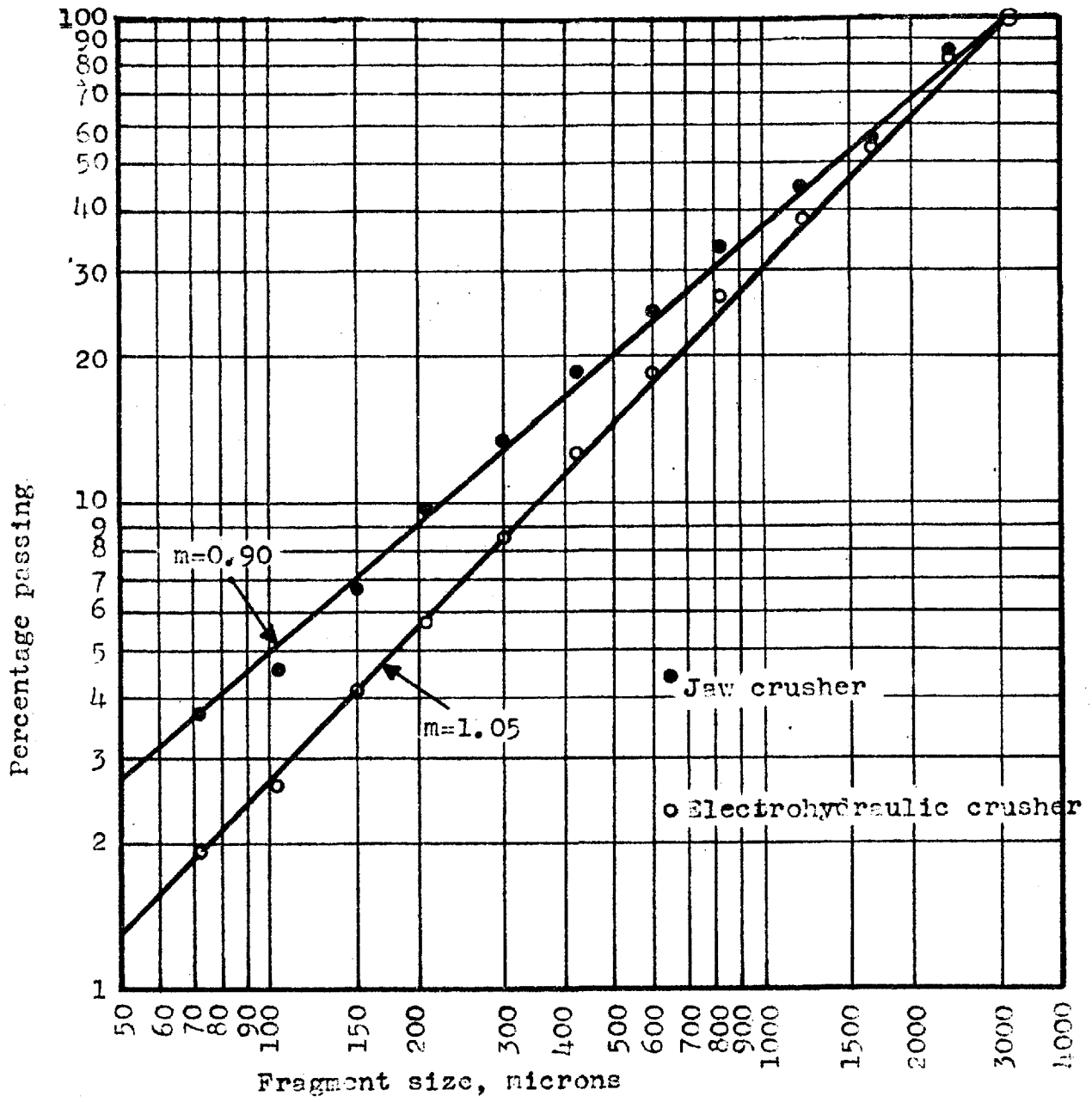   Feed size 1"-2"

Fig. 38   The comparative size distribution curves
           of Felsite. Feed size   1"-2".

Fig. 39   The comparative size distribution curves

of weathered Cornwall Granite. Feed size 1"-2".
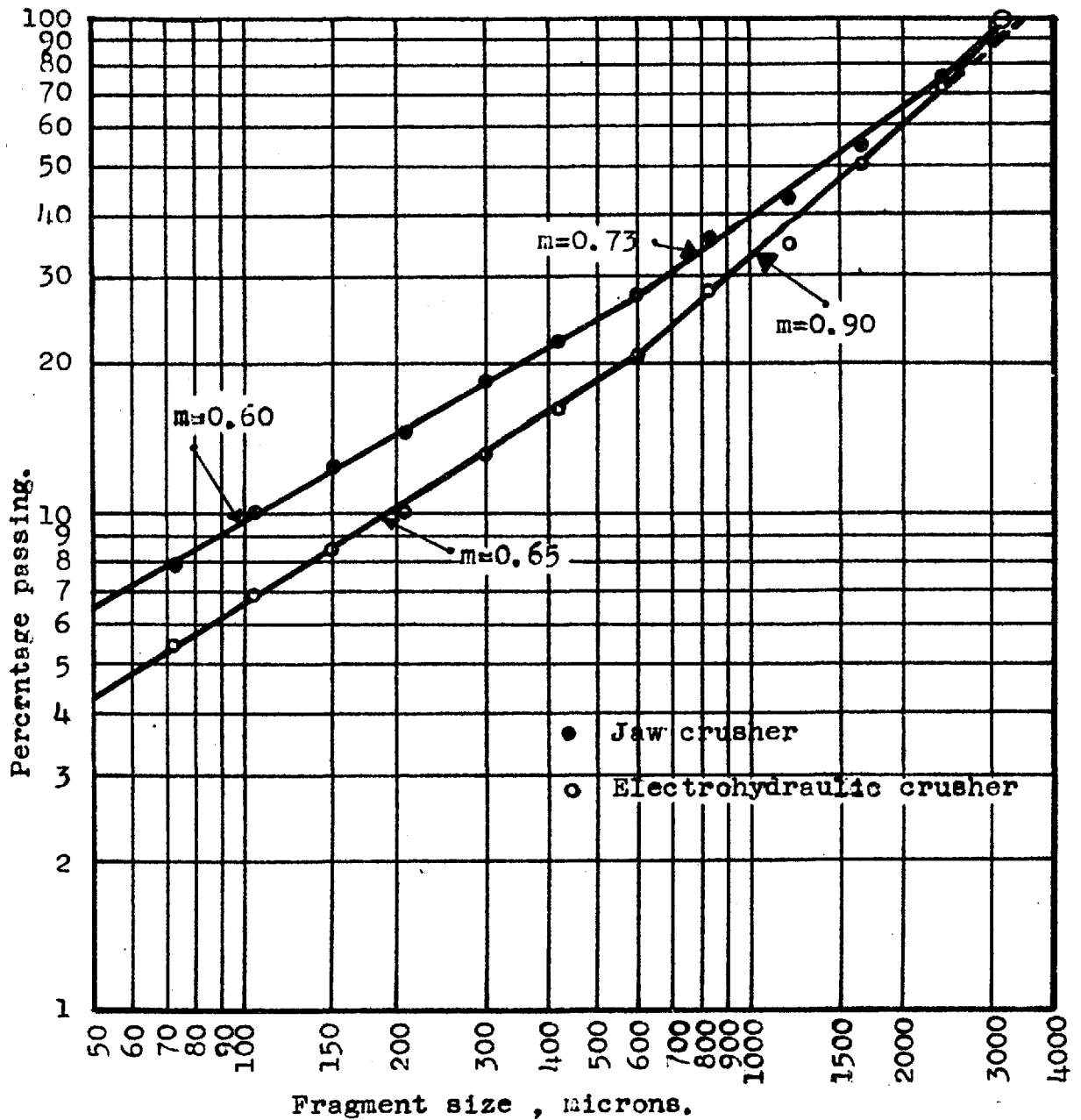
Fig. 40   The comparative size distribution curves

of Olivine Basalt. (Dumbuck Hill Quarry)

Feed size 1"-2"
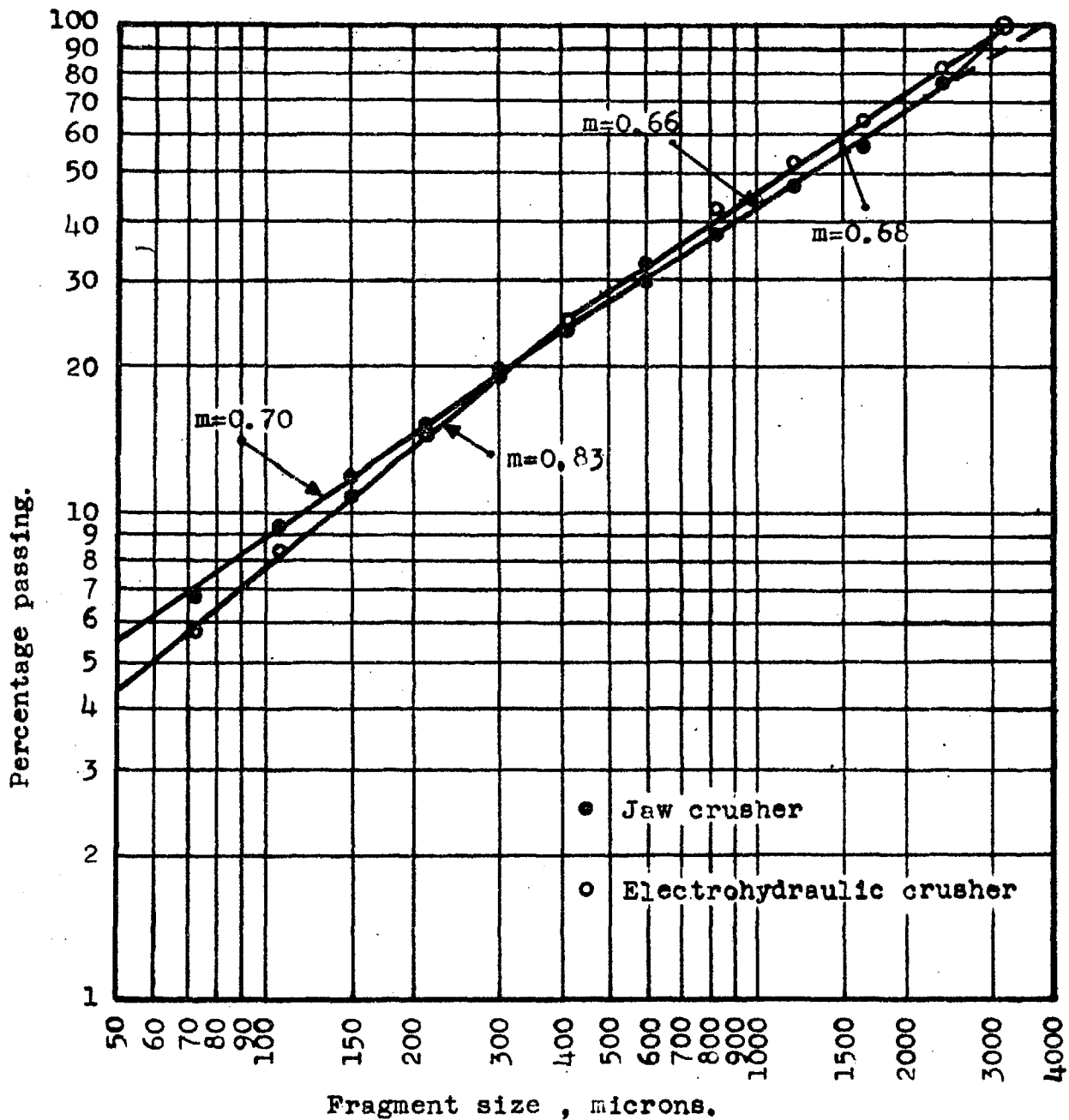
Fig. 42 The comparative size distribution curves

of Cassiterite ore (Gangue=Quartz+Calsite)
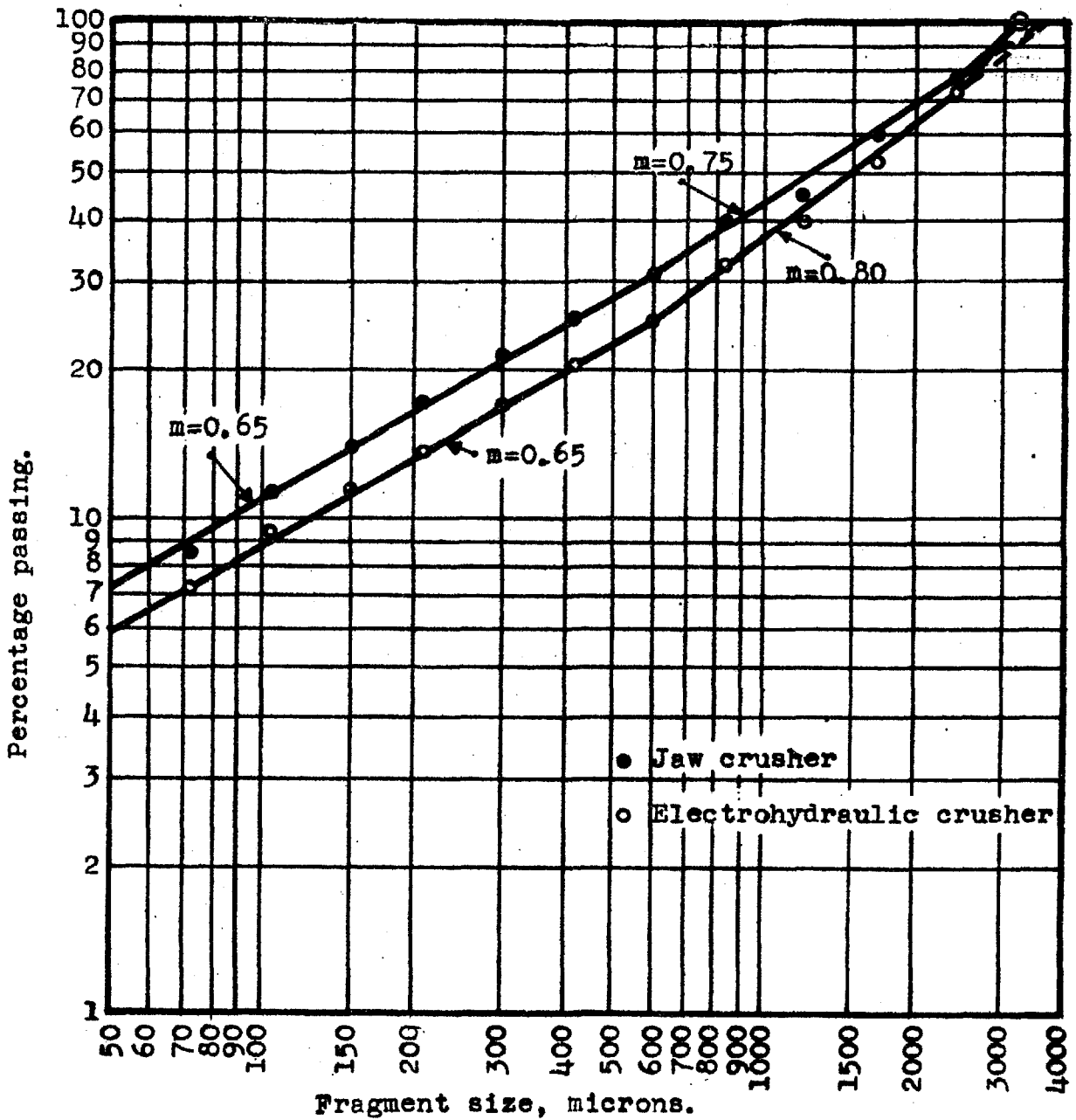
Feed size 1"-2".

Fig.43   The comparative size distribution curves
         of Pyroxene Andesite.(Moon's Hill Quarry)
         Feed size 1"-2"
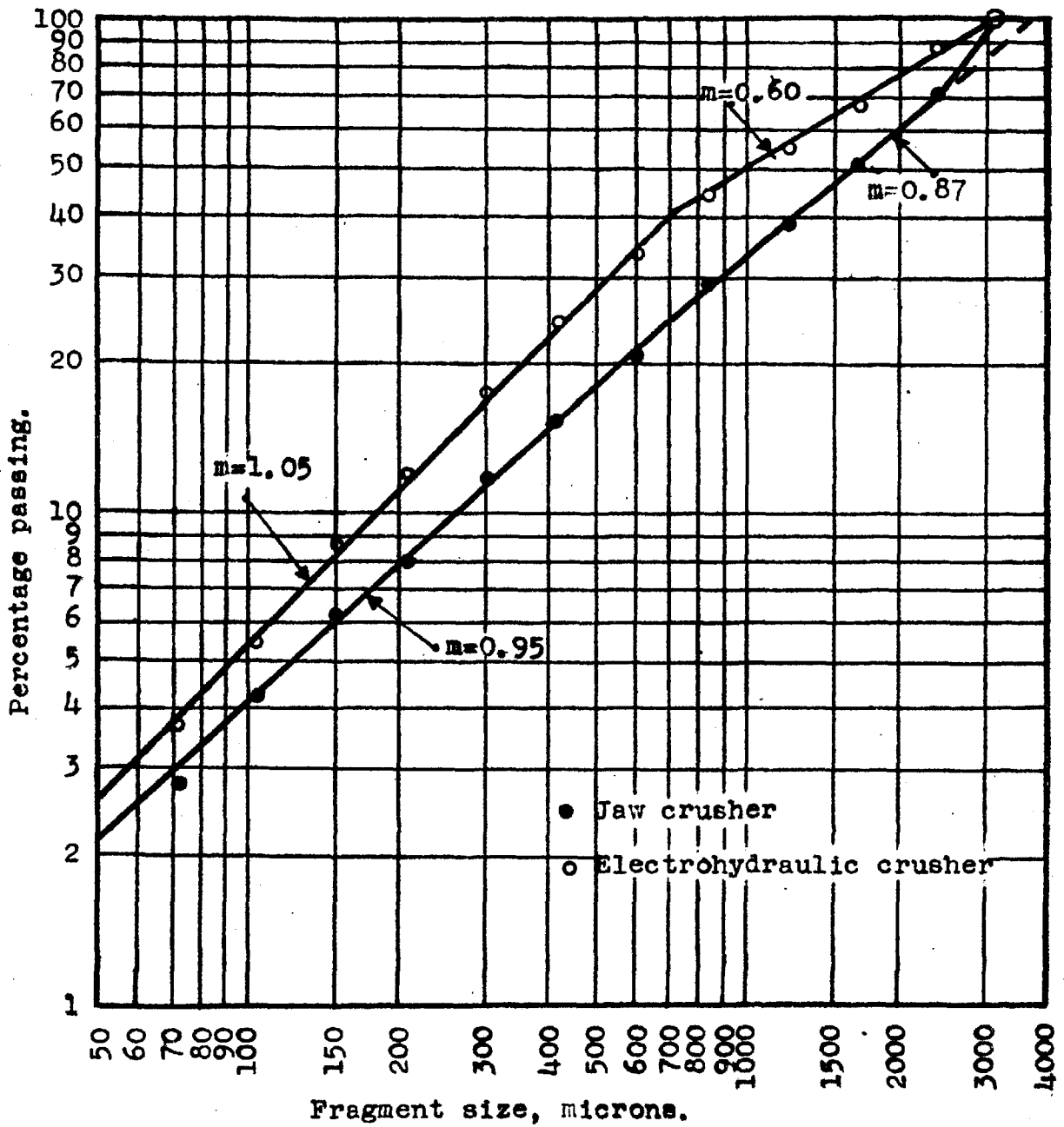
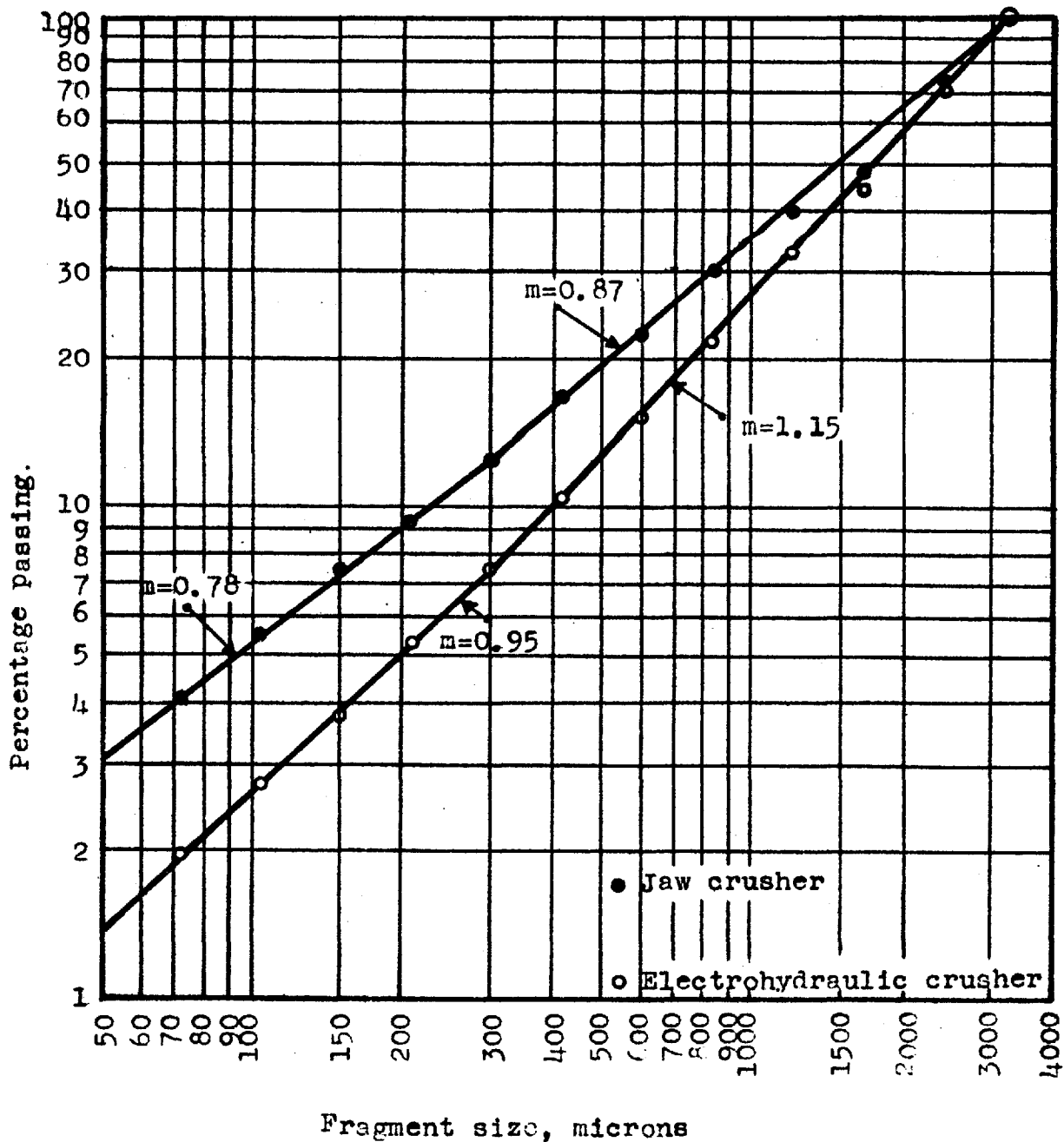Fig. 44. The comparative size distribution curves
of Quartz. Feed size 7/16"-1/4".
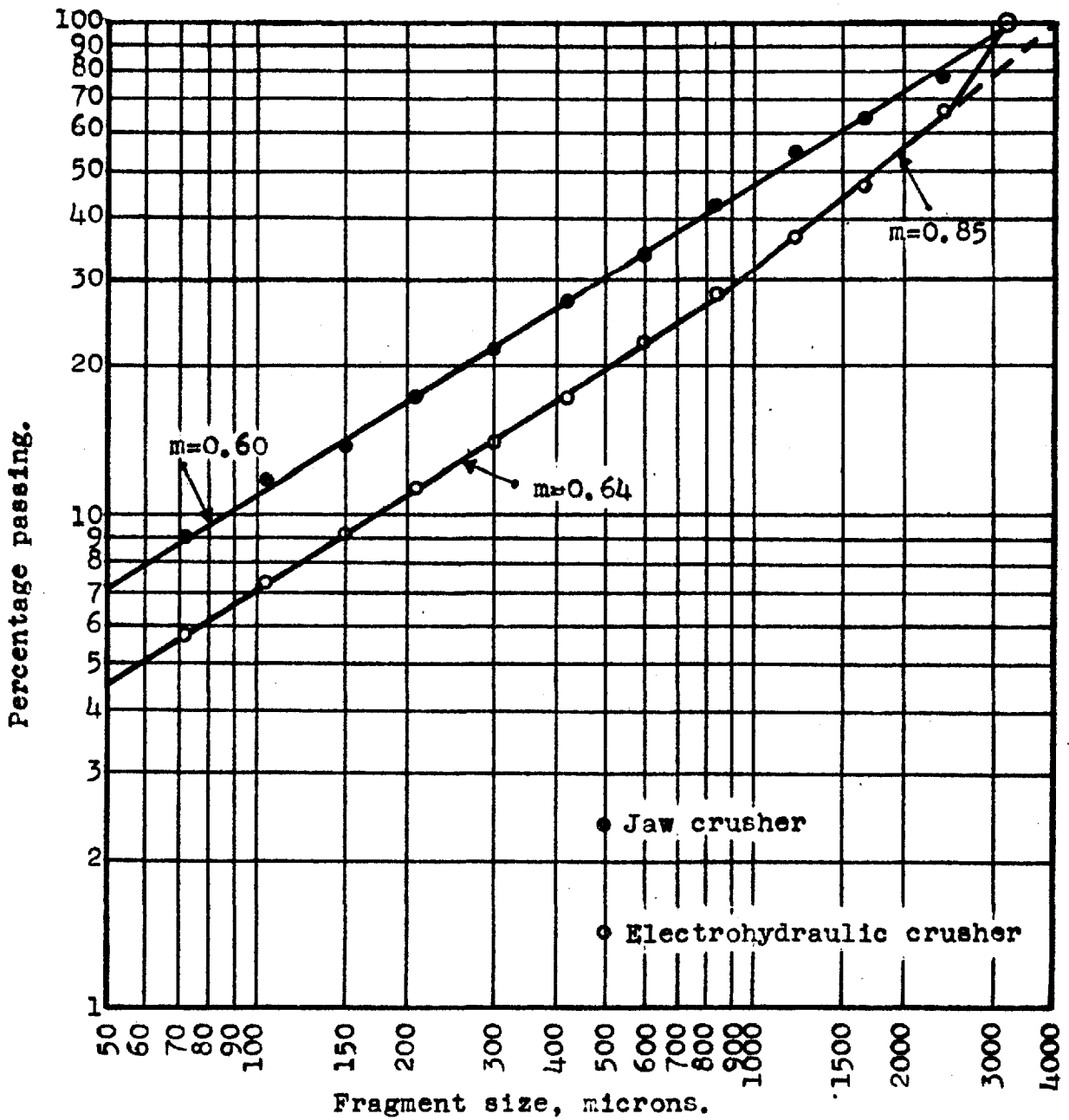
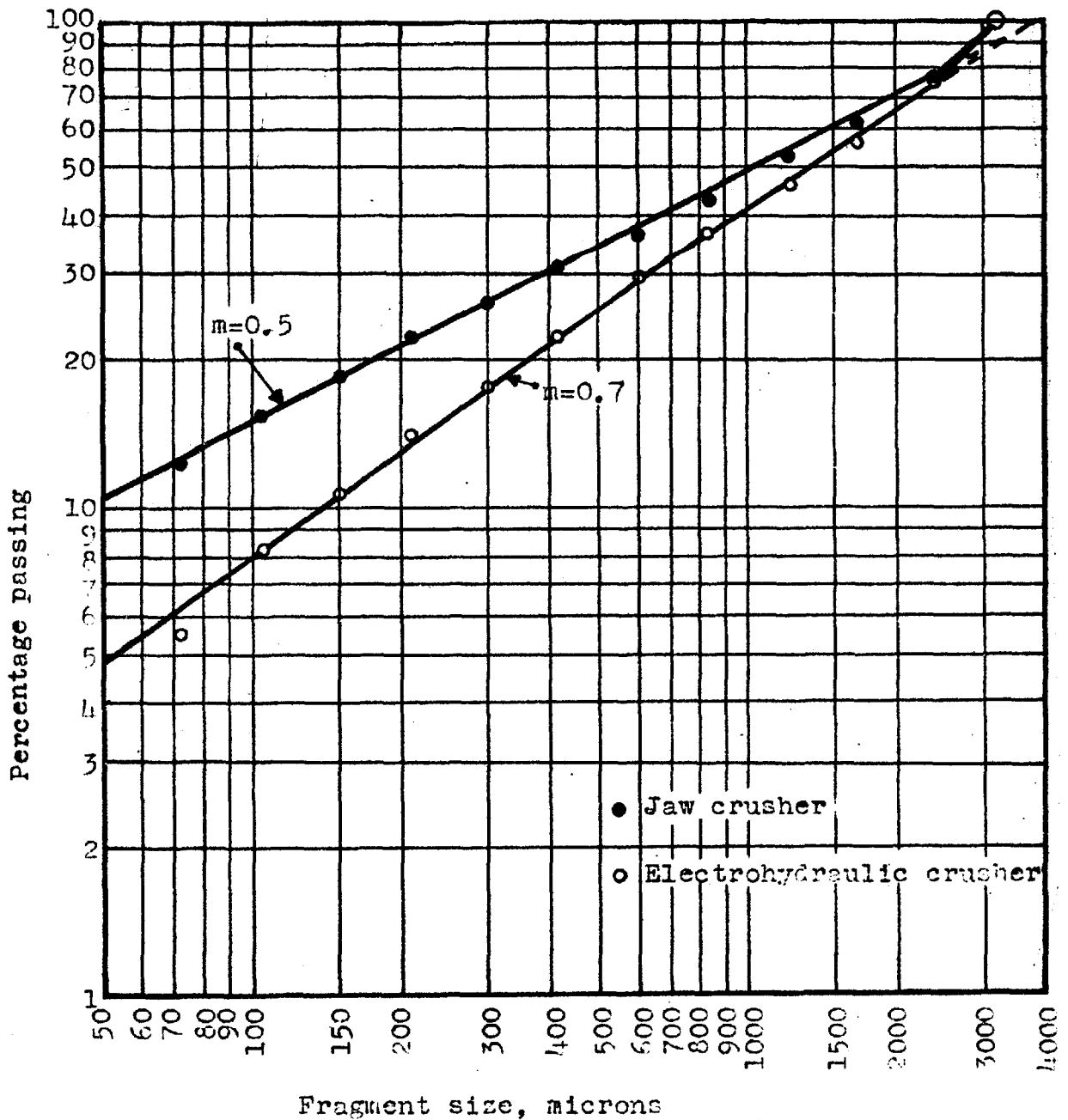Fig.45   The comparative size distribution curves

of Shale. Feed size 1"-2".

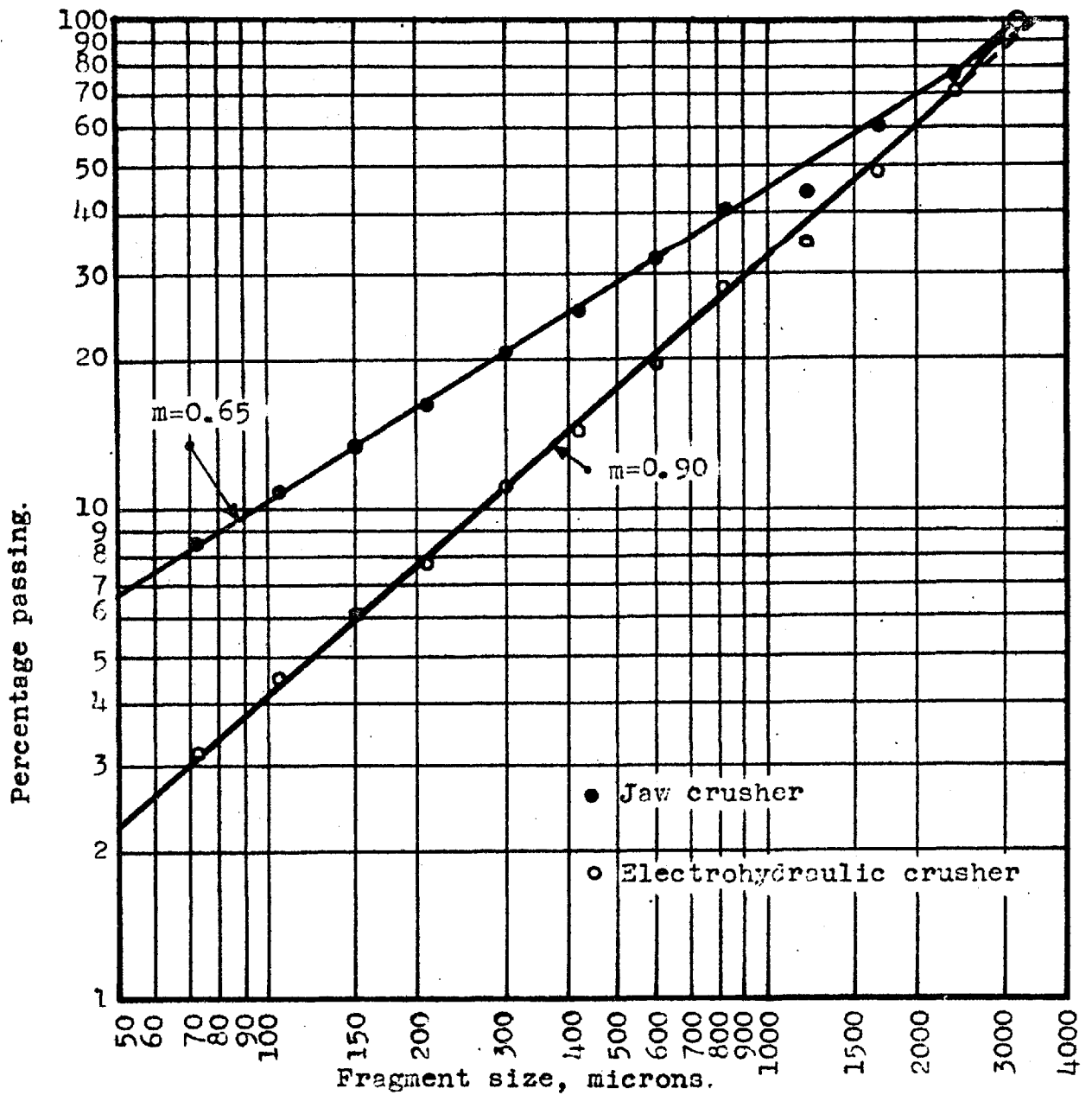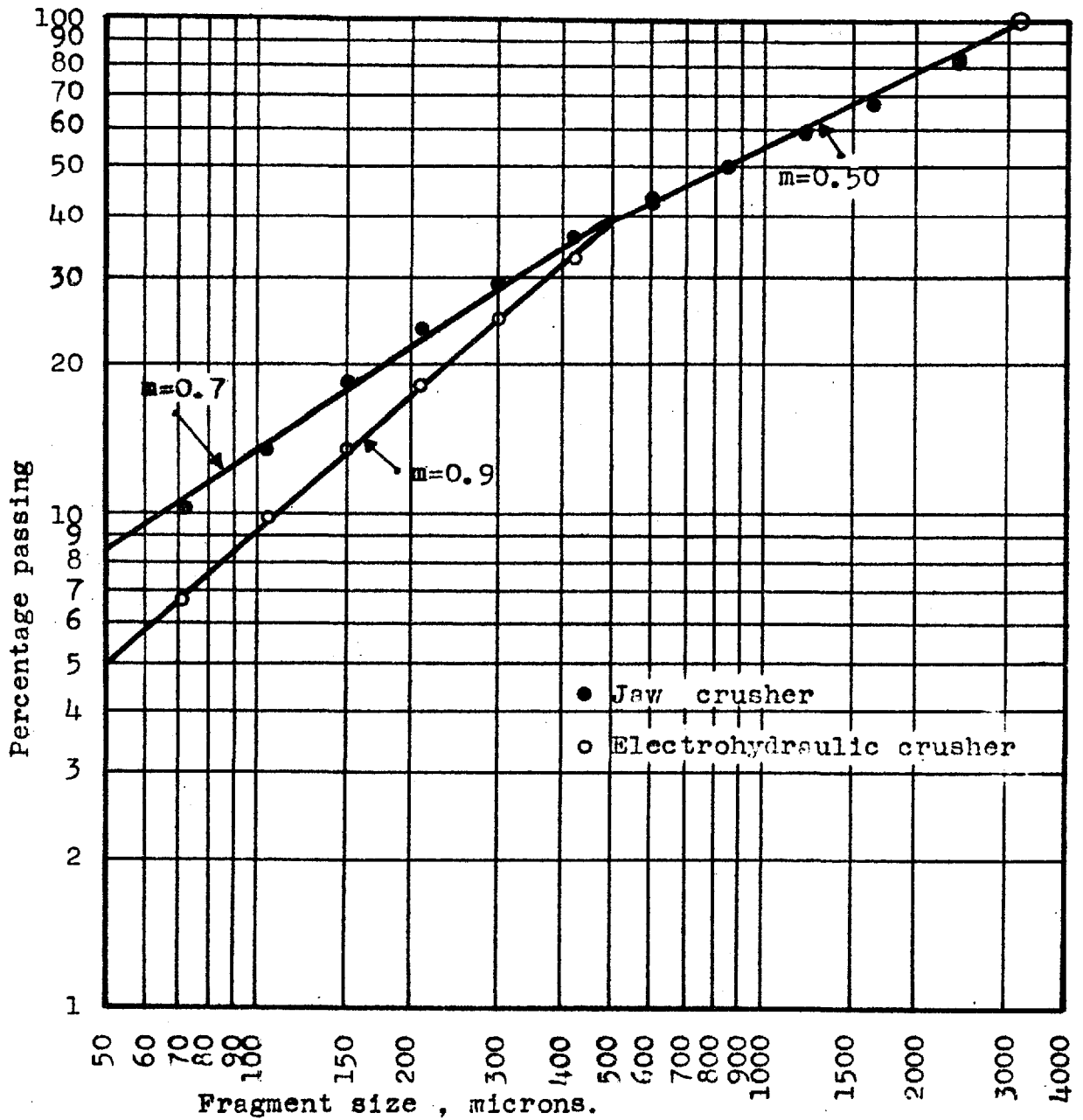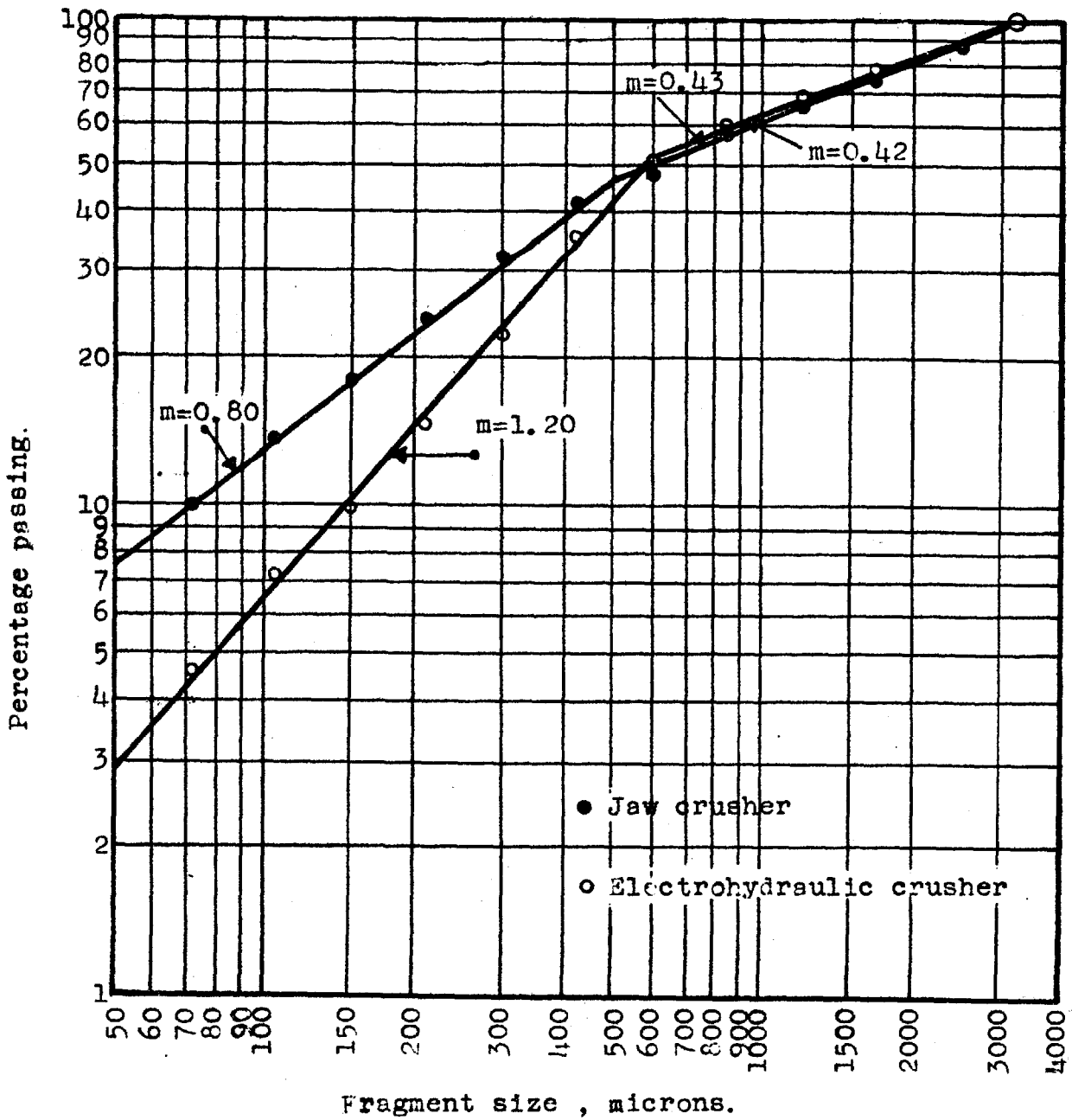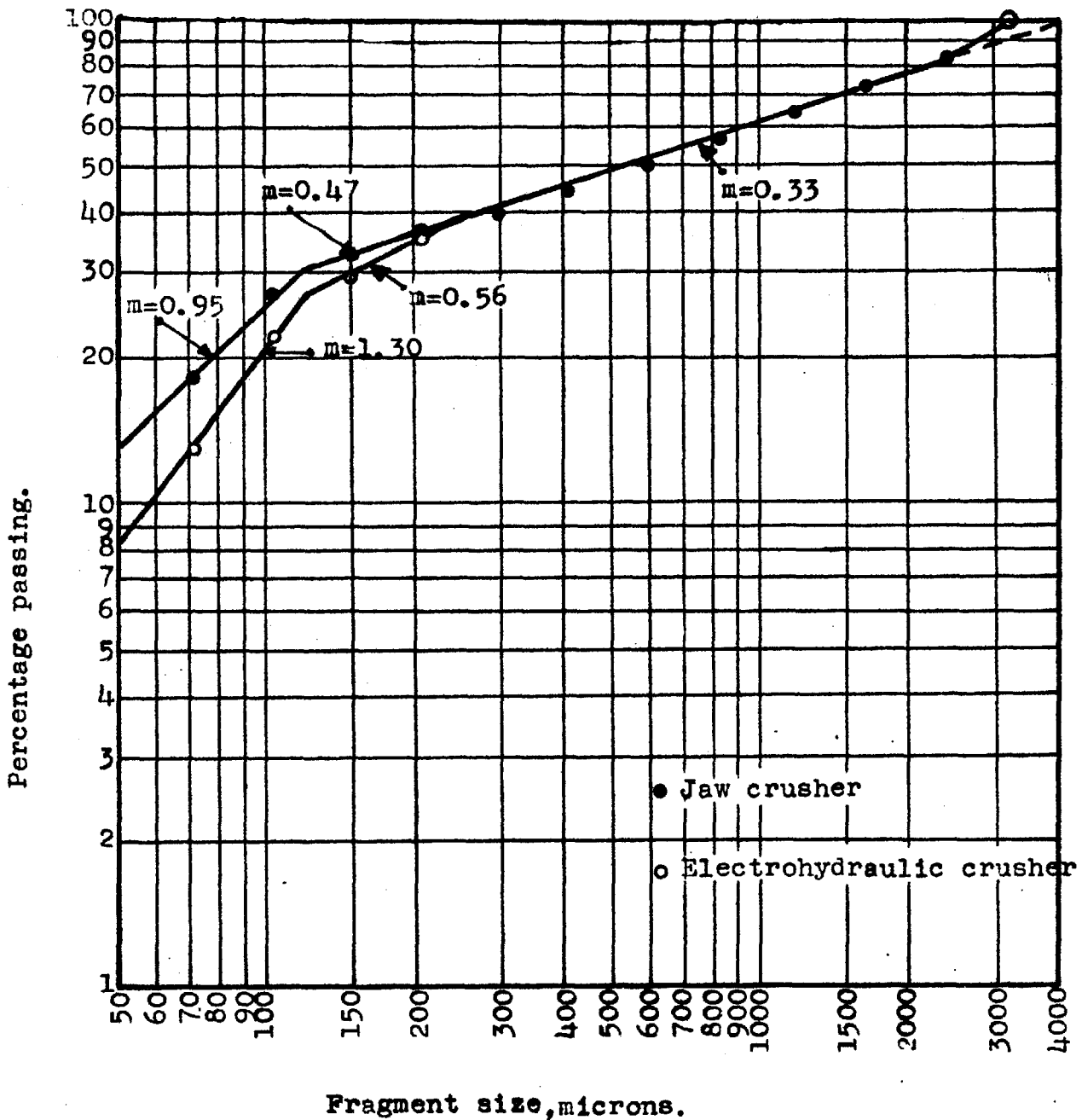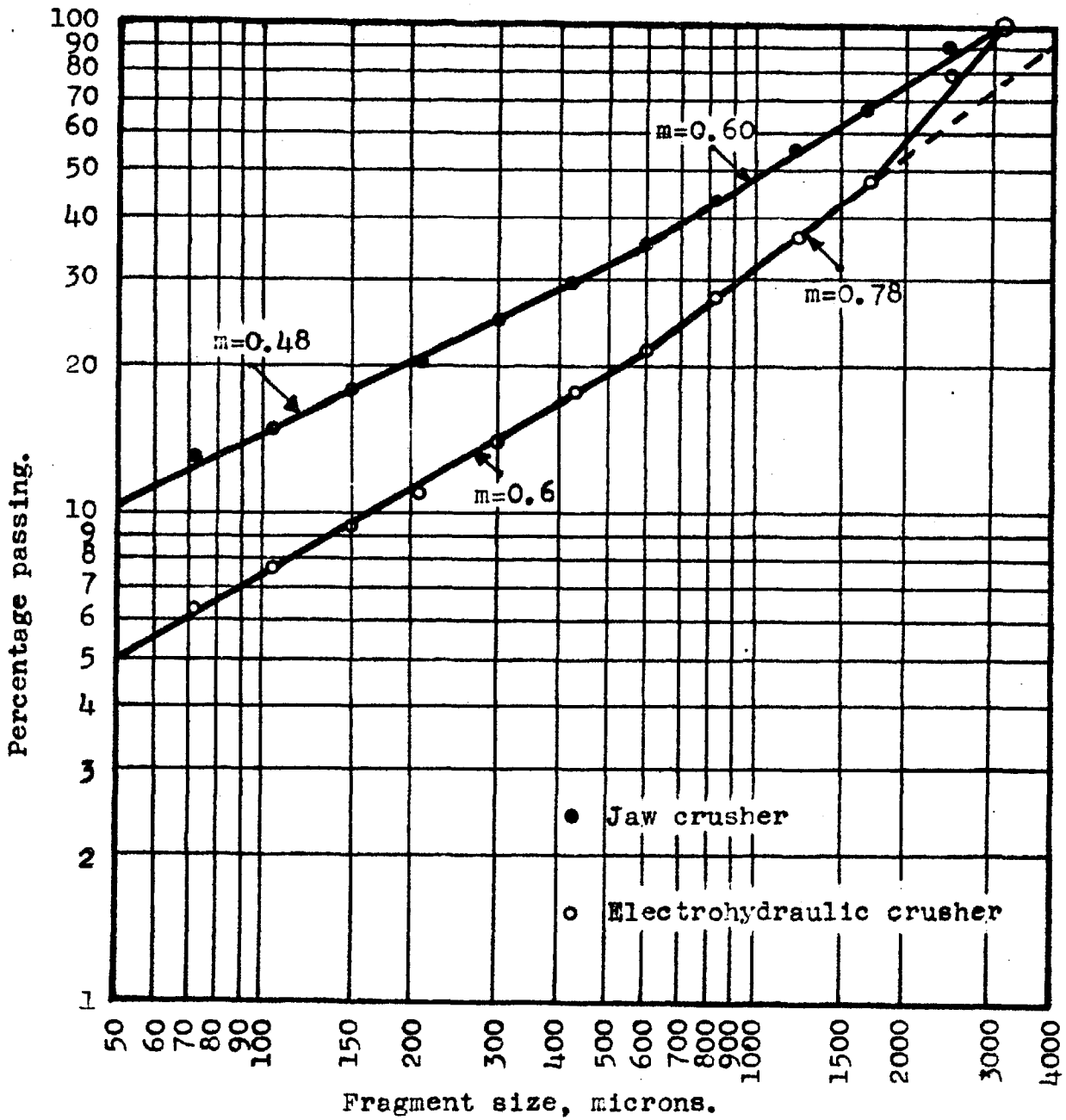Fig.46 The comparative size distribution curves of Limestone
Feed size 1/2"-1"

curves of electrohydraulic comminution products are always
steeper in the finer size ranges, than those of jaw crusher
products, i.e. less fine production compared to that of jaw
crusher. The size distribution curves of both products of
jaw and electrohydraulic comminution are not completely in
agreement with the Gaudin-Schumann distribution "law", but
it is interesting that they consist of straight line
segments. In most cases, they can be considered over a wide
range of particle sizes as a straight line which is in
aggreement with Gaudin-Schumann law. These results indicate
that size distribution function of a breakage is not a
simple function, on the contrary it is a complex function,
which presumably consists of breakage and selection functions,
and is highly dependant on the nature of the rock and type
of crushing method.

2.5.1   THE EFFECT CF VARYING FEED SIZE

The comparative size distribution curves of limestone
in electrohydraulic comminution and in jaw crushing , with
starting feed sizes of 1/2"-1" , 1/4"-1/2" and 1/8"-1/4"
are shown in Figs. 47 and 48 respectively. The comparative
size distribution curves of Flint in electrohydraulic
comminution and in jaw crushing with a feed size range of
1"-2" to 1/4"-1/8" are shown in Fig. 49 .
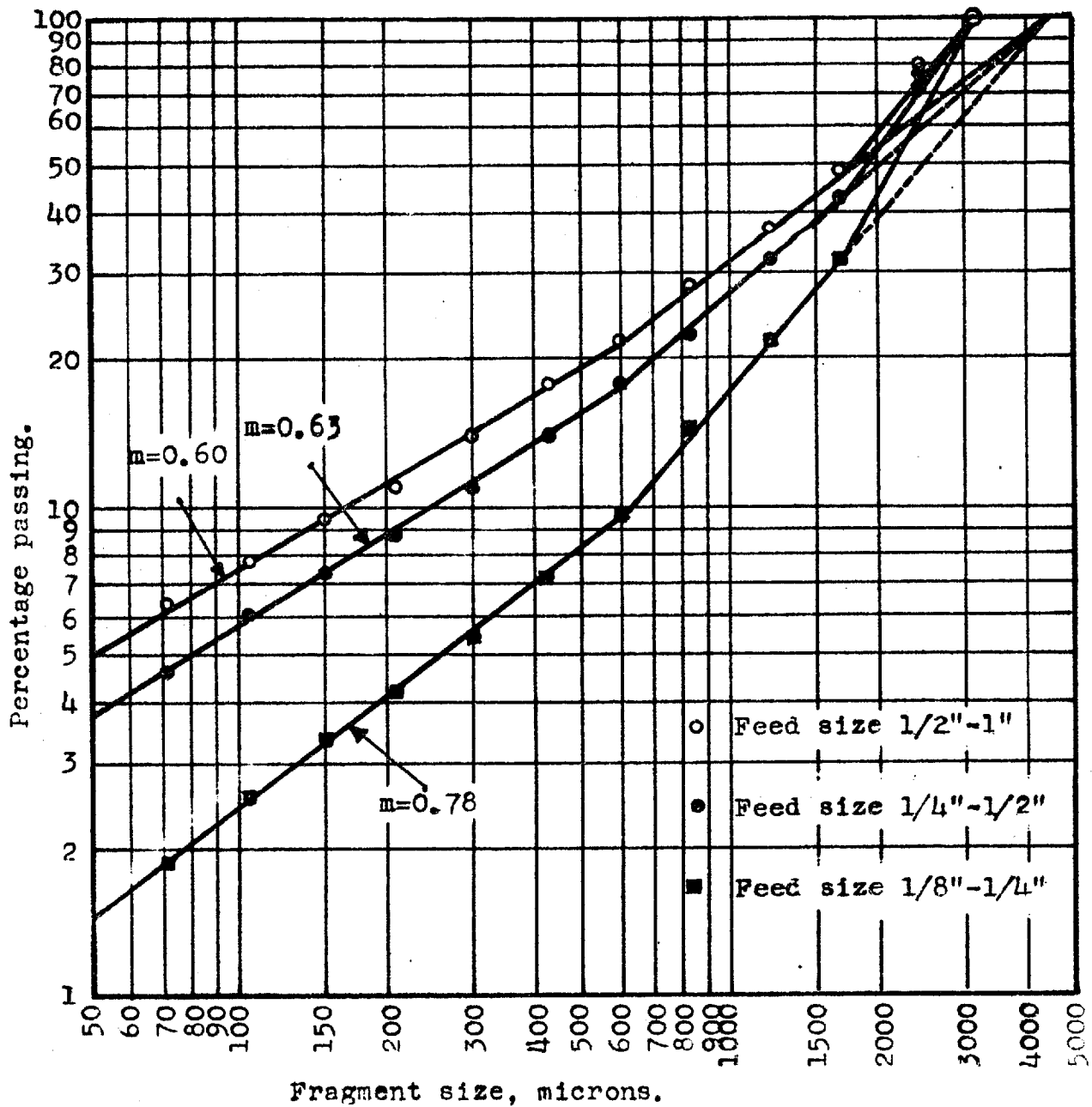
Fig. 47 The comparative size distribution curves of Limestone in
Electrohydraulic crushing, with varying feed size.
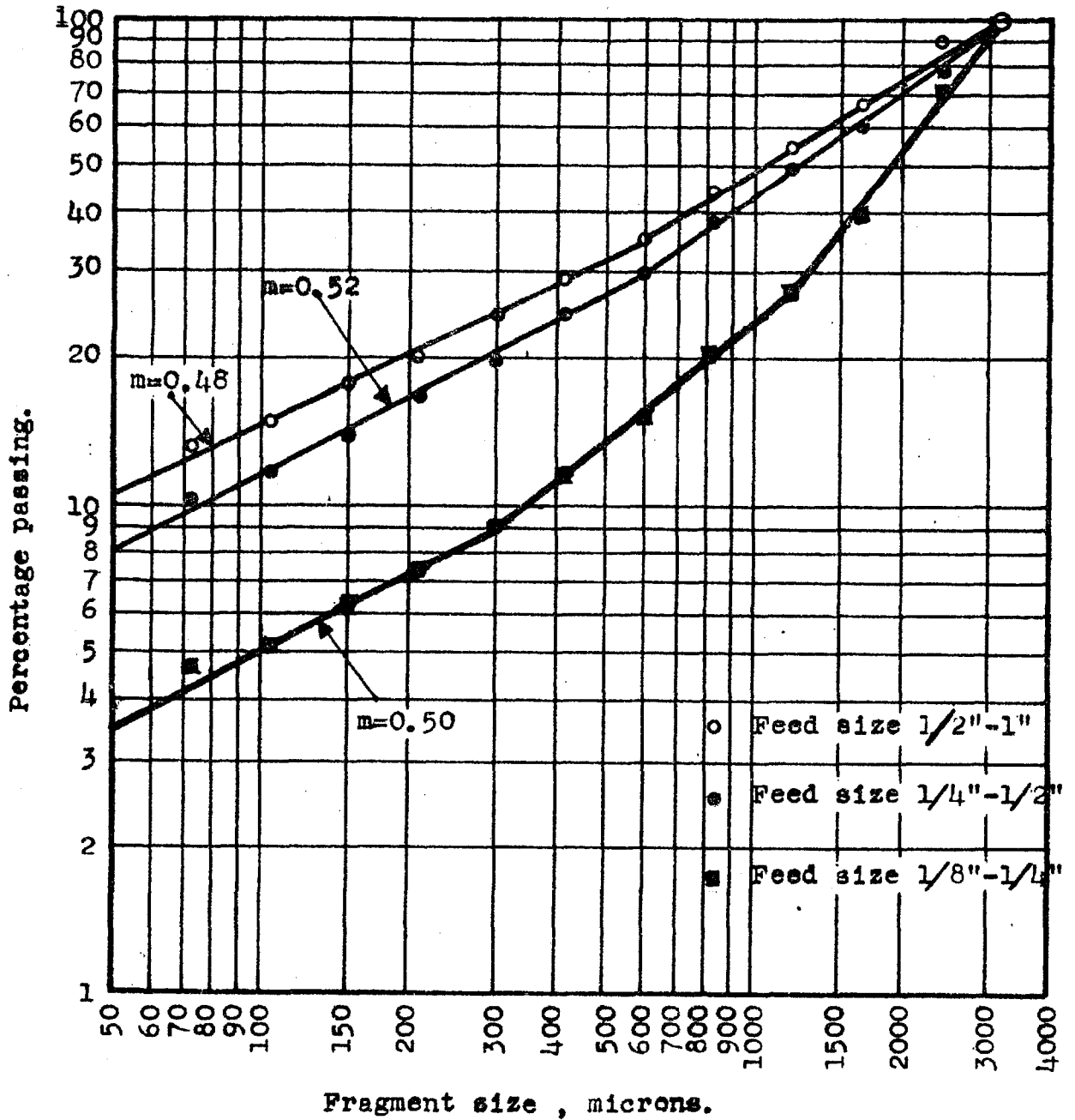
Fig. 48   The comparative size distribution curves of Limestone in
Jaw crusher, with varying feed size.
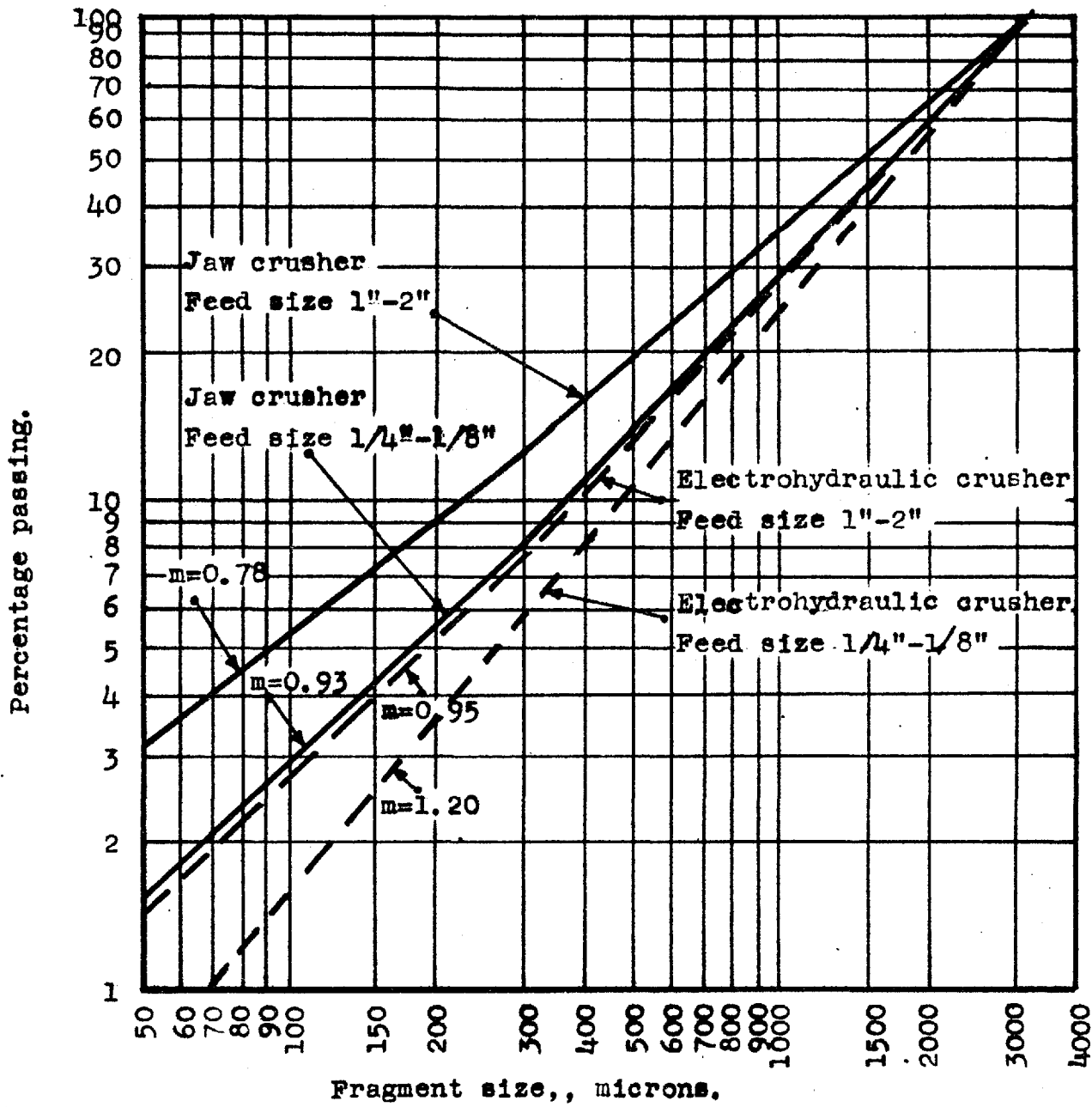
Fig.49   The comparative range of size distribution curves
of Flint. Feed size range 1"-2" to 1/4"-1/8".

The experimental results show that the size distri-
bution curves,i.e. slope of the curves , are very much
dependant on the starting feed size.The trend is clear from
the above figures, that the slope of the distribution
curves decreases with increasing feed size.For this reason,
in the comparative experiments the results of which are
given in Figs.32 to 46 , every precaution was taken to
keep feed size constant in both electrohydraulic comminu-
tion and in jaw crushing.

2.5.2   THE EFFECT OF THE NATURE OF ROCKS

In the size distribution curves , the effect of the
nature of the rocks is observed and pointed out by various
researchers [33]   in comminution operations.Comparative size
distribution curves shown in Figs.32 to 46 are very much
dependant on the rock nature.Inflexion points are the same
with very few exceptions for both electrohydraulic and jaw
crushing for certain type of rock.Although, few experiments
were done on this aspect, it seems that inflexion points
are constant for a given rock type.For example, size distri-
butions of grey flint pebbles show inflexion points at 300
microns for both electrohydraulic and jaw crushing (Figs.33
and 49).Another type of flint, "Flintag" from the Cement
Marketing Company was crushed.The size distribution of the

products have shown the same inflexion points at 300 microns for both electrohydraulic and jaw crushing, and the slope of the curves were of the same order as the grey Headley Heath flint products , considering starting feed size.

Fine grained red quartzite particles from the same company were crushed electrohydraulically and in the jaw crusher. The size distribution curves of both crushing operations were straight lines, similar to the previous fine grained grey quartzite size distribution (Fig.34), with slopes of comparable magnitudes.

The slope of the curves and inflexion points are tabulated for various rocks in the Tables 11, 12 and 13, as straight line curves, curves of concave down inflexion points and curves of concave up inflexion points respectively.

Table 11 Size distribution curves of some rocks, which consist of one straight line over a wide range of product size

Description of rock	Slope of the curve		Feed size
	E. H. C.	JAW	
Molochite	1.05	0.90	1/2"-1"
Quartzite (Fine grained)	0.70	0.50	1" -2"
Quartz-Diorite-Porhyrite	0.90	0.65	1" -2"
Average (except molochite)	0.80	0.57	

The main charecteristics of the rocks which are listed
in   Table 11, are that they consist of fine granular
crystalline structures, except molochite (row porcelain),
which is not a natural rock. Average slope of the curves
for two natural rocks (except molochite) is 0.80 for elec-
hydraulic crushing and 0.57 for jaw crushing.

Table 12 a. Size distribution curves of some rocks which
        consist of two straight line segments with
        concave down inflexion points

Electrohydraulic Comminution

Description of rock	Slope of first straight line segment (coarse range)	Slope of second straight line segment (fine range)	Inflexion point, microns	Feed size
Flint	1.15	0.95	300	1"-2"
Olivine-Basalt	0.90	0.65	600	1"-2"
Proxene-Andesite	0.80	0.65	600	1"-2"
Shale	0.85	0.64	800	1"-2"
Limestone	0.78	0.60	600	1/2"-1"
Average (except flint)		0.63		

Table 12 b. Size distribution curves of some rocks which
consist of two straight line segments with
concave down inflexion points

Jaw crushing

Description of rock	Slope of first straight line segment (coarse range)	Slope of second straight line segment (fine range)	Inflexion point, microns	Feed size
Flint	0.87	0.78	300	1"-2"
Olivine-Basalt	0.73	0.60	600	1"-2"
Proxene-Andesite	0.75	0.65	600	1"-2"
Shale		0.60		1"-2"
Limestone	0.60	0.48	600	1/2"-1"
Average (except flint)		0.58		

The main characteristics of the rocks which are listed in

Table 12 a and b, are that they consist of very fine

crystalline structures such as olivine-basalt and proxene

andesite and/or tend to be cryptocrystalline such as:

flint, shale and limestone. Average slope of the curves at

fine size range (except flint), is 0.63 for electrohydraulic

crushing and 0.58 for jaw crushing.

Table 13·a. Size distribution curves of some rocks which

consist of two straight line segments with

concave up inflexion points

Electrohydraulic comminution

Description of rock	Slope of first straight line segment (coarse range)	Slope of second straight line segment (fine range)	Inflexion point microns	Feed size
Albitized Olivine- Dolerite	0.76	0.90	420	1"-2"
Red Quartzite (coarse grained)	0.50	0.90	500	1"-2"
Felsite	0.42	1.20	600	1"-2"
Weathered Cornwall Granite	0.33/0.56	1.30	125/250	1"-2"
Cassiterite ore	0.68	0.83	420	1"-2"
Quartz	0.60	1.05	700	7/16"-1/4"
Average		1.03		

Table 13 b. Size distribution curves of some rocks which
consist of two straight line segments with
concave up inflexion points

Jaw crushing

Description of rock	Slope of first straight line segment (coarse range)	Slope of second straight line segment (fine range)	Inflexion point microns	Feed size
Albitized Olivine- Dolerite	0.39	0.75	420	1"-2"
Red Quartzite (coarse grained)	0.50	0.70	500	1"-2"
Felsite	0.43	0.80	500	1"-2"
Weathered Cornwall Granite	0.33/0.47	0.95	125/250	1"-2"
Cassiterite ore	0.66	0.70	420	1"-2"
Quartz	0.87	0.95	700	7/16"-1/4"
Average		0.81		

The main characteristics of the rocks which are listed in Table 13 a and b, are, that they consist of a fairly coarse granular crystalline structure. The average slope of the curves at fine size range is 1.03 for electrohydraulic crushing and 0.81 for jaw crushing.

Briefly , it appears from the above tables that the slopes of size distribution curves increase with increasing grain size of rock for both electrohydraulic and jaw crushing, and that electrohydraulic comminution gives invariably steeper slopes, i.e. sharper cut-off in the finer size range.

2.5.3 THE ROLE OF FREE CRUSHING

It is fairly well known from experimental results , that free crushing or so called single crushing should result in sharper resultant size distributions, since frictional forces between rock particles, which would produce most fines, are minimised. This fact is also demonstrated in electrohydraulic crushing. The crushing chamber shown in Fig.24 produces less sharp size distributions than the electrohydraulic comminution device shown in Fig.25 , which is working under much more free crushing conditions. Furthermore, single crushing with only one pulse,

which is perfect free crushing, resulted in the sharpest
size distribution. The resultant size distribution curves
of quartz are shown in Fig.50 .

Further experiments were performed in the electrohyd-
raulic comminution device shown in Fig.25 with the elec-
trode arrangement shown in Fig.15 .The particles of flint
and limestone were placed around the spark path manually
and the feed particles were subjected to a single pulse.
As expected, the size distributionsof products are
sharper than those of operations with multiple sparks.
The resultant size distribution curve of flint is shown
in Fig.51 and that of limestone in Fig.52 . As is clear
from these figures , the size distribution curves are
not only sharper , but also some inflexion points disap-
pear. This indicates that the size distribution functions
in single crushing are less complex than those of multiple
crushing, since selection functions which would presumably
result in inflexion points, disappear.

2.6   SELECTIVE CRUSHING AND LIBERATION IN
ELECTROHYDRAULIC COMMINUTION:

2.6.1   SELECTIVE CRUSHING

As was hinted in Chapter 2.1, effective selective
crushing is very likely possible in electrohydraulic

100
90
80
70
60
50

40

30

m=0.90

20

m=0.80

m=1.05

Percentage passing.

10
9
8
7
6
5

m=1.24

4

● Electrohydraulic crusher shown in
Fig. 24. (8kV, 10μF). Underwater crushing.

3

▣ Electrohydraulic crusher shown in
Fig. 24(8kV, 10μF). Some of the feed
particles in contact with air.

2

● Electrohydraulic comminution device
shown in Fig. 25. (35kV, 0.1μF)

○ Single crushing. (Single spark of
20kV, 5μF capacitor discharge)

1

50 60 70 80 90 100   150   200   300   400 500 600 700 800 900 1000   1500   2000   3000 4000

Fragment size , microns.

Fig. 50   Comparative size distribution curves of Quartz in
Electrohydraulic comminution. Feed size 7/16"-1/4"
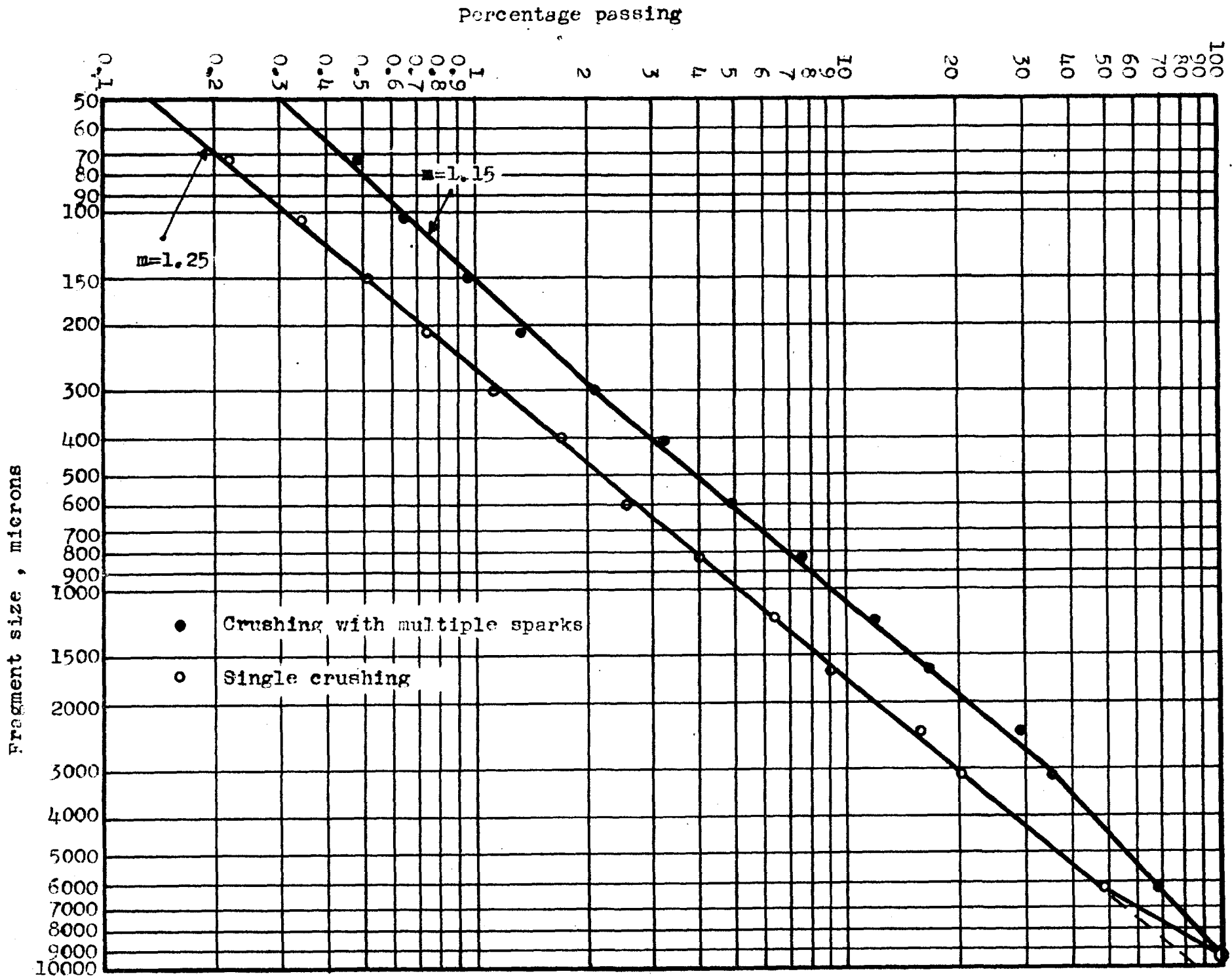
Fig. 51 The comparative size distribution curves of Flint   in single and multiple spark
electrohydraulic crushing. Feed size 1/2"-1"
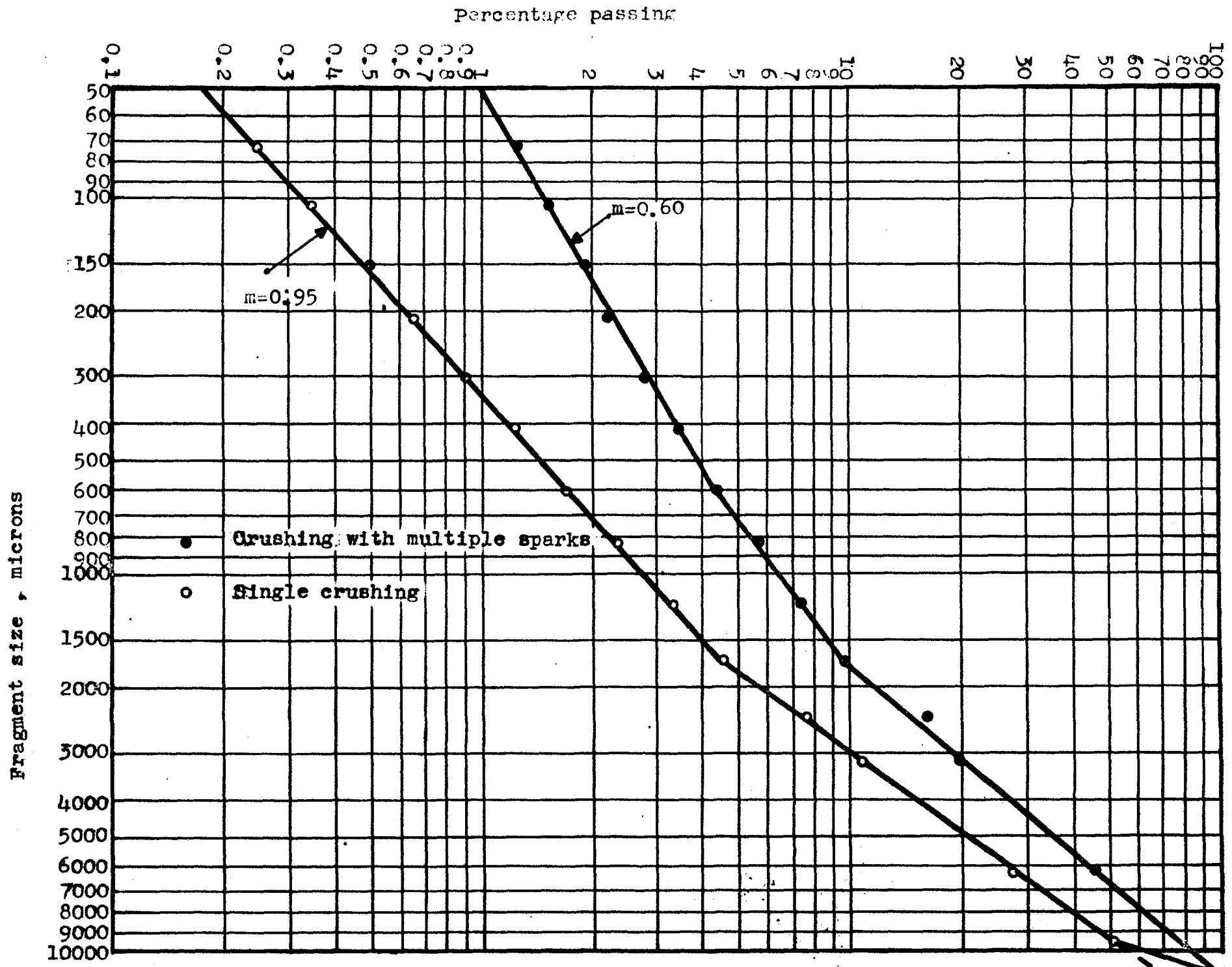
Fig. 52 The comparative size distribution curves of Limestone in single and multiple spark electrohydraulic crushing. Feed size 3/8"-1/2"

comminution by exploiting the differences between surface conductivities of two constituents. Especially in the coaxial annular electrodes arrangement shown in Fig.14 the selectivity should be very high, compared to the pointed electrodes system. In Fig. 53 a and b the selection areas of annular and pointed electrode systems are shown. The effective selection area in annular electrode system is :

$$A = \pi(R_1^2 - R_2^2) \text{ or}$$

substituting $R_1 = R_2 + 1$

$$A = \pi(2.R_2.1 + 1^2) \tag{15}$$

where 1 = gap length

R_1 = radius of outer ring electrode

R_2 = radius of inner circular electrode

The effective selection area in pointed electrode system is :

$$A = 2.\pi.1.R \tag{16}$$

where 1 = gap length

R = effective selectivity radius which would be a function of feed size and gap length 1

In the present electrohydraulic device(Fig.25), when 1 is 1 cm. , R_2 is 5.5 cm. then :

$$A = 12\pi$$

In the pointed electrode system , when 1 assumed to be 1 cm. and R very generously assumed 0.5 cm. , then :
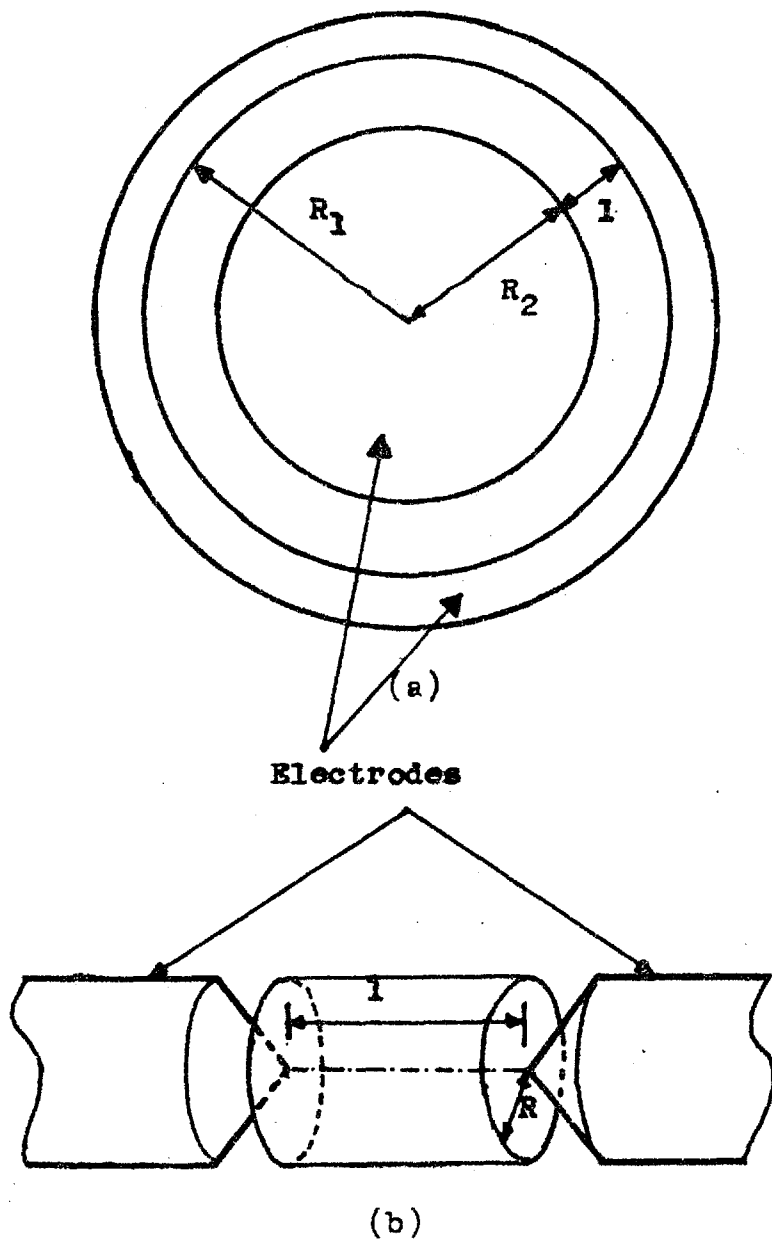
Fig. 53 Selection areas

    a. Annular electrode arrangement

    b. Pointed electrode arrangement

$A = \pi$

It seems, under the above conditions , that the annular electrode system should be about 10 times much more effective than the pointed electrodes.Furthermore, if the ability of the solid particles to provide shorter distance between two electrodes, is considered, the selectivity should be very high with annular arrangements.It is clear from Fig.14 that the sharp edges of both electrodes in the annular electrode arrangement are on the same plane as the resting surface of particles, so that one particle with a plane face can contact both electrodes with a straight line, while in pointed electrode system,diameters of electrodes, however small, would prevent a direct straight line contact of points of electrodes with a particle surfaee.

In order to investigate selectivity in electrohydraulic comminution some preliminary experiments were carried out with artificially prepared feeds of two constituents such as pyrrhotine (2 [FeS])-flint , flint pebbles-weathered granite , and limestone-felsite in the electrohydraulic comminution device shown in Fig.25 . The selective crushing was very effective in all experiments , depending on the order of assumed differences in surface conductivities and in the roughness   of surfaces of two constituents.The results are shown in Table 14 .

Table 14. Selective electrohydraulic comminution with
some artificially prepared feeds

0.1 μF , 35 kV disharge voltage ,
1 cm. underwater spark gap length,
demineralised water discharge medium,
about one pulse per two second repetition rate

Mixture (A) - (B)	Feed (1"-2") %(A)	Product (-1/4") %(A)	Probable cause of selectivity
Pyrrhotine-Flint	40	98.3	The difference between conductivities of two constituents is very great
Flint Weathered Pebbles-Granite	50	98.7	Flint pebbles were providing smooth surfaces, i.e. shortest distance between electrodes
Limestone-Felsite	50	72.0	Presumably different surface conductivities

The importance of selectivity in crushing operations is
great , since some preconcentration can be expected. It seems
from the above encouraging results that this feature alone
is of potential industrial importance to electrohydraulic

comminution, since:

(i.) High grade concentration operations are possible with relatively simple mechanical arrangements, during the electrohydraulic comminution process.

(ii.)The selective crushing should result in better libe-ration, since the shock wave source or shock wave front would be selectively positioned on a particle of two or more consti-tuents. Unfortunately no further experiments were made on this subject, due to lack of time.

2.6.2   LIBERATION IN ELECTROHYDRAULIC COMMINUTION

At the start of the studies, it was thought that electro-hydraulic comminution would produce better liberation than conventional methods , since the resultant tensile stresses would cause spallings, the main failures occurring at the interfaces where the bonds between mineral grains in the ore were weakest.However, more detailed analysis of the problem showed that this expectation was too sanguine.The interfaces between two mineral grains would be considered also to gene-rate reflected tensile stresses but, resultant tensile stress is developed at a certain distance to the interface, therefore it would not be effective across interface.

Geometrical analysis of the problem is given in Figs.54 to 57 .

Fig. 54 Four phases of transmission and reflection of a compressive stress wave at
an interface (Medium A/Medium B), where characteristic impedance ($\rho.c$) of
A is greater than that of B.
① Oncoming stress wave, ② Transmitted stress wave, ③ Reflected stress wave
④ Resultant stress.

Fig. 55 Four phases of transmission and reflection of a compressive stress wave at an interface (Medium A/Medium B), where characteristic impedance (ρ.c) of A is smaller than that of B.
① Oncoming stress wave, ② Transmitted stress wave, ③ Reflected stress wave
④ Resultant stress .
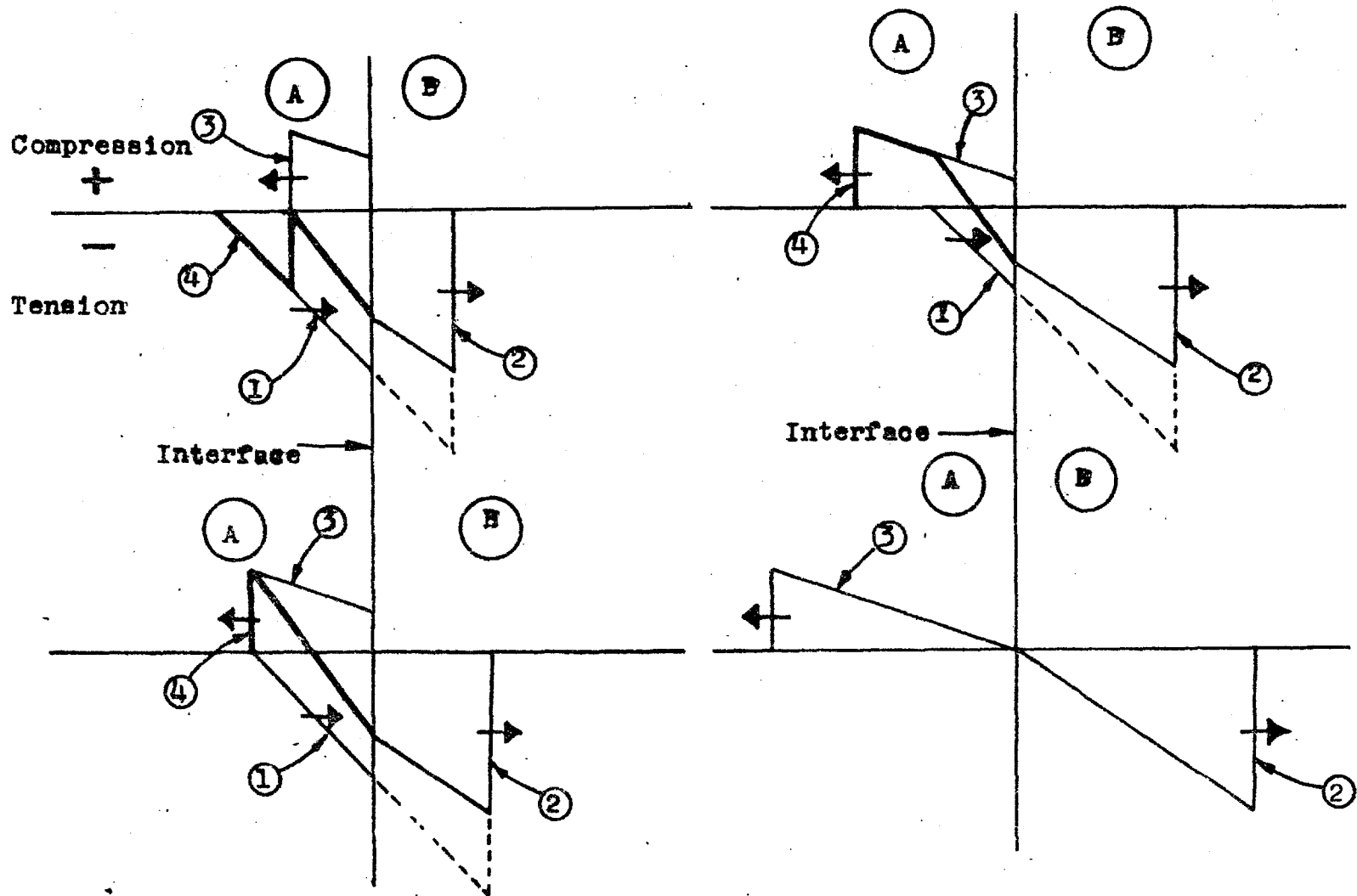
Fig. 56 Four phases of transmission and reflection of a tensile stress wave at an inter-
face (Medium A/Medium B) , where characteristic impedance (ρ.c) of A is greater
than that of B.

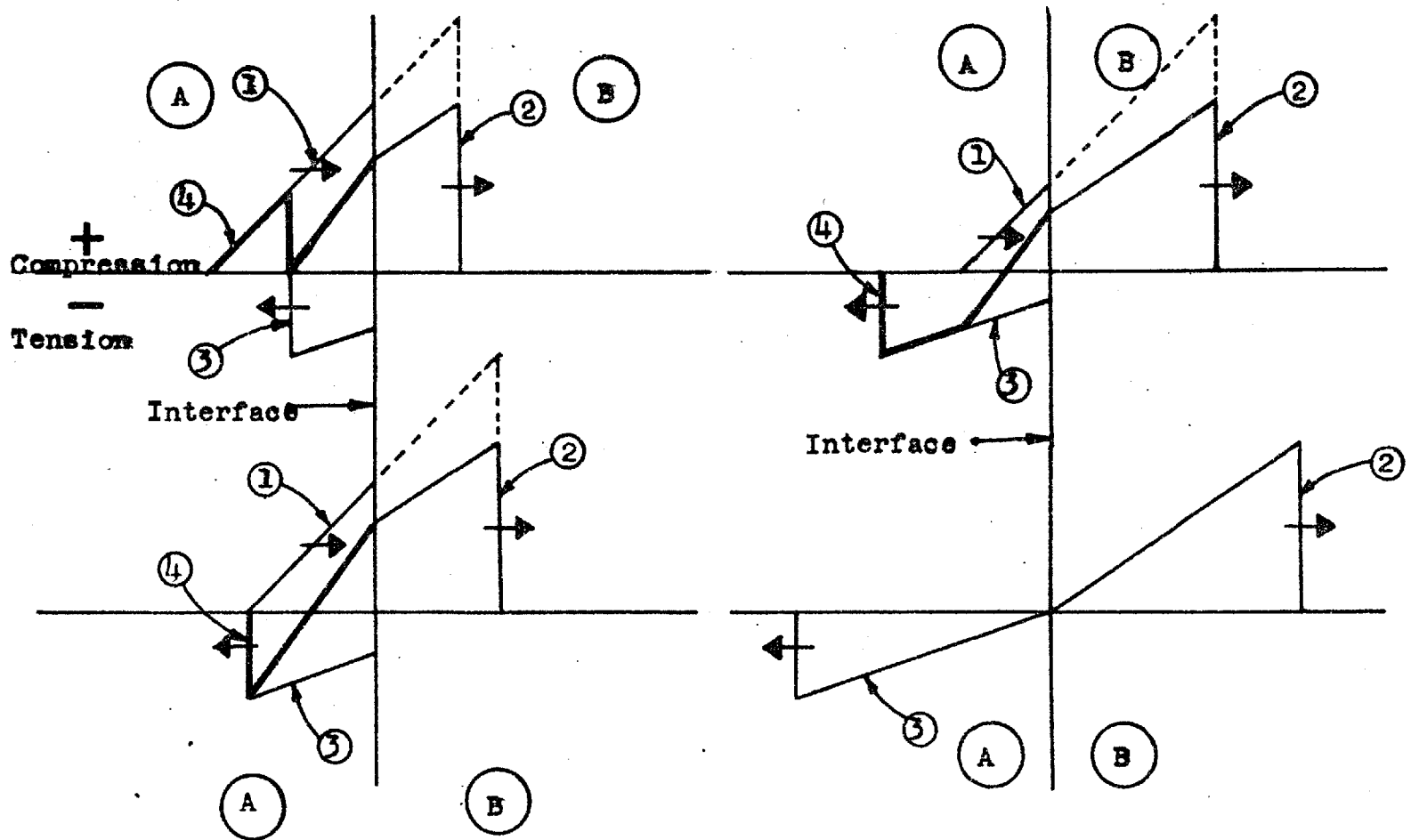① Oncoming stress wave, ② Transmitted stress wave, ③ Reflected stress wave
④ Resultant stress.

Fig. 57 Four phases of transmission and reflection of a tensile stress wave at an interface (Medium A/Medium B) , where characteristic impedance ($\rho.c$) of A is smaller than that of B.

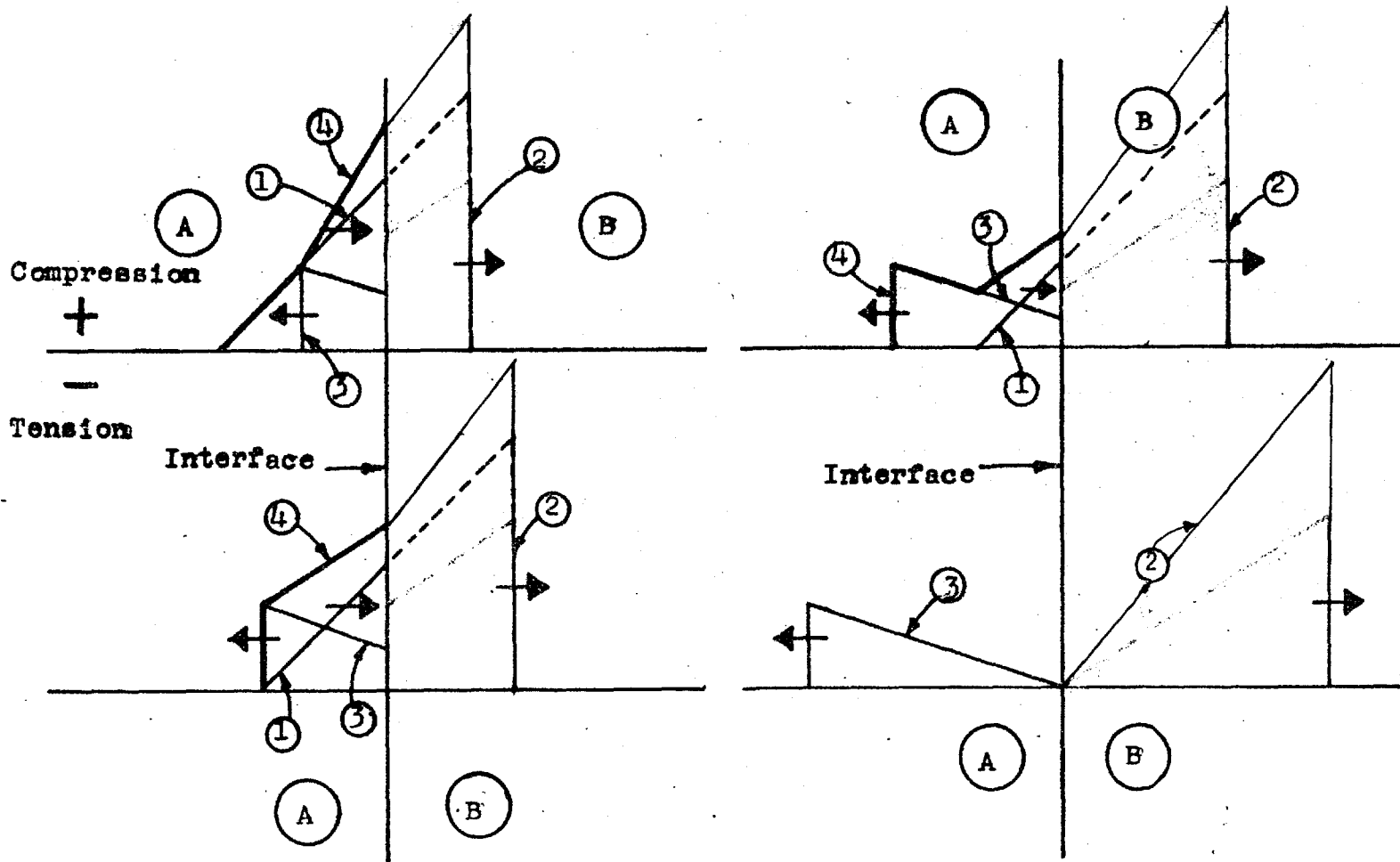① Oncoming stress wave, ② Transmitted stress wave, ③ Reflected stress wave, ④ Resultant stress.

The possible shock wave transmissions and reflections of a compressive longitudinal shock wave at the interfaces of two mineral grains of different acoustic impedances $(\rho.c)$ are shown in Figs.54 and 55 , with four phases. The oncoming compressive longitudinal stress wave is produced by spark disharge and transmitted to the solid particle directly. It is clear from these figures, that in no case is a tensile stress developed across the interface.

The possible transmissions and reflections of a tensile logitudinal wave at the interfaces of two mineral grains of different acoustic impedances are shown in four phases in Figs.56 and 57 . This longitudinal tensile stress wave could be produced at solid/water or Solid/air interface, and would be much more attenuated than the above compression stress wave, since the the shock wave should travel longer distance to reach the same interface. In Fig.56, the resultant tensile stress across the interface is less than the original stress of tensile wave, therefore, the probability for the preferance of interface of two mineral grains , in fracture development is not very high, unless there is a reasonable large difference between tensile strength of bonds across the interface and tensile strength of mineral grains.

In Fig.57 the resultant tensile stress across the interface is greater than the original intensity of tensile stress

wave, therefore the probability for the preferance of the interface of two mineral grains in fracture development is very high.

When it is considered from the work on the mechanism of electrohydraulic crushing , that the fractures caused by Hopkinson spallings play only a minor part in the main fracture mechanism   when particles are completely submerged in water , then it cannot be expected that electrohydraulic comminution would be outstandingly better at liberation than conventional methods. However , one is still justified in expecting a slight improvement due to Hopkinson spalling mechanism.

The role of hoop stresses is now considered in liberation. These form the highest stress concentrations in the middle of the shock wave front, in homogeneous materials. A simple mathematical treatment of the problem is shown in Fig.58 . The total hoop tensile force T_φ at the unit middle section or T_φ for $\varphi = 90^\circ$ is:

$$T_{90^\circ} = R.p$$

where R   radius of the shock wave front at time t

p intensity of shock wave front at time t

Tensile Force T_φ is given by the following formula:

$$T_\varphi = 2.R.\sin^2(\frac{\varphi}{2}).p \qquad (17)$$

This formula is computed for various φ's and the resultant
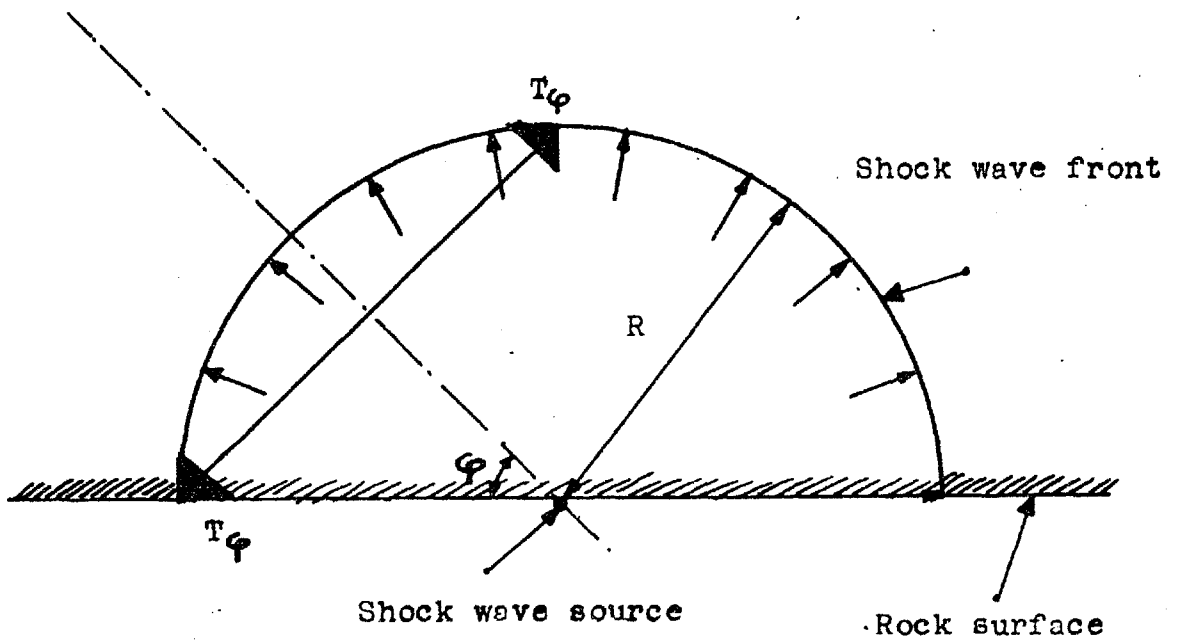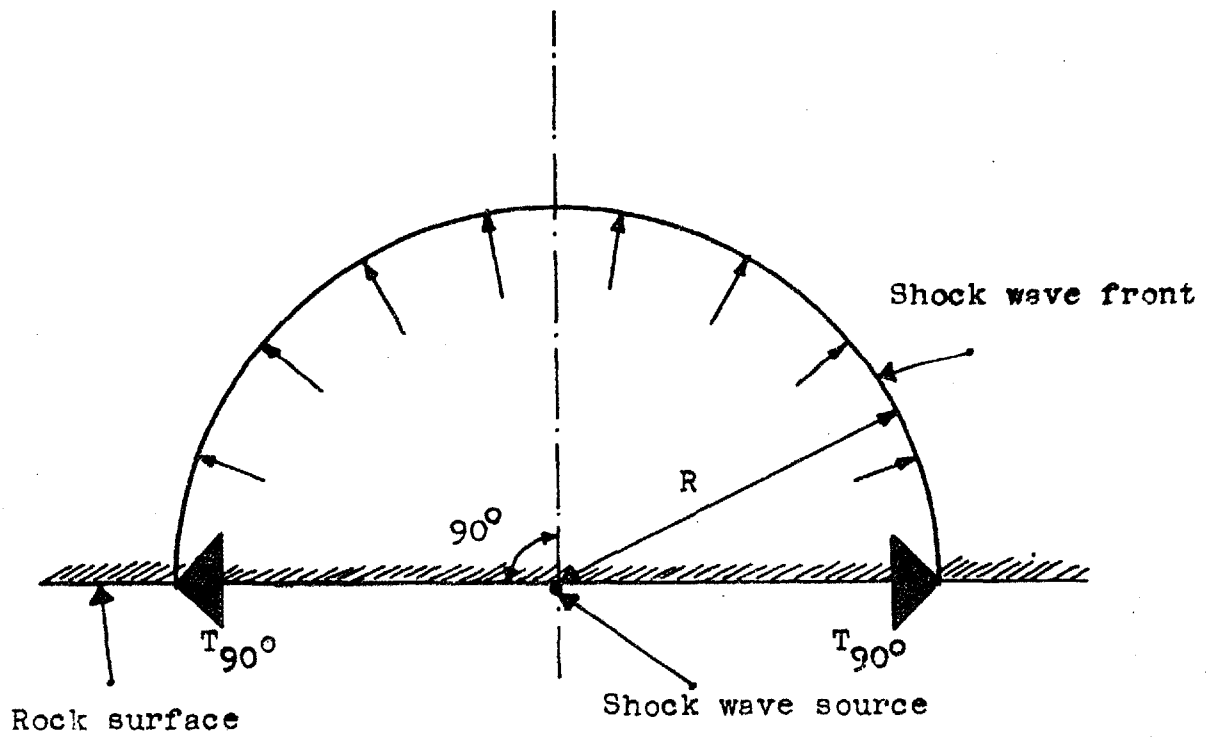
Fig. 58 Hoop Tensile force along shock wave front.

variation of the intensity of tensile force T_φ is shown

in Fig.59 .It is clear from these figures that the tensile

force falls very sharply from the middle of shock wave front.

Therefore, if the material has any weakness   due to bonding

of mineral grains, there is very little probability of that

weakness being selected during fracture   unless the weak-

ness   is very near to the peak of the front.Alternatively,

there must be a very significant difference between the

tensile strength of bonding and the tensile strength of the

mineral grains themselves.

However, as is mentioned previously, selective spark

discharge would be very helpful in addition to these weak-

nesses in the ore, since in this case the shock wave front

could be very favourably placed near the grains to be libe-

rated.Unfortunately, no experiments were performed in the

electrohydraulic comminution device shown in Fig.25 , which

is the most promising for better liberation , due to lack

of time , and since it was always very difficult to find

a suitable ore of two constituents of easy chemical analysis

and easy and effective separation methods.

However, some early experiments with two available ores

were done in the electrohydraulic crusher shown in Fig.24 .

in which,as explained in the above section, no significant

success would be expected, due to very little contribution

Shock wave front

Shock wave source   Rock surface
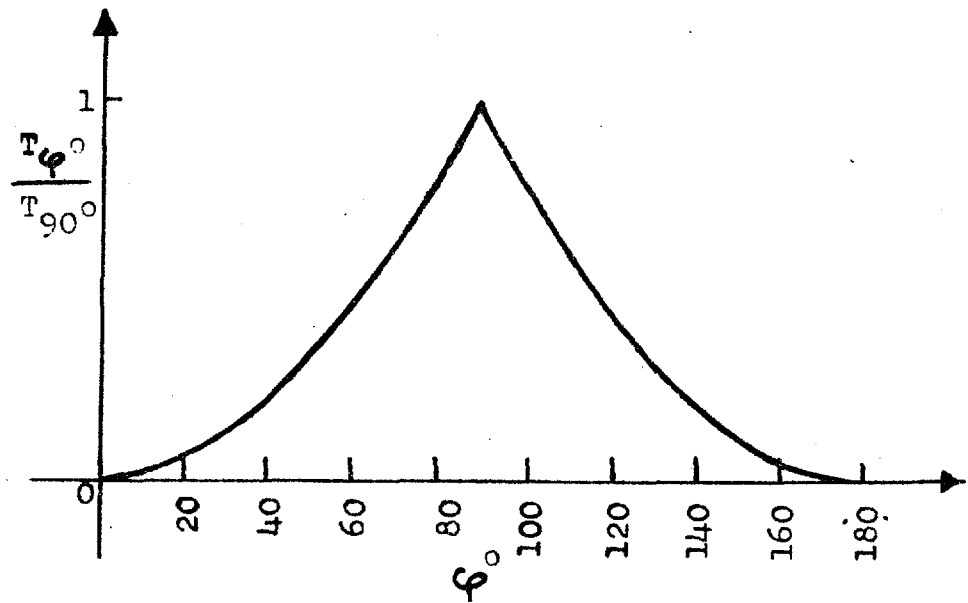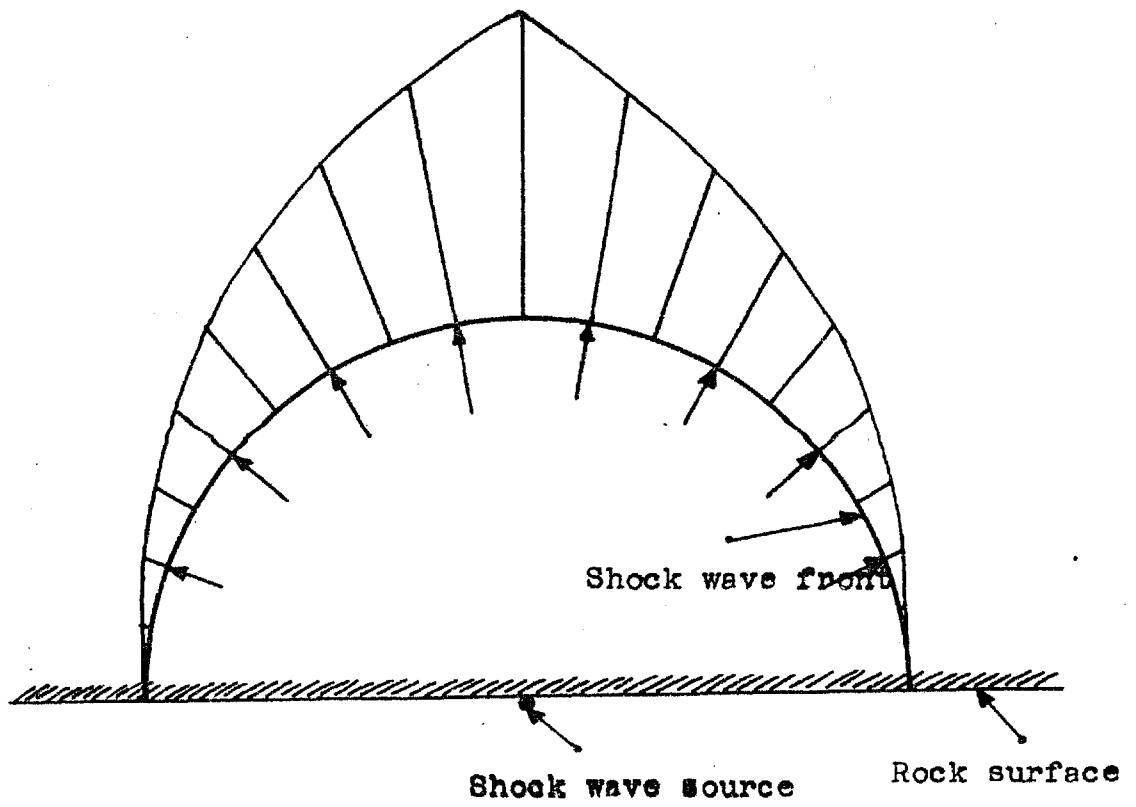
Fig. 59 Variation of the intensity of the Tensile force T_φ
along shock wave front.

of selectivity (Chapter 2.6.1) .

One of the ores was Pyrochlore-Carbonatite ore. Because
of the composition of the ore, which contained limestone,
some apatite and 4-5 % residue insoluble in cold dilute
hydrochloric acid (pyrite, magnetite, pyrochlore, some mica
and some silicates) it was impossible to get the real amount
of middlings and consequently percentage of liberation by
simple sink-float tests. However , with a sink-float test of
specific gravity near 2.76 (the specific gravity of limestone),
fully liberated limestone particles were floated from the
products of electrohydraulic crusher, a laboratory hammer
mill, a laboratory jaw crusher and a laboratory vibrating
mill , respectively. Assuming no significant selective
crushing, i.e. percentage of limestone   same   as in feed,
in all sizes of product, the calculated percentage of fully
liberated i.e. floated, limestone is plotted against average
particle size in Fig.60 . A small increase in liberation
with electrohydraulic comminution is clear from Fig.60
against jaw crusher and vibrating mill (a few percent).
However, there is no significant difference between elec-
trohydraulic comminution and hammer mill.

Another ore tested was a chromite ore from Turkey, which
was soft, since its serpentine constituent had been very
much weathered. Comparative samples of ore were crushed in a
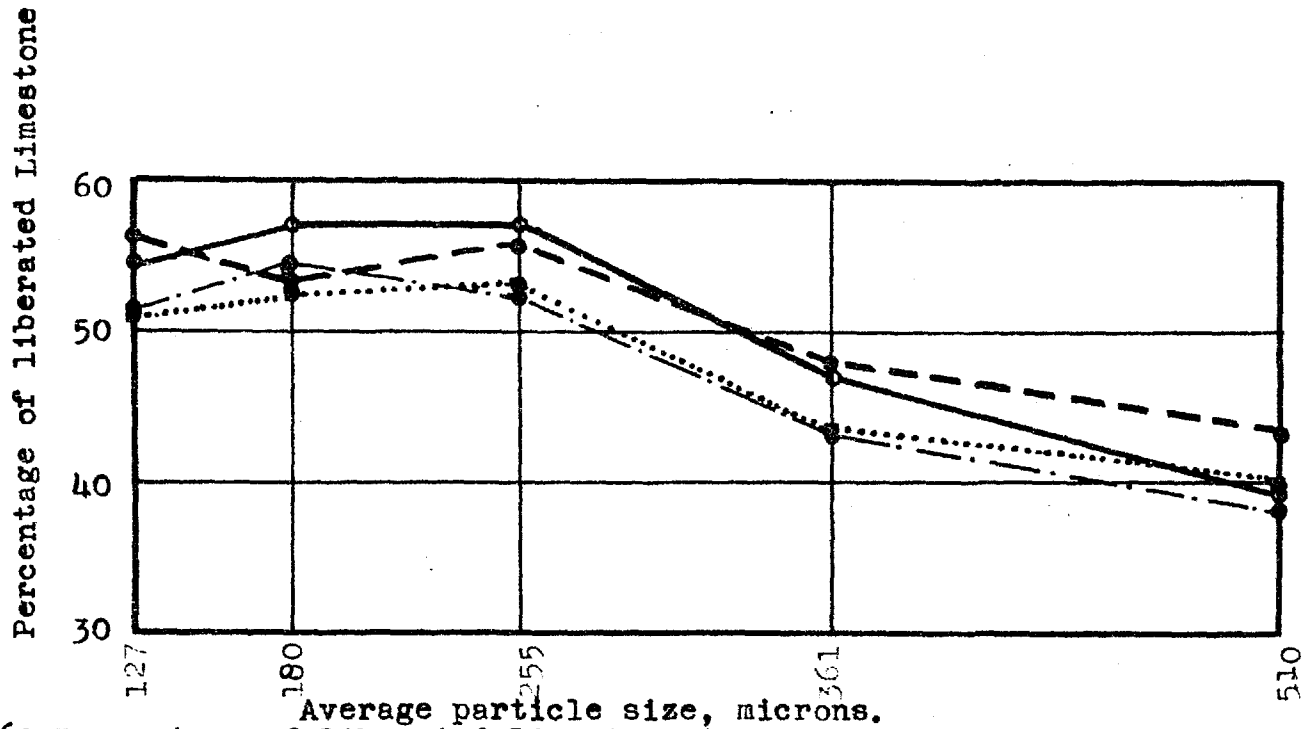
Fig. 60 Percentage of liberated Limestone in Pyrochlore-Carbonatite ore at various particle sizes:

o——o Electrohydraulic comminution.

●— —● Hammer mill

●——·—● Jaw crusher

■····■ Vibrating mill

laboratory hammer mill, in a laboratory jaw crusher, and electrohydraulically. As serpentine is softer than chromite , the fine sieve fractions of all products were found to contain more serpentine than coarse ones and feed , due to selective crushing. Therefore, for each fraction of crushed product, the serpentine content was determined approximately by measurements of mean specific gravity of fractions. By relating these quantities of serpentine to the amount of fully liberated serpentine which was floated by a heavy liquid of specific gravity of 2.6 (approximately specific gravity of serpentine), the percentage liberation of each fraction was found. The results are shown in Fig.61. It is clear from the figure that in the finer sizes, there is a small increase in liberation in electrohydraulic comminution, against the other methods (a few percent). However, the total liberation of all sieve fractions, which are shown in Fig.61 , have been calculated and found to be 50.6 % for electrohydraulic comminution, 50.4 % for hammer mill and 48.8 % for crushing in jaw crusher.

2.7   METAL WEAR IN ELECTROHYDRAULIC

COMMINUTION

One of the main characteristics of electrohydraulic comminution is to produce relatively contamination free
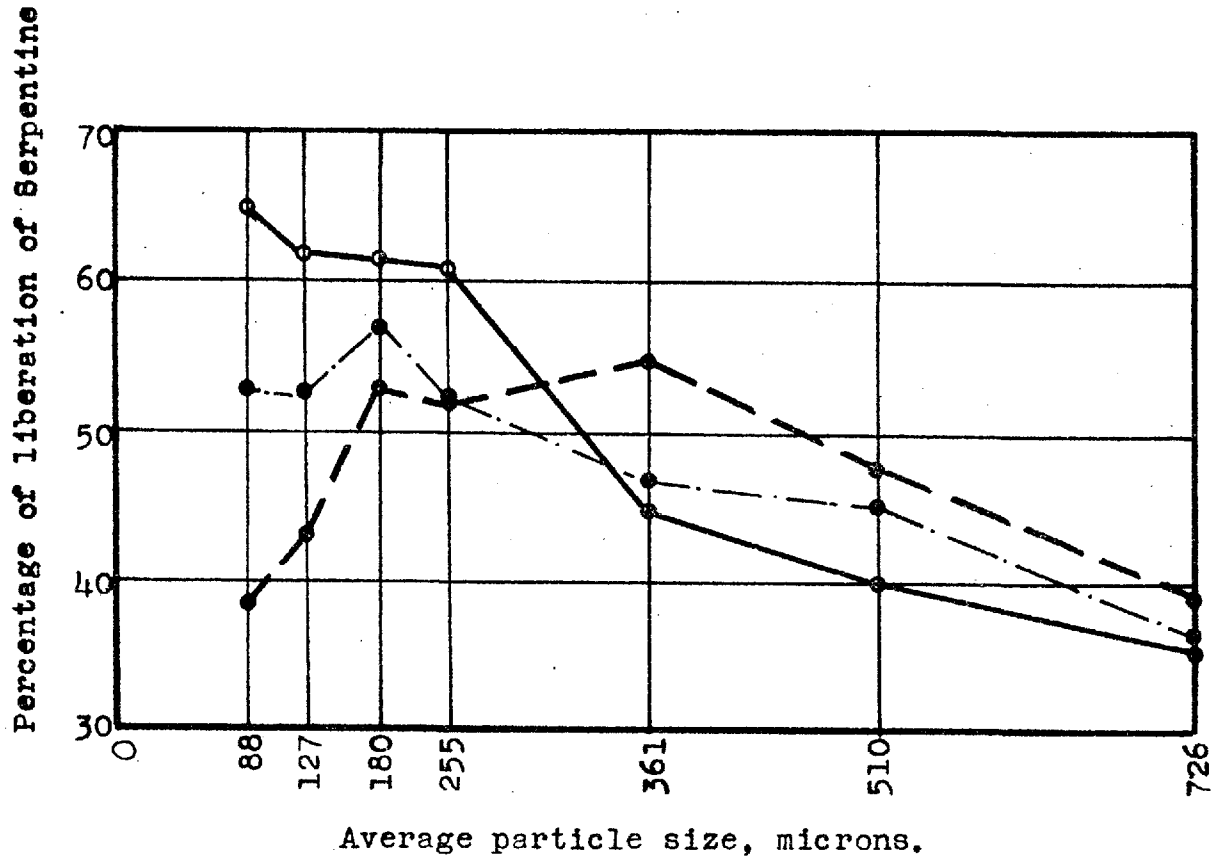
Fig. 61 Percentage of liberation of Serpentine in Chromite ore at various particle sizes:

○——○ Electrohydraulic comminution

●——● Hammer mill

●——● Jaw crusher

crushed products. Although no extensive experiments were performed on the metal wear with variations of the shape of the electrodes and types of metals used, in present studies, the metal wear of annular type of electrodes shown in Fig.14 , with 1 cm. spark gap , varies from 5 to 10 gr. per kWhr for stainless steel and for ordinary steel, respectively. The wear of the central circular high tension (+) electrode was also found slightly higher than that of the outer ring earth electrode. No such experiments were performed on the pointed electrode system. Maroudas et al.[10] have made some measurements on the metal wear of pointed electrodes and have found that metal wear varies from 15 gr. to 0.4 gr. with varying gap length of from 0.5 cm. to 2 cm., respectively for silver steel.

Although it seems that the metal wear in electrohydraulic comminution is relatively lower than in conventional comminution methods, the main advantages are as follows:

(i.) The metal wear of electrodes can be washed away from the product particles very easily, since they are very fine: on the contrary , in conventinal comminution the metal wear cannot be easily separated, since often it would coat the surfaces of the product particles and additionally , there would be fairly coarse grains of metal present.

(ii.) There is no limitation of using a special type of

metal or alloy in electrohydraulic comminution: on the
contrary, in conventional crushing and grinding methods a
special type of hard alloy should be used to prevent
excessive abrasion of working surfaces.

(iii.) The metal wear in electrohydraulic comminution
is not a function of the hardness and strength of the rock
to be crushed: on the contrary in conventional comminution
methods the wear is very much dependant on the hardness
and strength of the rock to be ground or crushed.

(iv.) The original surface properties of crushed
products can be maintained in electrohydraulic comminution
which is often impossible in conventional methods.This
might be valuable in Flotation and Electrostatic Separation
processes.

However, there is one significant disadvantage in
electrohydraulic   comminution, that is very highly
localized wear.

CHAPTER III   CONCLUSIONS

3.1   FRACTURE MECHANISM:

It is concluded, on both theoretical and experimental grounds , that the chief cause of fracture lies in tensile stresses due to hoop stresses and reflected tensile stresses. Geometry of specimen and type of loading are important parameters. For example, it was very easy to produce pure Hopkinson spalling in long, flat rectangular prisms, provided that the length of the specimen was greater than half width of the shock pulse, that the specimen was loaded at one end perpendicular to its longest axis, and that the energy of the discharge was enough to produce the required intensity of reflected tensile stress at the far end. On the other hand, when the type of loading was changed, in the same specimens, so that they were now loaded perpendicular to their shortest axes, it was very easy to produce pure hoop stress fracture.

3.1.1   HOOP STRESSES

There are some similarities between the static hoop stresses produced in a pressure vessel and the present dynamic hoop stresses, mainly in that the highest tensile stress distribution is across the shortest radial section. Also the dynamic hoop stresses have their peak at the inner surface of the specimen.

There is however one significant difference. In the

static case, the hoop stresses rapidly disappear when the first complete crack develops in the pressure vessel, because of the release of pressure. In the dynamic case , the pressure (intensity of shock wave front) is not released after production of the first crack, which simply halves the length of arc subject to hoop stress by the wave front. (see Fig.58) Therefore, if there is still a sufficient length of arc remaining for the front to produce large enough hoop stresses , ($T_{\varphi} = 2.R. \sin^2(\frac{\varphi}{2}).p$ (17)), further cracks will develop.

There is as yet no satisfactory quantitative explanation of the remarkable symmetry of the radial cracks. Rinehart's[18] explanation of angular symmetry, based on the critical impact velocity, is for infinite bodies and does not take into account the shape of specimen. From the observed fracture patterns, it seems that angular symmetry depends largely on the geometry of the specimen, and the angle between radial fractures depends on the intensity of the shock wave front.

3.1.2   HOPKINSON SPALLING

For Hopkinson spalling , and for fractures due to concentrations of reflected tensile stresses, the size of the feed should be greater than half the wave length , in order to achieve efficient crushing .

3.2 PRODUCTION OF INTENSE REFLECTED WAVES IN ORDER TO INCREASE COMMINUTION EFFICIENCY

The reflection coefficient for the waves outgoing from the particles should be increased in order to increase the efficiency of electrohydraulic comminution through the agency of Hopkinson spalling and of fractures due to concentrations of reflected tensile stresses. This was achieved by starting the pulse at one face of a particle in a dense medium, e.g. water, while keeping the other faces in air, so that the reflection coefficient was practically unity. Almost a net doubling of crushing efficiency was observed in the experiments.

3.3 SIMULTANEOUS MULTIPLE SPARKS

Using two sparks, produced simultaneously by two exploding wires, across or along a rectangular prism, reinforcement of dynamic hoop stresses and also reinforcement of reflected tensile stresses, were observed. From the above observation it is suggested that the use of multiple sparks in electrohydraulic comminution might increase efficiency for the following reasons:

a. Some particles which with one spark i.e. one shock wave front, would be only deformed elastically, might be

fractured by reinforcement of the stresses produced by simultaneous wave fronts.

b. If they are generated simultaneously near to each other, a steep resultant shock wave front can be generated, which might be more efficient than individual shock wave fronts in crushing. However, this latter point remains to be proven.

3.4 SELECTIVITY

The tendency of the spark discharge to follow solid surfaces between two electrodes, and the resultant selective crushing of mixed feed , is a discovery made during these studies. As the preliminary tests showed, the selective electrohydraulic comminution can result in a concentration process, which is very sensitive to certain electrical properties. A thorough study of the phenomenon remains to be made, but it seems at the moment, that bulk conductivity, surface conductivity, and surface roughness play a major role in the selectivity between rocks and valuable minerals.

3.5 LIBERATION

Unlike the above studies on selectivity in crushing , using an annular electrode system, the experiments with a

pointed electrode system have shown little better libera-
tion than those of conventional methods. By combining better
selective crushing, using annular electrode system with libe-
ration studies a better liberation might be expected; however,
these experiments have yet to be performed.

3.6   SHAPE

Electrohydraulic comminution resultsin a remarkable cubic
particle shape. This is a very desirable feature for coarse
aggregates used in road making and concrete , where the
percentage of flaky material is limited by British
Standards [42,43] .

From the mineral technological point of view this feature
would be also desirable, especially in gravity separation
methods, since in a certain size range the settling veloci-
ties due to specific gravity would not be confused by
variations in particle shape ; consequently more effective
separation would be possible between two mineral grains.

3.7   SIZE DISTRIBUTION

Sharper size distribution is a very desirable feature in
comminution processes. The product size is predetermined for
an effective liberation of mineral grains in mineral
technology, and less over-crushing means both a saving in

energy and a saving of valuable minerals, e.g. during
desliming in a floatation process. In the production of
coarse aggregates, the aim of quarries is to produce less
fines which are considered as a loss of material and
discarded.

It seems from the experimental results that the size
distribution curves depend very much on the nature of the
rock, especially the grain size , for both electrohydraulic
comminution and jaw crushing.

Generally, the coarse grained rocks give higher slopes
than fine grained, amorphous, cryptocrystalline rocks in
log-log plot. They are partially in agreement with the
Gaudin-Schumann size distribution "law".

CHAPTER IV   APPENDIX:

THE ELECTROHYDRAULIC EFFECT AS A SCIENTIFIC

RESEARCH TOOL

4.1   INSTRUMENTATION

A geometric shape could be loaded accurately by the
exploding wire technique, because of the very small volume
of the exploding wire or foil. Also, it is possible to pro-
duce several sparks simultaneously with a high degree of
temporal precision.

An investigation has been started by the auther to use
electric resistance strain gauges for measurement of the
stresses produced by shock waves due to underwater discharge.
In order to eliminate electrical interference, the first
step was to shield the experimental assembly completely and
to use coaxial cables for strain gauge circuit. In spite of
these efforts electrical interference on the strain gauges,
which is proportional to the distance to the discharge circuit,
i.e. spark gap , was considerably high. A cylindrical synthetic
rock specimen, in which two opposite sensing 1/2" strain
gauges were placed during casting , was prepared, as shown
in Fig.62 .Using air discharges of 5 µF capacitor (underwater
discharge would have fractured the specimen, and the aim was
only to investigate the electrical interference on the strain
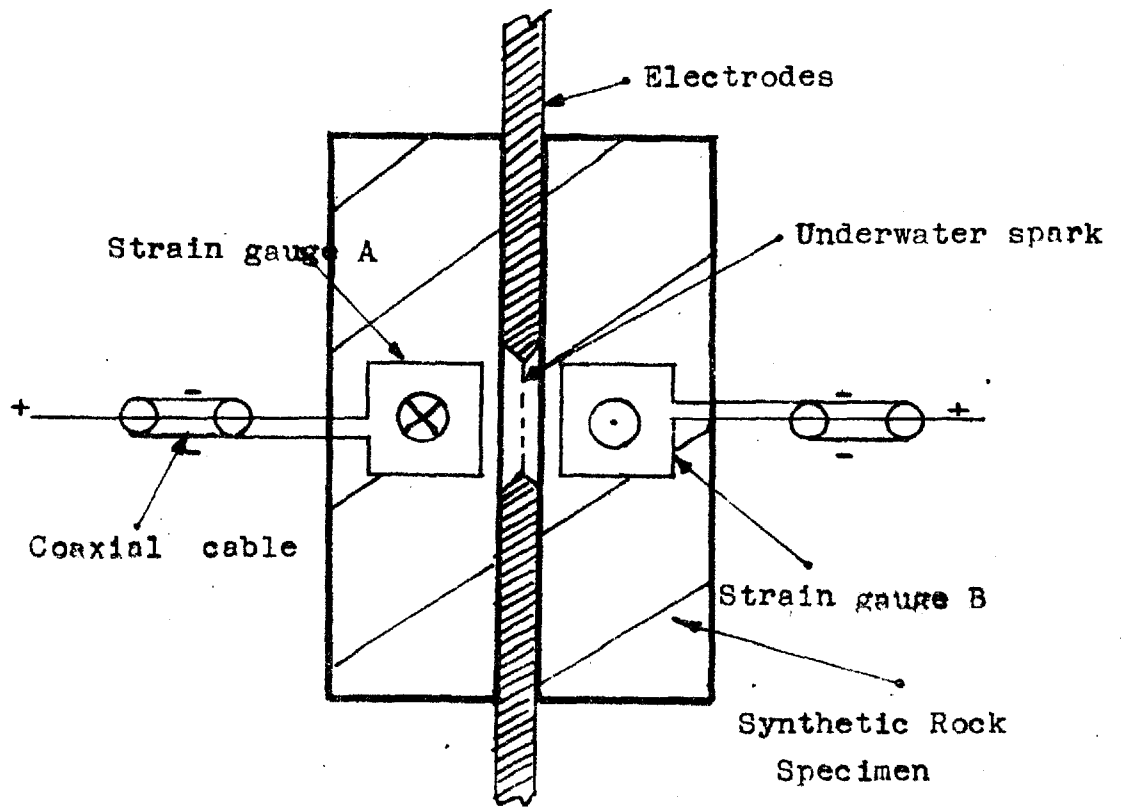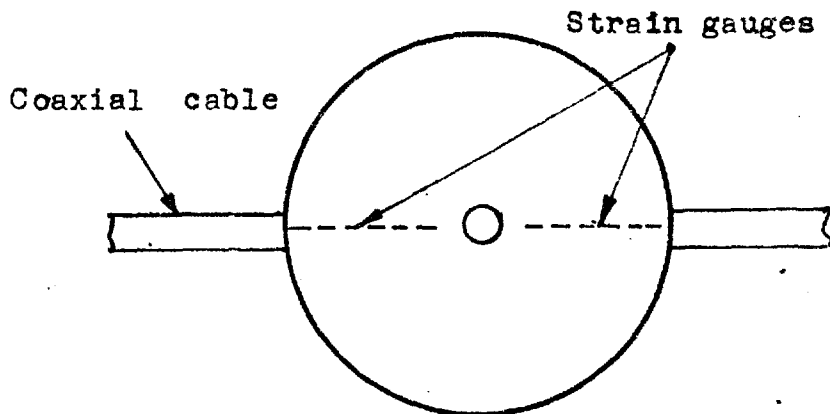
Fig. 62 The experimental arrangement in order to eliminate
electrical interference during discharges, using
two opposite sense strain gauges.

gauges) ,the interferences on the two strain gauges were recorded on the oscilloscope screen. The photographs of the recorded traces are shown in Figs.67 and 68 .Analysis of photographs are given in Figs. from 63 to 66 .

Using a two channel (A,B) oscilloscope, the above two traces were added algebraically together, but this was not very easy, since for summing up each channel required reverse triggering polarities.This performance was achieved using external triggering, which was connected to the earth of the coaxial cable of one of the strain gauge, so that channel (A) was being triggered say at (+) polarity, while channel (B) was being triggered at (-) polarity.The figures 64 and 66 show the resultant interferences. Intensity at the second peak was about 0.2 Volts , corresponding 4 kV discharge voltage.

At 8 kV discharge voltage, the second peak of inter-ferences were about at 1.8 V for strain gauge (A) and 2.8 for strain gauge (B). It seems from these figures that the interference is not linear with varying voltage.Therefore, with increasing discharge voltage more difficulties would be expected.

Another development was to use a high transient direct current of 300-400 Volts and a few miliseconds duration for strain gauge measurements, in order to make the above
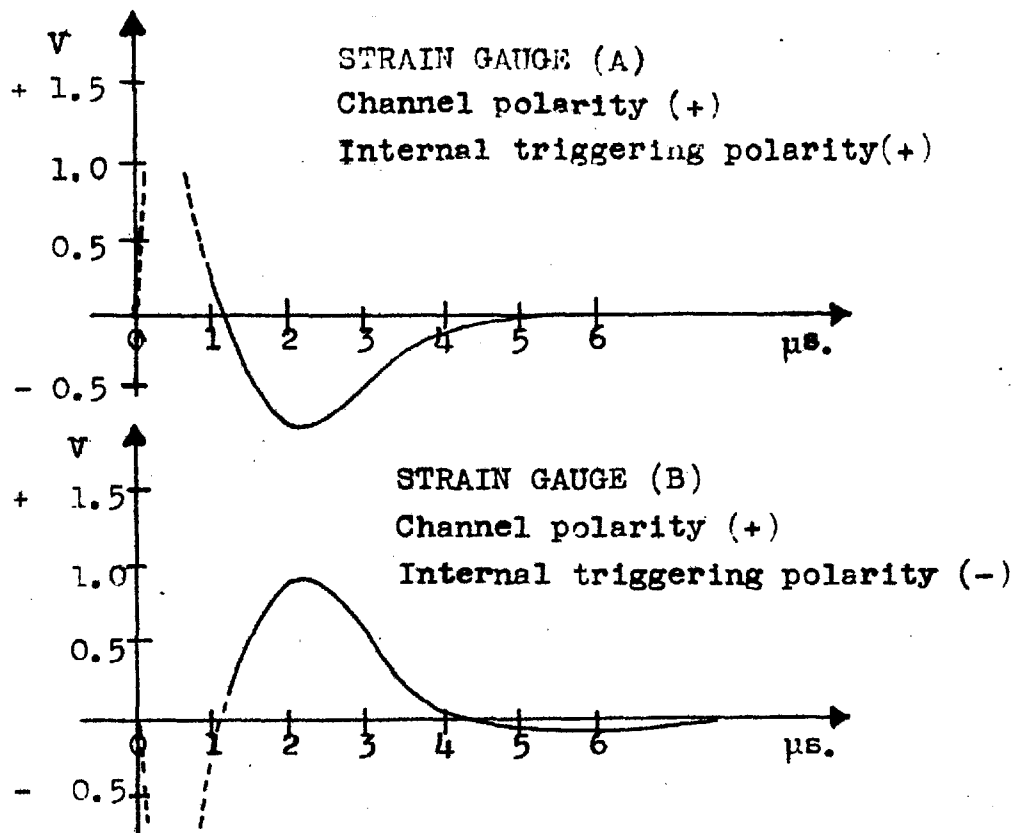
Fig. 63 Oscilloscopic traces of electrical interference during
discharges; 5 µF capacitor at 4 kV discharge voltage.

Fig. 64 The resultant interference trace of both strain gauges.
The interferences have been added algebreically together
using two channels of one oscilloscope.
5 µF capacitor at 4 kV discharge voltage.

STRAIN GAUGE (A)
Channel polarity (+)
Internal triggering polarity(-)

STRAIN GAUGE (B)
Channel polarity (+)
Internal triggering polarity (+)

Fig. 65   Oscilloscopic traces of electrical interference during
         discharges. 5   µF   capacitor at 4 kV discharge voltage.

Channel polarity (+)
External triggering polarity(-)

Channel polarity (-)
External triggering polarity (-)

Fig. 66 The resultant interference trace of both strain gauges.
        The interferences have been added algebreically together
        using two channels of one oscilloscope.
        5 µF capacitor at 4 kV discharge voltage.

Fig.67 Photographs of oscilloscopic traces of
electrical interference during discharges.
5 µF capacitor at 4 kV discharge voltage.
Analysis of traces are shown in Figs.63 and 65.
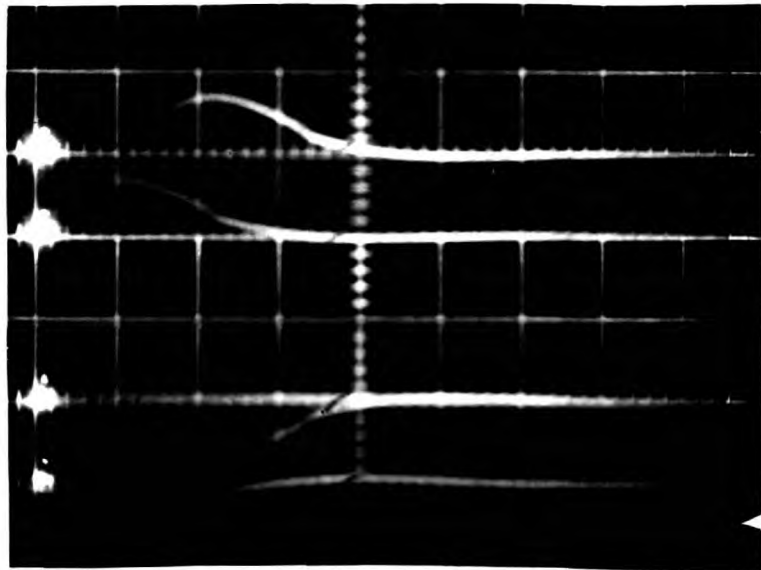
Fig.68 Photographs of resultant oscilloscopic
interference trace of both strain gauges.
5 µF capacitor at 4 kV discharge voltage.
Analysis of traces are shown in Figs.64 and 66.

resultant interference negligible. In preliminary experiments, the strain gauges have been able to withstand a transient direct current of 300-400 Volts of milisecond duration.

The experiments on this subject were discontinued, since the project was thought to be a research topic of considerable duration.

However, the above preliminary experiments show that, with very careful preparation methods, two reverse sense strain gauges coupled with transient direct currents of high voltages, can be used giving fairly negligible resultant interferences in the stress determinations on artificial and natural rock samples.

4.2   ROCK MECHANICS

Once instrumentation of stress-strain measurements is solved , the electrohydraulic effect would be used very widely as a research tool in Rock Mechanics. Especially, dynamic loading caused by explosives would be scientifically investigated using exploding wire, or foil or bare underwater spark.

The geometric models of rocks could be loaded accurately by cylindrical shock wave fronts produced by exploding wires and planar wave fronts produced by exploding foils, and also by several different shock wave fronts

simultaneously e.g. cylindrical and planar wave fronts simultaneously.

Also very high repetition rates can be generated by bare sparks for vibration studies.

Bore-hole blasting can be reproduced in small scale models by electrohydraulic discharges. In bore-hole blasting , both the size of the burden and the wave length of the stress pulse are of the order of metres, while the duration of the pulse is hundreds of microseconds. In electrohydraulic crushing the length of stress pulse is of the order of cm. and the duration is microseconds .Hence, bore-hole blasting could be correctly modelled, on a conveniently small scale using electroacoustic pulses, keeping the same ratio of specimen size to wave length of stress pulse as in rock-blasting. Moreover the electroacoustic pulse is more cylindrically uniform than that from explosives, because the whole length of the spark is exploded at practically the same time, while in explosives there is the detonation velocity along the line of explosive to be taken into account.

Some properties of explosions can be investigated. In electroacoustic sparks, the energy and shape of the wave front can be regulated closely.

4.3   DYNAMIC LOADING OF ENGINEERING MATERIALS

The behaviour of engineering materials namely, metals, plastics,concrete, etc. are very important in design problems of structures , machines, and missiles.Dynamic loading of these materials with transient stresses are also often encountered in actual conditions , but unfortunately is not well explained.Therefore, a precise scientific research tool in dynamic stress-strain studies could be very useful , and the same considerations which apply to the use of electrohydraulics in research on rock mechanics, might be expected to become in some cases of general use in the dynamic study of engineering material .

REFERENCES

(1) T. SVEDBERG   "Über die elektrische Darstellung einiger neuen colloidalen Metalle" Berichte der Deutschen Chemische Gesellschaft. Vol. 38, p. 3616, 1905

(2) G. I. POKROVSKIY and K. P. STANYUKOVICH   Izvestia Akad. Nauk. Ser. Fiz. Vol. 8, p. 214, 1944

(3) W. SCHAAFFS   "Untersuchungen an Funkenschallwellen mit Hilfe von Röntgenblitzen" Zeitschrift für Naturforschung. Vol. 4 (A), p. 463-472, 1949

(4) F. FRÜNGEL and H. KELLER   "Stoss-Schallquellen, Grundlagen und Analogie zu Sprengstoffumsetzungen" Zeitschrift für Angewandte Physik. Vol. 9 (3), p. 145-147, 1957

(5) B. H. BERGSTROM   "The electrohydraulic crusher" Eng. and Min. Jour. Vol. 162, p. 134-136, 1961

(6) L. A. YUTKIN   "The electrohydraulic effect" Mashgiz, Moskva, Leningrad, 1955

(7) N. G. MAROUDAS and R. F. TAYLOR   A. E. R. E. M 1261 , 1963

(8) N.G.MAROUDAS   "Electrohydraulic comminution"

                           Brit.Chem.Eng.

                           Vol.12 (4),p.558-562,1967

(9) N.G.MAROUDAS   "Apparatus for electrohydraulic

                           crushing"

                           British Patent no:1021786 , 1965

(10) K.W.CARLEY-MACAULY,   "Energy consumption in electrohydrau-
     J.W.HITCHON and   lic crushing"
     N.G.MAROUDAS   Trans.Inst.Chem.Engns.

                           Vol.44,p.T395-T404,1966

(11) N.G.MAROUDAS and   "An improved electrohydraulic
     E.YIGIT   comminution apparatus"

                           British Patent appl. no:26651,1966

(12) N.G.MAROUDAS ,   "Mechanism of electrohydraulic
     H.A.JOHNSTON and   crushing"
     E.YIGIT   Second European Symposium on

                           Comminution.Amsterdam Sept.1966

                           Dechema-Monographien,Verlag Chemie,

                           Vol.57,p.551-582, 1967

(13) E.A.MARTIN   "Experimental investigation of high

                           energy density, high-pressure

                           arc plasma"

                           Jour.Appl.Phys.

                           Vol.31, no:2,p.255-267,1960

(14) F. FRÜNGEL   "High speed pulse technology"Vol. I
Academic Press Newyork London 1965

(15) A. S. ZINGERMANN   "The dependance of the pressure at the
front of a shock wave upon steepness
of the energy pulse front when an
electrical discharge takes place in
a liquid" Soviet Phys. Tech. Phys.
Vol. 1, p. 2454-2455, 1957

(16) Y. F. EPSTEYN ,   "New methods of crushing rocks"
E. I. ARSH and   Moscow, p. 46-70, 1960
G. K. VITORT

(17) J. S. RINEHART and   "Behaviour of metals under impulsive
J. PERSON   loads"
Dover Publ. Inc. Newyork 1965

(18) J. S. RINEHART   "The role of stress waves in the
comminution of brittle rock-like
materials" Inter. Symp. on stress wave
propagation in materials.
p. 247-269, 1960

(19) T. H. HUETER and   "Sonics"
R. H. BOLT   John Wiley and Sons Inc. 1962

(20) D. G. CHRISTIE   "Reflection of elastic waves from
boundary" Phil. Mag. London
Vol. 46, p. 527-541, 1955

(21) H. SCHARDIN   "Ergebnisse der Kinematographischen
Untersuchung des Glasbruchvorganges"
Glastechnische Berichte.
Vol. 23, p. 1-10; 67-69, 1950

(22) F. SAUTER   "Der elastische Halbraum bei einer
mechanischen Beeinflussung seiner
Oberfläche (zwei dimensionales Problem)"
Zeitschrift für Angewandte Mathematik
und Mechanik. Vol. 30, p. 203-215, 1950

(23) P. R. RITTINGER   "Lehrbuch der Aufbereitungskunde"
Berlin 1867

(24) F. KICK   "Das Gesetz der proportionalem
Widerstand und seine Anwendung"
Leipzig 1885

(25) F. C. BOND   "The third theory of comminution"
Trans. AIME, Min, Eng.
Vol. 4 , p. 484-494, 1952

(26) F. C. BOND   "Bond Indexes tabulated"
Vol. 5 , P. 315-316, 1953

(27) K. SCHÖNERT,   "Die Festigkeit kleiner Glaskugeln"
H. UMHAUER and   Glastechnische Berichte.
H. RUMPF   Vol. 35, p. 272-278, 1962

(28) K. SCHÖNERT and   "Versuche zur Zerkleinerung von
H. RUMPF   einzelteilchen zwischen zwei Flächen"

First European Symposium on
Comminution. Frankfurt 1962
Verlag Chemie und VDI Verlag
p. 108-127, 1962

(29) R. T. HUKKI and   "The relationship between net energy
     I. G. REDDY   input and fineness in comminution"
Second European Symp. on Comminution.
p. 313-339, 1967

(30) H. E. ROSE   "A comprehensive theory of the
comminution process"
Second European Symp. on Comminution.
p. 27-62, 1967

(31) K. SCHÖNERT   "Modellrechnungen für Zerkleinerungs-
prozesse mit den Ergebnissen der
Einzelkornversuche"
Second European Symp. on Comminution
p. 241-280, 1967

(32) F. C. BOND   "Crushing and grinding calculations"
Allis-Chalmers Inds. Press Dept. 1955

(33) E. OCELLA   "L'influence de la nature du minerai
sur la distribution granulométrique
des produits de fragmentation"
Second European Symp. on Comminution
p. 847-866, 1967

109

(34) B.BEKE   "Principles of comminution"
Publ.House of Hungarian Academy of
Sciences,Budapest 1964

(35) J.R.HOSKING   "A comparison of the tensile strength,
crushing strength and elastic proper-
ties of eleven roadmaking rocks"
Qua.Man.Jour.Vol.39,p.200-211,1955

(36) S.L.WINDES   "Physical properties of mine rock.I"
U.S.Bureau of Mines R.I.4459,1949

(37) S.L.WINDES   "Physical properties of mine rock.II"
U.S.Bureau of Mines R.I.4727,1950

(38) B.E.BLAIR   "Physical properties of mine rock.III"
U.S.Bureau of Mines R.I.5130,1955

(39) J.S.RINEHART   "Dynamic fracture strength of rocks"
VII Symp.on Rock Mechanics.
Pennsylvania State University
Vol.1,P.205-208,1965

(40) E.HOEK and   "Brittle fracture propagation in rock
Z.T.BIENIAWSKI   under compression" Int.Jour.of Frac.
Mech.Vol.1,no:3,p.137-155,1965

(41) D.F.COATES   "Rock mechanics principles"
Dept.of Mines and Tech.Sur. Ottowa,
Mine Branch Monograph 874, 1965

(42) BRITISH STANDARD   "Specification for aggregates from
     882,1201:1965   natural sources"

(43) BRITISH STANDARD   "Single-sized gravel aggregates
     1948:1953   for roads"

(44) BRITISH STANDARD   "Single-sized roadstones and
     63:1951   chippings"

(45) F.A.SHERGOLD   "A study of the granulators in the
                               production of road making aggregates"
                               Road Res.Tech.Paper 44,1959

(46) BRITISH STANDARD   "Methods for sampling and testing of
     812:1960   mineral aggregates sand and filler"

(47) P.J.F.WRIGHT   "The properties and specification of
                               aggregates for concrete"
                               Quar.Man.Jour.Vol.46 (9),p.371-379,
                               1962

(48) F.C.BOND   "Control particle shape and size"
                               Chem.Eng.p.1-4,1954

(49) D.S.MONCRIEFF   "The effect of grading and shape on
                               the bulk density of concrete
                               aggregates" Mag.of Conc.Res.
                               Vol.5 no:14,p.67-70,1953

(50) J.R.HOSKING   "An investigation into some factors
                               affecting the results of bulk density
                               tests for aggregates"Cement,Lime and
                               Gravel.Vol.31 no:11,p.319-326,1961

(51) F.A.SHERGOLD   "The percentage voids in compacted
gravel as a measure of its angularity"
Mag. of Conc.Res.
Vol.5 no:13,p.3-10,1953

(52) F.A.SHERGOLD   "The assesment of shape in roadmaking
aggregates"
Roads and Road Construction.Jan.1953

(53) M.F.KAPLAN   "The effects of the properties of
coarse aggregates on the workability
of concrete" Mag. of Conc.Res.
Vol.10 no:29,p.63-74,1958

(54) J.W.KIRK   "Impulse forming by electrical
discharge methods"
Sheet metal ind. p.533-540,1962

(55) J.F.PARR   "Hydrospark forming shapes space-age
metals"The Tool Eng.
Vol.44 no:3,p.81-86,1960

(56) U.S.PATENT   Eng.and Min.Jour.
no:3207447   Vol.167 no:1,p.98-99,1966

(57) J.S.RINEHART   "Fracturing under explosive loading"
Chem.Eng.Prog.Vol.55no:2,p.59-64,1959

(58) J.S.RINEHART   "Fracturing by spalling"
WEAR 7 ,p.315-329,1964

(59) J.H.CHARLES and J.S.RINEHART   "Coupling between unconfined cylindrical explosive charges and rock" Int.Jour.of Rock Mech.and Min.Scien. Vol.2,p.13-24,1965

(60) D.G.CHRISTIE and H.KOLSKY   "The fracture produced in glass and plastics by the passage of stress waves"Jour.Soc.Glass Tech. Vol.36,p.65-73,1952

(61) D.G.CHRISTIE   "An investigation of cracks and stress waves in glass and plastics by high speed photography"Jour.Soc.Glass Tech. Vol.p.74-89,1952

(62) H.KOLSKY and Y.Y.SHI   "Fracture produced by stress pulses in glass-like solids"Proc.Phys.Soc. Vol.72,p.447-453,1958

(63) P.H.COLE   "Underwater explosions" Princeton University Press, 1948

(64) K.HINO   "Theory and practice of blasting" Nippon Kayaku Com.Ltd. 1959

(65) U.LANGEFORS and B.KIHLSTRÖM   "Rock blasting" John Wiley and Sons Inc. 1963

(66) M.A.COOK   "The science of high explosives" Reinhold Publ. Corp. 1963

(67) I.W.FARMER   "New methods of fracturing rocks"

Min.and Miner.Eng.p.177-184,1965

(68) C.MITTAG   "Die Hartzerkleinerung"

Springer Verlag   1953

(69) W.GRÜNDER   "Aufbereitungskunde" Vol.II

Hermann Hübener Verlag   1957

(70) M.H.MILLER   "The effect of stress wave duration

on brittle fracture"

Int.Jour.of Rock Mech.and Min.Scien.

Vol.3,p.191-203,1966

(71) C.O.HARRIS   "Introduction to stress analysis"

The Macmillan Com.Ltd. 1959

(72) E.J.PRYOR   "An Introduction to mineral dressing"

Mining Publ.Ltd. 1955

(73) A.F.TAGGART   "Handbook of ore dressing"

John Wiley and Sons Inc. 1953

(74) A.M.GAUDIN   "Principles of mineral dressing"

Mcgraw-Hill book Com.   1939

(75) I.M.FYFE and   "Explosive wire induced cylindrical

waves in solids"

Exploding Wires.Vol.3,p.257-265

Plenum Press Newyork 1964

(76) J.A.KERSAVAGE   "Pressure environments created by

wires exploded in water"

Exploding Wires.Vol.2,p.225-233

Plenum Press Newyork 1962

(77) A.F.TAGGART   "Elements of ore dressing"

                            John Wiley and Sons Inc. 1965

(78) R.GUILLOT   "Le problème du broyage et

                            son évolution"

                            Collection de l'A.N.R.T. 1960

(79) F.BIRCH ,   "Handbook of physical constants"

     J.F.SCHAIRER and   Gelogical Society of America

     H.C.SPICER   1942

(80) I.SZABO   "Mathematische Formeln und Tafeln"

                            Verlag von Wilhelm Ernst und Sohn,

                            Berlin 1959

The Mechanism of electrohydraulic crushing

By N. G. Maroudas, D.I.C., Ph.D., A.M.I.Ch.E.,
H. A. Johnston, B.Sc. (Min. Eng.), A.M.S.A.I.M.M., and
E. Yigit, M.Sc. (Min. Eng.),
Department of Mining and Mineral Technology, Imperial College,
London, U.K.

Summary

The partition of shock-wave stress between water, air and solid particle is examined theoretically, with reference to the efficiency of electrohydraulic comminution. The exploding wire technique is presented as a new experimental tool for the generation of a pure line source of mechanical impulse. Comparison is made between experimental fracture patterns for single particles and the fracture patterns predicted from shock-wave theory. It is concluded that, contrary to the assumption of the original Russian workers in this field, cavitation damage plays little or no part in electrohydraulic comminution, and that breakage is chiefly due to the radial fractures which are produced by an expanding cylindrical or spherical wave front.

Zusammenfassung

Die Aufteilung einer Druckwelle auf Wasser, Luft und Feststoffteilchen wurde im Hinblick auf den Wirkungsgrad der elektrohydraulischen Zerkleinerung theoretisch untersucht. Der explodierende Draht wurde als neue experimentelle Methode zur Erzeugung einer reinen Linienquelle mechanischer Impulse vorgestellt. Ein Vergleich zwischen dem experimentellen Bruchverlauf für Einzelteilchen und dem durch die Druckwellentheorie vorhergesagten Bruchverlauf wurde unternommen. Es wurde gezeigt, daß, im Gegensatz zu den Annahmen der russischen Forscher, die als erste auf diesem Gebiet arbeiteten, die Zerstörung durch Kavitation nur einen kleinen oder gar keinen Anteil an der elektrohydraulischen Zerkleinerung hat. Die Zerkleinerung wird in der Hauptsache durch radiale Brüche bewirkt, die durch eine expandierende zylindrische oder sphärische Druckfront erzeugt werden.

Résumé

On a examiné théoriquement la répartition de la charge des ondes de choc entre l'eau, l'air et la particule solide du point de vue de l'efficacité de la comminution électrohydraulique. On présente ici la méthode du fil éclatant comme moyen de produire expérimentalement une source pure linéaire d'impulsion mécanique. On compare les types de fracture obtenus expérimentalement pour des monoparticules avec les modèles de fracture déduits de la théorie des ondes de choc. On conclut que la cavitation joue très peu de rôle dans la comminution électrohydraulique, ce qui est contraire à l'hypothèse des chercheurs russes qui furent les premiers à étudier ce phénomène, et que la fragmentation est due surtout aux fractures radiales occasionnées par l'avance d'une onde de choc cylindrique ou sphérique.

Introduction

It is well known that the electrical energy stored in a capacitor can be discharged between underwater electrodes to produce high pressure acoustic pulses, which are capable of disrupting solids in the vicinity of the spark.

Fracture of brittle solids by underwater sparks appears to have originated with Russian workers, although some experiments were done in the Research Laboratories of the Allis-Chalmers Manufacturing Corp. [6] in U.S.A. as early as 1952. In 1955 Yutkin [4] published his book "The Electrohydraulic Effect" in which he described how electrohydraulic impulses were used to break, cut and drill rock, to pump and atomise liquids and to hammer metals.

At the United Kingdom Atomic Energy Research Establishment, Harwell, a small crusher was built in 1959. Crushing efficiencies lower than those of conventional crushers, but twenty times higher than those obtained on previous electrohydraulic crushers [6], were obtained by reducing the inductance of the spark circuit to 0.1 microhenries [8], [9], [10], [11]. More recently the U.S. Patent [12] of an electrohydraulic crusher working with multiple sparks in an air-water-rock slurry has been published. So far no published research has been devoted to an investigation of the mechanism of electrohydraulic comminution. It has been implied by various authors (e.g. Yutkin [4], Bergstrom [6]) that comminution is the result of a compressive pressure followed by cavitation, due to growth and collapse of the spark channel. However, a little though would show that the cavitation hypothesis is not only vague but implausible. Cavitation could, at most, exert a ~~force~~ ↑pressure of 1 atm. suction, which is not enough to fracture ceramic materials.

The present paper is a report on some studies aimed at investigating more precisely the mechanism of rock-breakage in electrohydraulic crushing.

Theoretical considerations

The underwater spark produces initially a cylindrical shock wave front which becomes more spherical as it expands (Fig. 1).
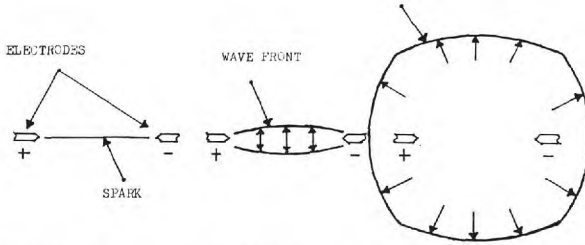
Fig. 1 Expansion of shock wave front in spark discharge. The arrows show the direction of expansion.

The following treatment is based largely on that of Rinehart [13]. A shock wave can create both dilatational (longitudinal) and distortional (shear) disturbances in an elastic medium (Fig. 2). In longitudinal disturbance the particle motion at the front of the disturbance is parallel to the direction of propagation of disturbance, particle motion being in the same direction for compression and in the opposite direction for tension. In shear disturbance the particle motion is perpendicular to the direction of propagation.

Fig. 2 Dilatational and distortional waves

553

The velocities of longitudinal and shear waves are given by the following formulae:

$$C_L = \left(\frac{3K\,(1-\nu)}{\varrho\,(1+\nu)} \right)^{1/2} \tag{1}$$

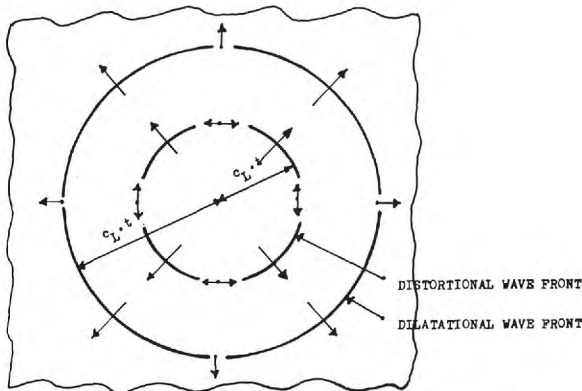where C_L Velocity of longitudinal wave
          K Bulk modulus of material
          ϱ Density of material
          ν Poisson ratio of material

$$C_S = \left(\frac{G}{\varrho} \right)^{1/2} \tag{2}$$

where C_S Velocity of shear wave
          G Rigidity modulus of material
          ϱ Density of material

The velocity of shear waves (C_S) is usually about one half that of the longitudinal velocity (C_L).

Longitudinal waves are of primary importance in the production of fractures in rock, because they have higher velocities than shear waves and are capable of producing tensile stresses within the bodies.
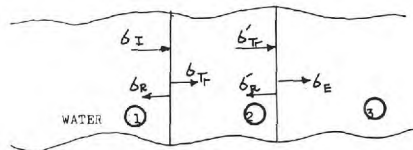

Fig. 3   Partition of the stress for a plane shock wave striking an immersed body

A solid particle in water, subjected to a longitudinal wave is shown in Fig. 3. The compressive stress of the wave which reaches the solid body from the spark is σ_I. This stress divides into two components at the first interface between water and the solid body (interface water/solid). One component is the reflected compressive stress, σ_R, and the other component is the transmitted stress, σ_{Tr}. This latter transmitted longitudinal stress wave travels within the body and reaches the second interface (interface solid/water). On the way σ_{Tr} loses some of its original intensity, depending on the distance which it has travelled and the absorption factor of the rock. Let this attenuated pulse now be called σ'_{Tr}. At the interface solid/water σ'_{Tr} divides into two components. The one component is the reflected tensile stress σ'_R and the other is transmitted compressive stress σ_E.

The formulae for reflected and transmitted stresses, for normal incidence, according to Rinehart, are as follows:

$$\sigma_R = \frac{\varrho_2\, C_2 - \varrho_1\, C_1}{\varrho_2\, C_2 + \varrho_1\, C_1} \cdot \sigma_I \tag{3}$$

Resultant sign in the above formula indicates the type of the reflected stress: $+$ for compression and $-$ for tension.

$$\sigma_{Tr} = \frac{2 \cdot \varrho_2\, C_2}{\varrho_2\, C_2 + \varrho_1\, C_1} \cdot \sigma_I \tag{4}$$

where σ_I intensity of the stress of shock wave
σ_R intensity of the stress of reflected wave
σ_{Tr} intensity of the stress of transmitted wave.

ϱ_1, ϱ_2, C_1, C_2 are the respective densities and velocities of propagation of elastic disturbances in two materials. The quantity $\varrho \cdot c$ is called the characteristic impedance of the materials and has the dimensions of momentum per unit volume.

More complex relationships describe the reflection of an elastic wave striking an interface obliquely. In general, either longitudinal or shear waves will generate reflected and transmitted waves of both types, with the original energy being partitioned between them.

Table 1   Partition of stress between glass and water. For a shock wave ranging from 5 to 200 Kbars. Symbols as in Fig. 3.
Assumed no attenuation, i.e. $\sigma'_{Tr} = \sigma_{Tr}$ Stresses are in Kbar, $+$ compression, and $-$ for tension.

$\varrho_w c_w$	σ_I	σ_R	σ_{Tr}	σ'_R	σ_E	$\dfrac{\sigma_R}{\sigma_I} = \dfrac{\sigma'_R}{\sigma_{Tr}}$
2.7	$+\ 5$	$+\ 3.4$	$+\ 8.4$	$-\ 5.8$	$+\ 2.6$	0.69
3.4	$+\ 10$	$+\ 6.2$	$+\ 16.2$	-10.0	$+\ 6.2$	0.62
4.5	$+\ 20$	$+10.5$	$+\ 30.5$	-16.0	$+\ 14.5$	0.53
5.3	$+\ 30$	$+13.9$	$+\ 43.9$	-20.4	$+\ 23.5$	0.46
6.4	$+\ 50$	$+19.4$	$+\ 69.4$	-26.8	$+\ 42.6$	0.39
8.3	$+100$	$+27.2$	$+127.2$	-34.3	$+\ 92.9$	0.27
11.0	$+200$	$+27.4$	$+227.4$	-31.1	$+196.3$	0.14

The predominant feature of electrohydraulic comminution is that it occurs when a solid body in the vicinity of the spark is struck by the expanding cylindrical shock wave [11]. Hence the solid is subjected to four sorts of stresses.

1) Normal compressive stress of the longitudinal wave of the cylindrical wave front (Fig. 5)
2) Hoop stress, as in a pressure vessel, due to the cylindrical wave front of the compressive stress of the longitudinal wave within the body (Fig. 5)
3) Reflected tensile stress of the longitudinal wave at the solid/water interface, which would produce Hopkinson spalling (Figs. 6 and 7)
4) Compound tensile stress concentrations, due to reinforcement of reflections from the corners of the solid (Fig. 8) and to the interferences among tensile and shear stresses.

Consider a cubic shape loaded as in Fig. 4: the section OCC'O' parallel to the direction of wave propagation would be subject to the hoop stresses and the section ABB'A' perpendicular to this direction

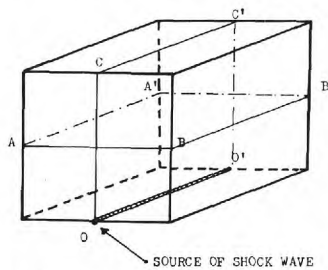Fig. 4 Cubic prism loaded by a linear source along the axis of one external face

would be subject to tensile stresses after reflection at the upper interface. These two sections are equal; hence it would appear from the following considerations that the most likely mode of damage would be due to hoop stresses.
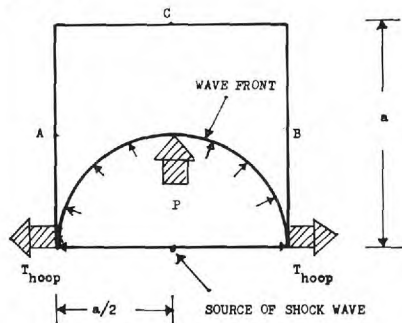

Fig. 5 Cross section of a cubic shape subjected to a cylindrical shock wave front

556

1) Firstly, we may discount compression damage, caused by the purely compressive stress of the wave front (i. e. force P, Fig. 5.), because the compressive strength of the rock is very much higher than its tensile strength.

2) In Fig. 5., the total hoop tensile force T_{hoop} along the unit section OC which is produced by the cylindrical compressive wave front, as in pressure vessel is:

$$T_{hoop} = \tfrac{1}{2}\,aP \tag{5}$$

where a Diameter of wave front
　　　 P Compressive pressure at the wave front at distance a/2 from the source.

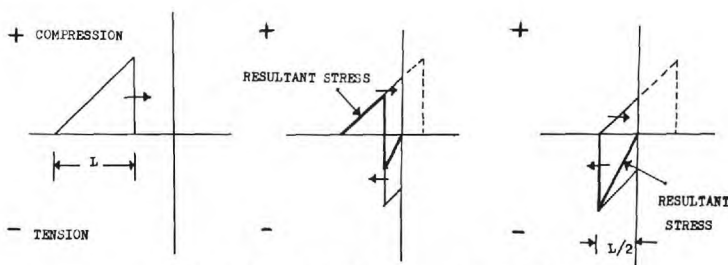The hoop stress distribution along the section is not uniform, being highest at the source.

Fig. 6   Wave reflection at a free surface

3) The probability of fracture by Hopkinson spalling is less when the rock is immersed in water, for the following reasons:

a) Only a fraction of the intensity of the stress wave is reflected at the solid/water interface. For example, for a glass/water interface at 20 Kbar the reflection coefficent σ_R/σ_{Tr} is only 0.5 (Fig. 3 and Table 1).

b) After reflection the highest resultant tensile stress occurs at the distance of half a wave length in the case of steep triangular wave form (Fig. 6). Thus it would be difficult to produce spalling in the smaller specimens of rock if the peak pressure of resultant stress after reflection were only slightly higher than the dynamic tensile strength of the material. This situation is summarised in the following formulae for the thickness of the slab and for the number of slabs:

$$l = LT/2P \tag{6}$$

where   l Thickness of the slab
　　　　 L Length of shock wave
　　　　 T Dynamic tensile strength of material

$$N = L/2l = P/T \qquad (7)$$

where N Number of slabs

$$L = tc \qquad (8)$$

where   t   Duration of the pulse
          c   Velocity of the propagation of the pulse.

$$\text{If } T \div P$$

$$N = 1 \text{ and } l = L/2$$

Therefore the size of the specimen D must be greater than L/2

Let us define as follows the tensile force, $T_{Hopkinson}$, exerted by a reflected wave on the unit section AB of Fig. 7.

$$T_{Hopkinson} = aP_a' \qquad (9)$$

where P_a' average resultant tensile intensity of the reflected wave front.
          a   length of section.
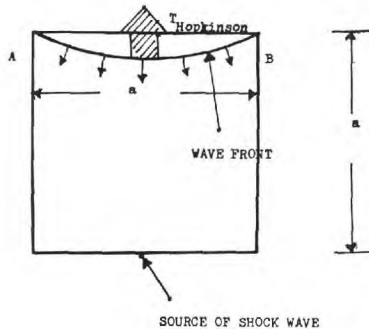
Fig. 7   Reflection of a cylindrical shock wave front at the opposite face to the source, neglecting the reflections at the sides

In Fig. 7, a unit section AB, perpendicular to the direction of wave propagation is subjected to a total tensile force $T_{Hopkinson}$

$$T_{Hopkinson} = \int_0^a P' da \qquad (10)$$

where P' intensity of the resultant tensile stress along the section
          a length of the section.
P' varies along the section because

(i) The angle of incidence of the wave varies

(ii) The distance to wave front from boundary to develop peak resultant tensile stress after reflection, which would be half the wave length in the case of a triangular wave front, varies in both cases due to the curvature of the wave front.

Thus the tensile stress distribution along the wave front is not uniform being highest in the middle.
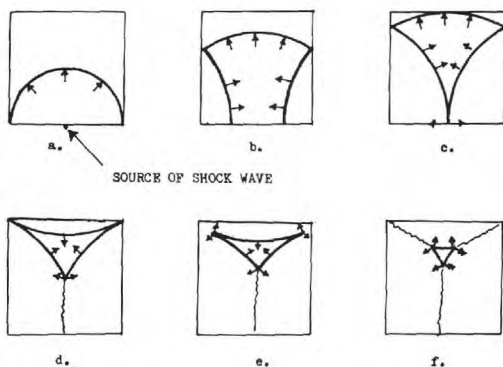

Fig. 8   The concentration of reflected tensile stresses at a square section

The above considerations of fracture by Hopkinson spalling due to single reflections are also valid for their concentrations which would produce corner fractures (Fig. 8). For instance, corner fractures cannot start from the very tip of the corner, although most diagrams depict them in this fashion.

When we compare T_{hoop}, $T_{Hopkinson}$ and P with each other, assuming that half the wave length is smaller than the size of specimen and P is the same order as $T_{(hoop, Hopkinson)}$, then it follows that:

1) P cannot compare with $T_{(hoop, Hopkinson)}$ as a cause of fracture, because the compressive strength of rocks is about 20 times higher than their tensile strength.

2) It would seem from equations (5) and (9) that $T_{Hopkinson}$ is twice as great as T_{hoop}. But, as mentioned above, even at 90° angle of incidence for the glass/water interface, the coefficient of reflection is 0.5 (for a longitudinal wave at 20 Kbar). For angles other than 90°, shear stresses are reflected. (For example for a material of Poisson ratio 0.25, the angle of incidence ranging from 60° to 80°, practically all the energy goes into the shear wave).

Considering also the attenuation of the intensity of the wave during travel and the impossibility of reflections developing their peak pressures along a curved wave front at the same time, because of varying

distances to the reflection points, it would appear that the hoop tensile force is more favourable than the other two for crack initiation.

Experimental equipment

Experiments were designed to elucidate the mechanism of electro-hydraulic fracture by studying the fracture patterns produced in various specimens of regular geometry and uniform mechanical properties.

A synthetic rock-like material was mainly used, consisting of a mixture of graded quartz sand and epoxy resin. This material was more uniform than natural specimens; on the other hand it had a more rock-like grainsize distribution than, say, glass or clear resin, while being stronger than plaster-of-paris or cement mixtures. The size distribution of the sand was as follows:

Mesh	18—25	25—36	36—52	52—72	72—100	—100
%	6	17	22	22	11	22

Geometry of grains was cubic.

The resin was Epikot 815 with hardener Epikure T (Shell Chemical Co. Ltd.). The mixture consisted of 800 parts of graded sand, 100 parts of Epikot 815 and 20 parts of Epikure T, by weight. After mixing the constituents with each other, as uniformly as possible, the product was cast into moulds of various shapes, then tamped by hand to consolidate the mass. Approximate physical properties of the synthetic rock were as follows:

s.g. = 2.07
Porosity = 0.072
Velocity of sound = 3,600 m/sec = 11,800 ft/sec
Static compressive strength = 800 kg/cm^2 = 11,500 p.s.i.
Static tensile strength = 100 kg/cm^2 = 1,500 p.s.i.
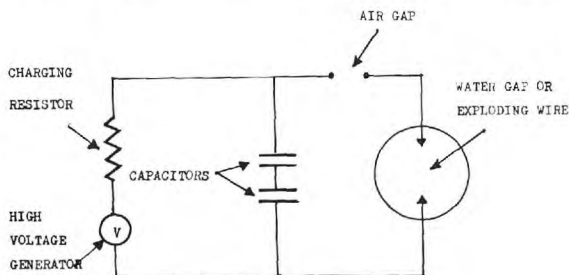Dynamic Young's modulus = 2.7 x 10^5 kg/cm^2 = 4 x 10^6 p.s.i.

Fig. 9   Electrical circuit

The electrical pulse was generated by two capacitors (each of 10 KV, 20 Micro F) connected in series. The circuit is shown in Fig. 9. In the

experiments, the electrical loop between capacitors and underwater electrodes was kept reasonably small in order to reduce inductance (see refs. [8], [9], [11]), but no special effort was made in this direction, as efficiency was not the prime object of the present study. The inductance of the circuit was found to be about 1-2 Microhenries from the oscilloscope measurements. Photographs of these oscilloscope traces showed that the reproduceability of any spark was within the accuracy of the measuring instruments, i.e. within $5^0/0$ overall, without taking any special precautions. The crushing chamber used in the experiments is shown in Fig. 10. A cylindrical wave front was generated by the use of exploding wires, 1 to 4 cm long and 36 s.w.g. (193 Microns) in diameter.
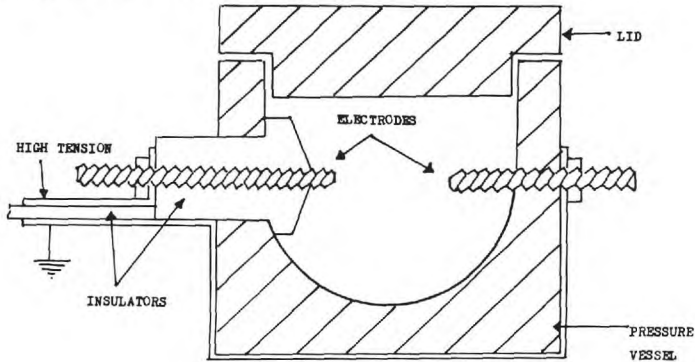

Fig. 10   The crushing chamber

Experimental Results

The experiments were classified under five different headings, A to E, as follows:

A. Internal Loading of Specimens

Cylindrical, square, rectangular and triangular prisms of synthetic rock used in the experiments. The specimens had holes along their axes. The exploding wire was either placed in the hole and confined by water around it or else it was tamped inside the specimen during casting to obtain more effective confinement. Experimental arrangements are shown in Fig. 11.

Photographs of some of the observed fracture patterns are reproduced in Figs. 12 and 13. All the fracture patterns show a remarkable radial symmetry. The main cracks seem to have traversed the statically weakest radial sections of the specimens. These lines of fracture are analogous to those caused by hoop stresses in the static loading of a cylindrical pressure vessel. This observation suggests that dynamic

561

WATER

EXPLODING WIRES

ELECTRODES

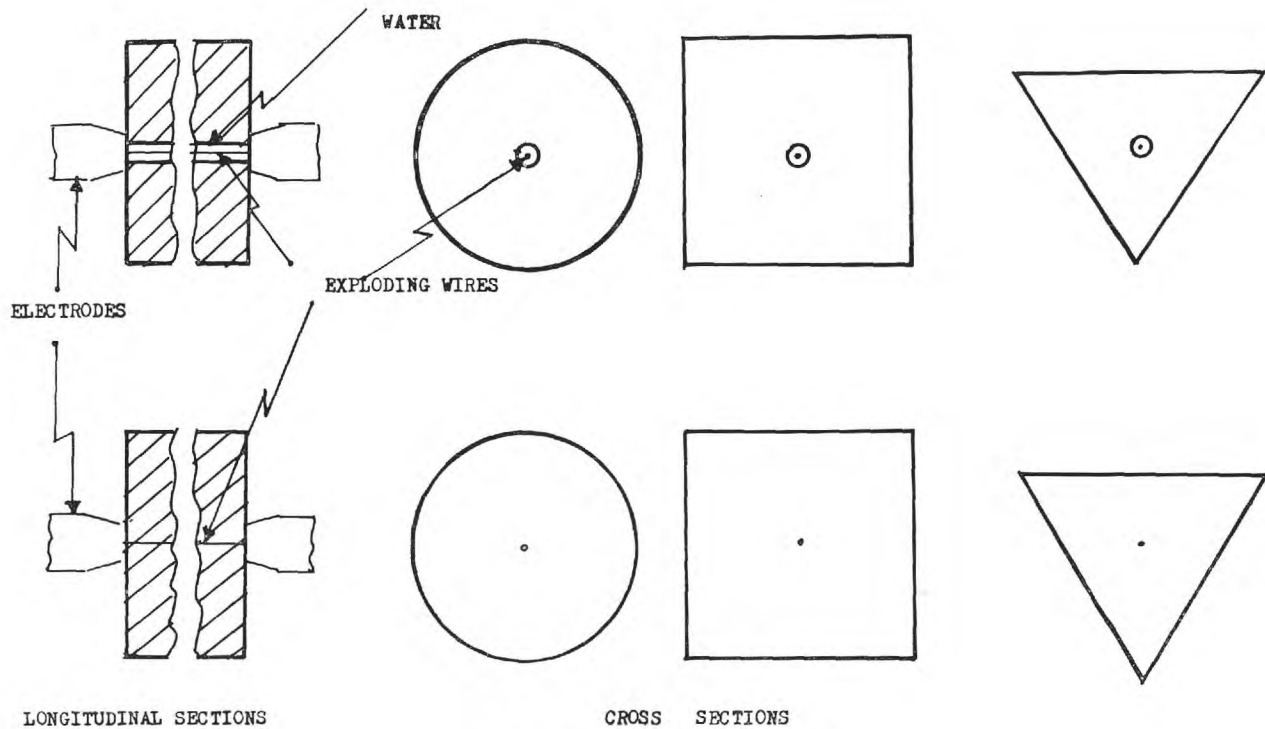LONGITUDINAL SECTIONS

CROSS SECTIONS

Fig. 11 Internal loading of prisms

hoop stresses are at work in the present case. However, it might be objected that, in square and triangular prisms, the second stage cracks through the corners (Fig. 12B, C and 13D, E) might easily have
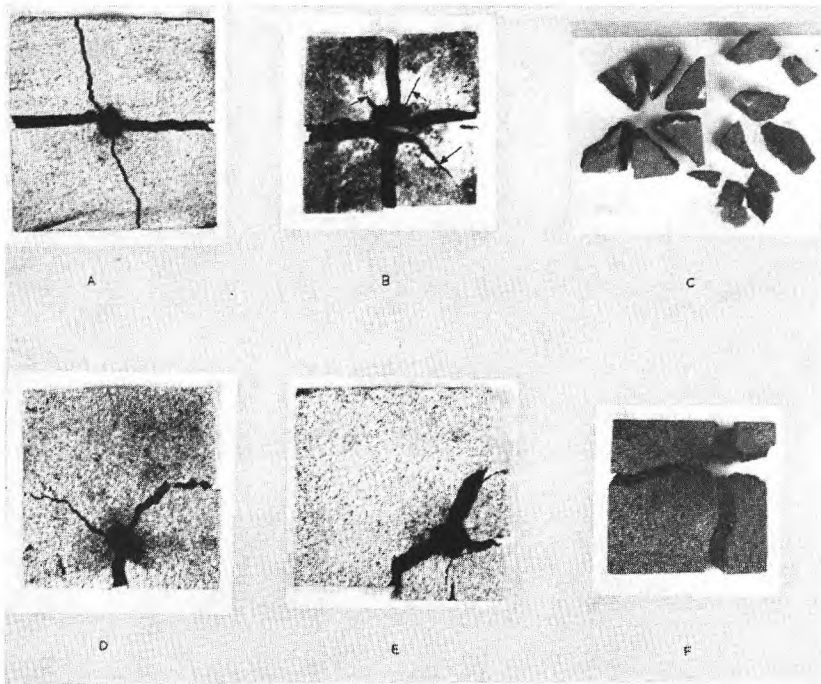
Fig. 12   Fracture patterns in square prisms. The arrows show the cracks which have been started but not completed

been caused by tensile stress concentrations due to reflections at the corners, which is the usual mechanism for corner fractures (cf Fig. 8). But many cases were found where the cracks were started from the inside of the specimens (Figs. 12B, 13D and E). In order to be attributable to reflections, these cracks would have had to have been started nearer to the corners. It is possible that tensile stress concentrations after reflections might have caused further propagation of cracks initially formed by the earlier hoop tensile stresses in these regions. However, no spalling or scabbing was found, such as could have been attributed to the action of reflected waves, thus reinforcing the conclusion that breakage was initiated solely by hoop stress.

Signs of compression damage, attributable to a purely compressive shock wave front were also looked for. Practically no such effects were found.

In the static case the highest tensile stresses occur in the inside of the pressure vessel. In the above specimens, the presence of incomplete cracks, starting from inside, show that the analogy with static hoop stresses holds for the present case of dynamic loading. To investigate this further, cylinders were used, which were reinforced with a polythene or copper ring around their axis. Just enough energy
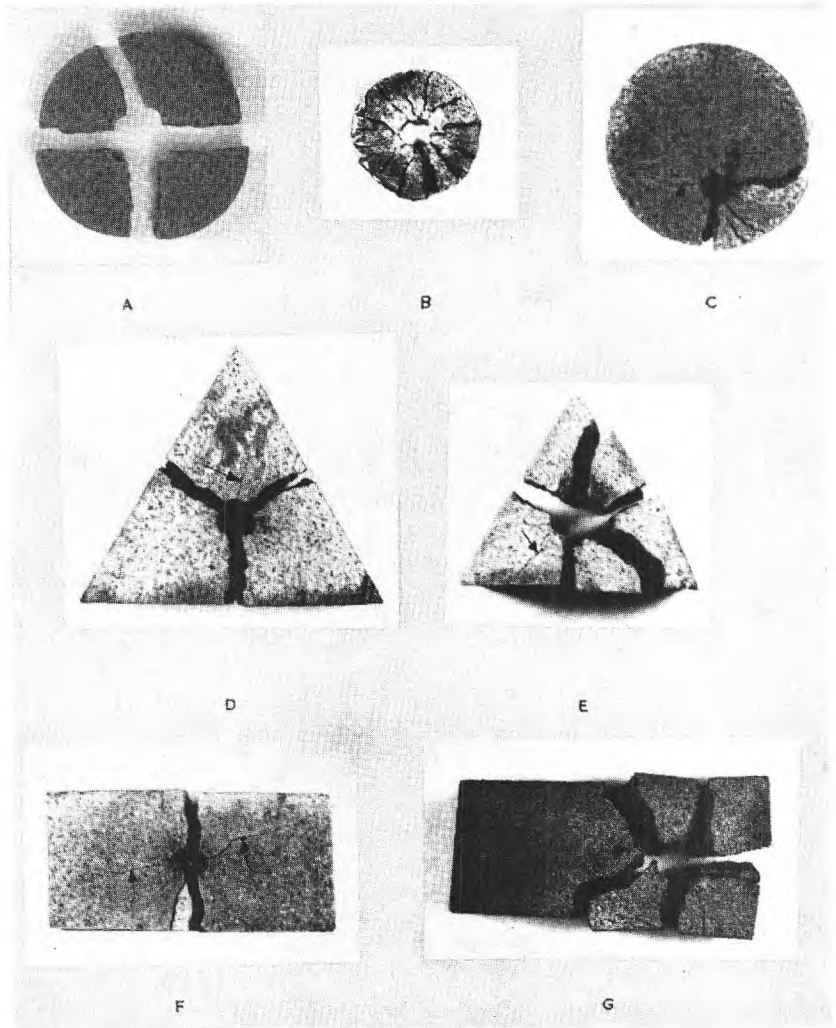
Fig. 13   Fracture patterns in prisms. Arrows show started cracks.

was given to start cracks but not to complete them. Fig. 14A shows the fracture of a cylinder with polythene ring reinforcement. An exploding wire was placed in the axis of the cylinder during casting. The propagation of the cracks from the inside is clearly visible.
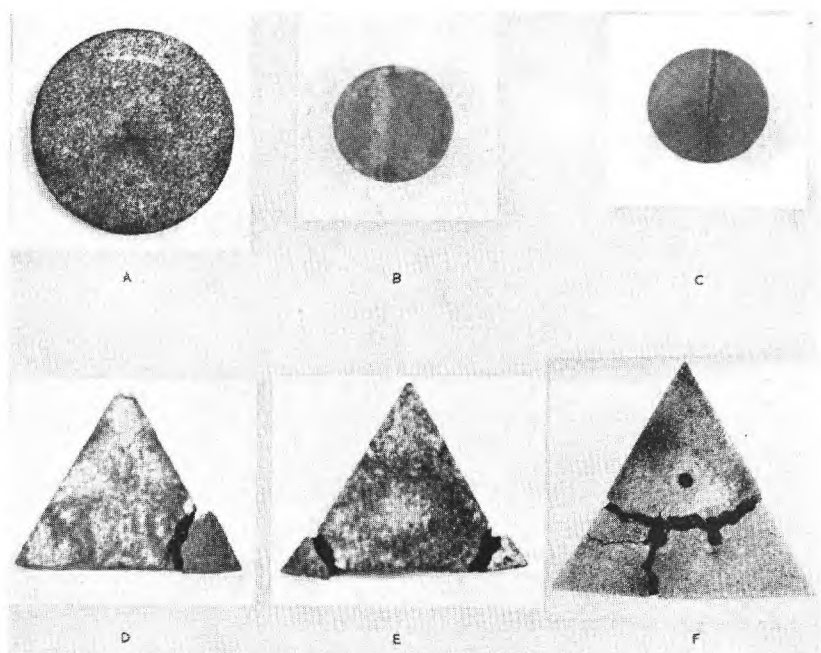
Fig. 14 Miscellaneous loading of prisms by exploding wires
A Cylinder, internal loading, with polythene ring reinforcement
B Cylinder, surface loading wire in water, no apparent damage
C Cylinder, surface loading, wire in air, showing "crush zone"
D, E Triangles, external loading, with one and two wires respectively
F Triangle, internal loading, three wires

From the above observation also it would seem that the highest hoop tensile stress in dynamic loading occurs nearest to the axis of the cylinder.

B. External loading of the specimens

Experiments were performed by placing the exploding wire on the external faces of square, rectangular, triangular and cylindrical prisms of synthetic rock (Fig. 15).

565

In Fig. 15A a square prism was subjected to the pulse while immersed completely in water. There is no sign of spalling, scabbing, corner fracturing or compression damage. The crack which has been started but not completed, seems due to hoop stresses, although it
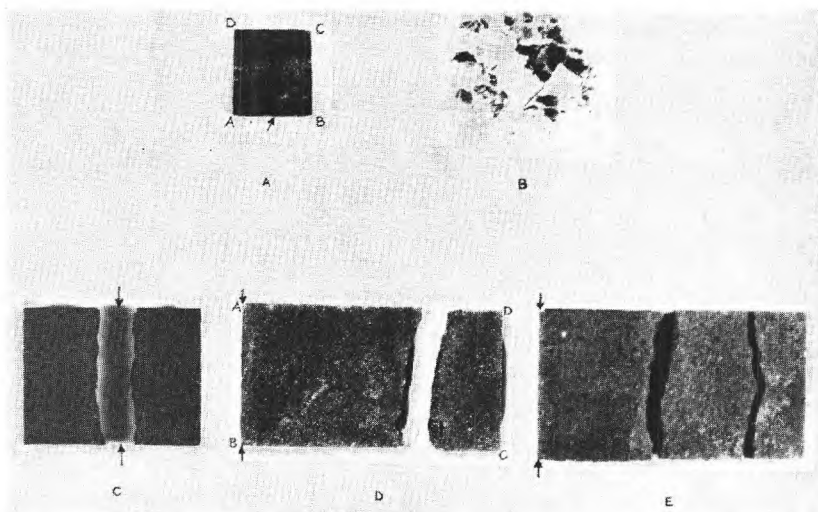
Fig. 15   Fracture of square and rectangular prisms subjected to a cylindrical shock wave front along the axis of one external face. Arrows show position of exploding wire.

coincides with the probable concentrations of reflected tension waves (Fig. 8c). The circumstantial evidence in favour of the hoop fracture hypothesis is that there were signs within the crack of copper from the exploding wire, showing that the crack was initiated immediately after the explosion. If the crack had been caused by concentration of reflected tension waves, the gases would presumably have already escaped from the open face, or been absorbed by the water. There is also no sign of any corner fractures, whereas if there really had been a high enough concentration of reflected tension waves at the face AB, there would presumbly also have been concentrations of reflected tension waves near the corners C and D. Another significant observation in favour of crack initiation by hoop stresses is the invariable coincidence of the positions of the starting crack and the wire. If the exploding wire were to deviate, say, by a distance x from the axis of symmetry of the face AB, then the line of concentration of the reflections from the surfaces AD and BC should in turn deviate from the wire by a distance 2x. There was never any sign of deviation of the crack from the place where the exploding wire was placed.

566

Bearing in mind the observations on Fig. 15A it would seem that the fracture in Fig. 15C was also produced by dynamic hoop stresses. Because of the long, flat geometry of the specimen in Fig. 15C the corner fractures should have been started earlier than the concentration of the reflections at the middle of the bottom face, and because of the attenuation of shock wave, corner fractures should have been caused by stronger concentrations. However, there are no signs of corner fractures, spalling, scabbing or compression damage.

In Fig. 15D, a similar long, flat rectangular prism is shown, but this time loaded along one of the two smallest faces. In this way the tendency to fracture by hoop stresses was minimised because of the low curvature of the shock wave front compared to the ~~width~~ length of section AB. For Hopkinson spalling, on the other hand, there were two advantages in this geometry of loading.

1) The large ratio of the length BC (7 cm) to width AB (2 cm) and to shock wave length L (7 cm) respectively.

2) Because of the distance of the reflection face to the source, the shock wave front at this distance, was fairly planar, and thus favourable to Hopkinson spalling.

One spall of about 1.8 cm thickness was produced. No compression damage, corner fractures, cracks due to concentration of reflected waves or hoop stress fracture were observed. Thus experiment and theory are qualitatively in accord, showing the relative influence of geometry and type of loading on the resulting fracture.

C. Production of more effective reflected tensile waves

1. Efficiency of reflection

The efficiency of reflection is an important parameter in the production of higher tensile stresses. For this reason the reflection coefficient should be increased. This was done practically by starting the pulse in a dense medium, e.g. water, while keeping all the opposite faces of the specimen in contact with air. Thus, referring to Fig. 3, medium 1 would be water, medium 2 would be rock and 3 air. Because of the very low impedance of air ($\varrho c = 4 \times 10^{-4}$) the reflection coefficient σ_R/σ_I is almost unity, i.e. practically the whole intensity of the wave is reflected. The same specimens as in Fig. 15A and D were fractured while their upper faces were kept in contact with air.

In Fig. 15B, a similar prism to that used in Fig. 15A was subjected to the pulse, but it was only half immersed in the water, its upper surface being in contact with air. Reflected tensile stresses and their concentrations played an important role in the resultant fractures.
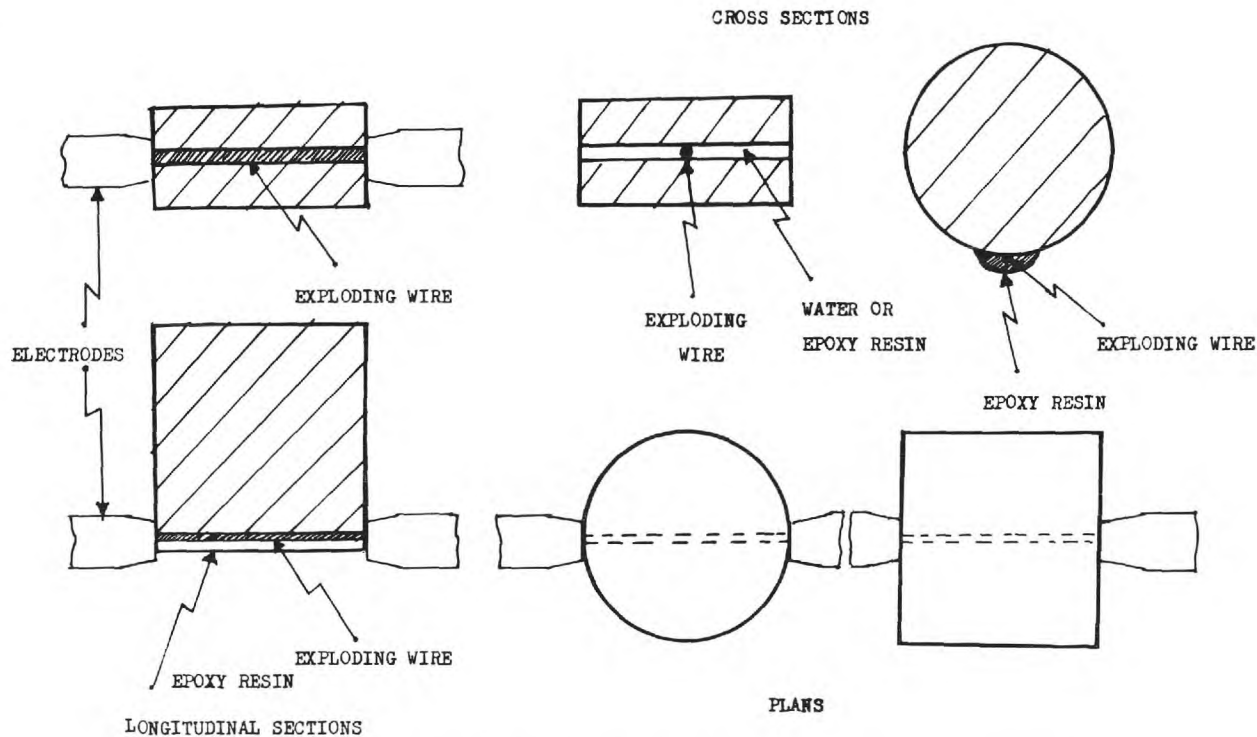
Fig. 16 Experimental arrangement for study of reflections. The exploding wire is magnified to be seen clearly.

Many fragments are visible, the products of spalling and scabbing. Hoop stress fractures were also visible in the broken material. The difference between Fig. 15A and B is very clear.

In Fig. 15E a similar prism to that used in Fig. 15D was subjected to the pulse, but with its upper surface in contact with air. Two rectangular spalls of about 1.8 cm thickness were produced.

From the equation (7) for the number of spalls, N,
$$N = P/T = 2 \qquad \text{for Fig. 15A}$$
$$= 1 \qquad \text{for Fig. 15D}$$

The tensile strength of the specimen, T, is the same in both experiments. Hence the peak pressure, P, of the reflected pulse in Fig. 15E must be about twice as great as in Fig. 15D.

In order to investigate further the comminution efficiency of reflected shock waves at the free surfaces, specimens were fractured in three different ways.

a) Completely submerged in water.
b) With the lower half submerged in water and the upper half in contact with air.
c) With all the outer surfaces completely in air.

In all three cases the exploding wire was held between two slices of specimen, either with a very thin layer of water and the help of an elastic band, or else by a thin layer of solidified epoxy resin. The experimental arrangements are shown in Fig. 16. The specimens were of synthetic rock, a sandstone and a granite, respectively.

(I)   With the specimen completely in water the fracture pattern was usually either a single split or a cross (Figs. 17A, C and 18A).

(II)   With the specimen half in air, half in water, the slice of specimen in contact with air was crushed into many small pieces (slabs, scabbing and corner fractures), while the underwater slice of rock was fractured into two pieces only (in the case of sandstone and synthetic rock) or into about 4 pieces (in the case of granite) (Figs. 17B and 18B).

(III) With the specimens completely in air, they were all broken into many small pieces, with some fines. The granite produced most fines. (Figs. 17D and 18C, F).

2. The effect of reflections on energy consumption

Energy consumptions were calculated in terms of Bond Index and also as Joule/cm². Results for a specimen of granitic rock are shown in Table 2. (Fig. 18F).

Table 2 Energy consumption for granitic rock

Type of fracturing	Initial Size cm	Reduction Ratio	Energy Consumption KWh/T	Bond Index KWh/T	Joule/cm²
(a) Specimen under water	3.0	4	2.1	47	2.1
(b) Half of specimen in air	3.0	6	1.8	20	0.65
(c) Specimen in air	3.1	11	1.8	17	0.31

In Table 2 the Bond Indexes are much lower than any previously recorded for electrohydraulic crushing. The last figure especially is close to the Bond Index of 15 for granite in conventional grinding [22]. The above experiments show clearly the importance of efficient reflections in electrohydraulic crushing.

Further experiments were performed in a crushing chamber of the type shown in Ref. [9]. Some quartz particles were crushed to observe the increase in comminution efficiency due to free surfaces. In case A, the feed was completely under water. In case B, the electrodes only were covered by water, and the rest of the feed was left in contact with air. Energy consumptions are shown in Table 3. The efficiency of comminution has been almost doubled, as shown by the ratio A/B ÷ 1.8. However, further work must be done with different types of rock and feed size in order to make a critical comparison with conventional fine crushing.

Table 3 Energy consumption for quartz particles.
A: Feed completely under water, B: Only the electrodes covered by water.

Feed Size	7/16" — 1/4"			1/4" — 1/8"		
	A	B	A/B	A	B	A/B
Average K.V.	8.07	8.08		8.04	8.01	
Average Bond Index	208.1	107.7	1.93	164.9	87.7	1.88
Average joule/cm²	1.30	0.78	1.67	1.32	0.72	1.86

D. Analogies with bore-hole blasting

In bore-hole blasting, both the size of the burden and the wave length of the stress pulse are of the order of metres, while the duration of the pulse is hundreds of microseconds. In electrohydraulic crushing the length of stress pulse is of the order of cm and the duration is

microseconds. Hence it was thought that bore-hole blasting could be correctly modelled, on a conveniently small scale, by using electro-acoustic pulses in specimens of cm size, thus keeping the same ratio of specimen size to pulse wave-length as in rock-blasting. Moreover,
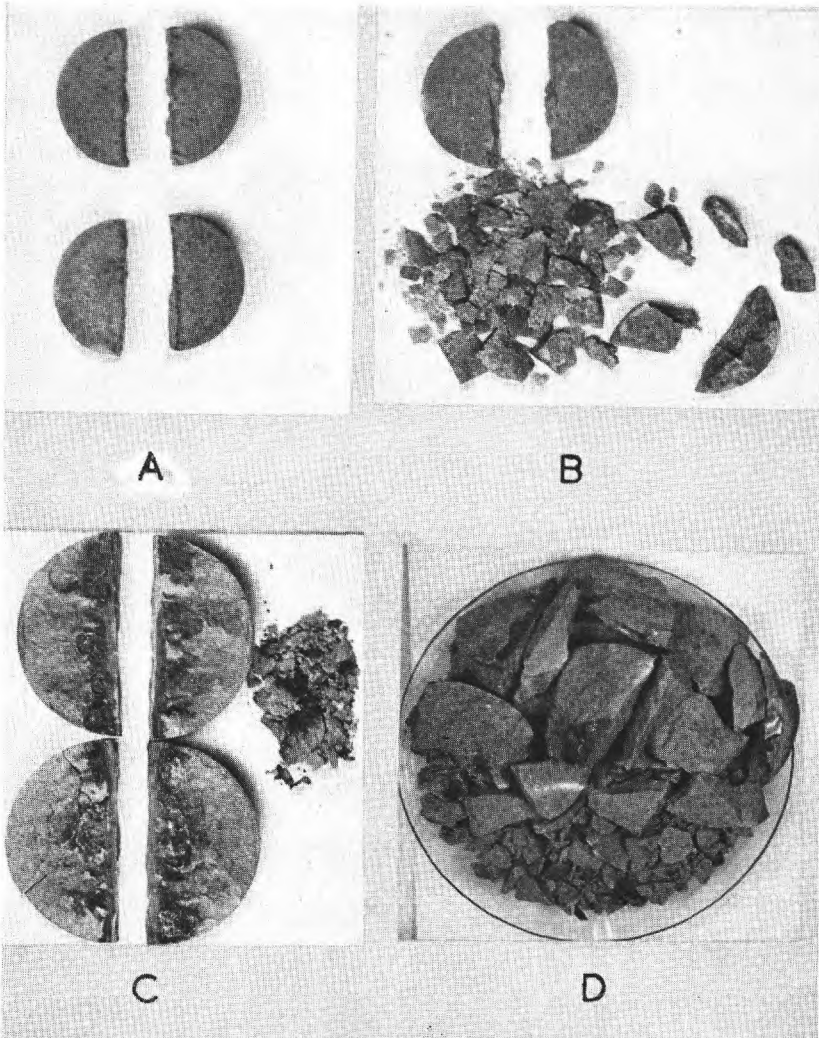

Fig. 17   Effect of single pulse on a synthetic and natural rock. Synthetic (A, B) and natural (C, D) sandstone, loaded in contact with water (A and C) and air (B and D).

the electro-acoustic pulse is more cylindrically uniform than that from explosives, because the whole length of the spark is exploded at practically the same time, while in explosives there is the detonation velocity along the line of explosive to be taken into account.

a) Single bore-hole blasting:

Fig. 19 shows the fracture of a cubic specimen of concrete. The spark was in the bottom of the borehole, just in the middle of the cube. The fracture pattern is similar to those obtained in rock blasting by explosives, and is an example of the so-called "critical fracture of crater". Radial cracks due to dynamic hoop stresses are visible, as well as the more familiar "cratering" observed in rock blasting. However, no "crush zone" was observed around the borehole. The causes of discrepancy were further investigated. In an attempt to obtain a "crush zone", some cylindrical slabs of synthetic rock were subjected to shock waves which were not strong enough to produce fracture by tensile stresses.
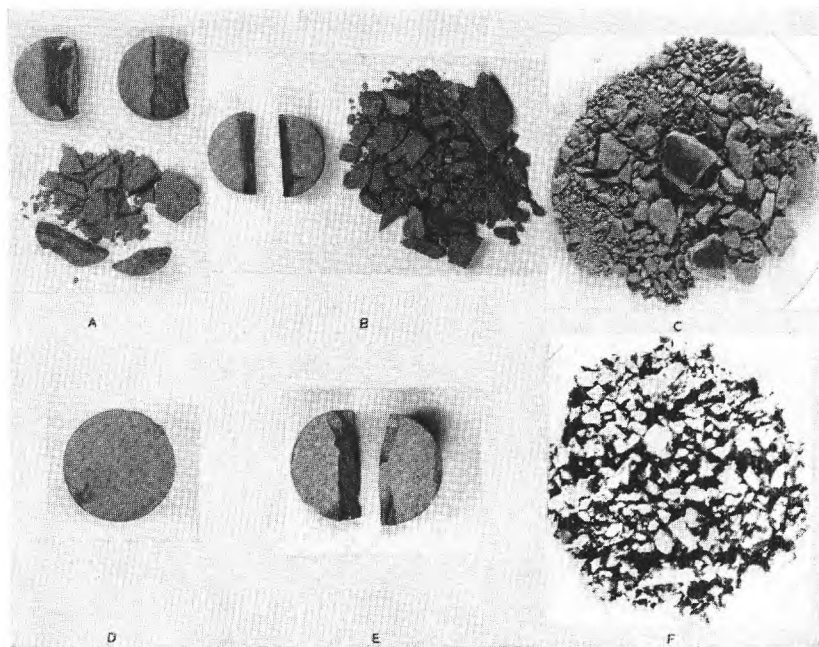
Fig. 18   Effect of single pulse on natural rocks. Specimens A to E are sandstone and F is Cornish granite.
A, D: Specimen completely immersed in water.
B, E: Half in air — half in water.
C, F: Completely in air.

In Fig. 14B the specimen was subjected to the shock wave while completely submerged in water. No damage seems to have been produced. In Fig. 14C the wire was exploded with the loaded face completely in air and the wire merely lying on top of the
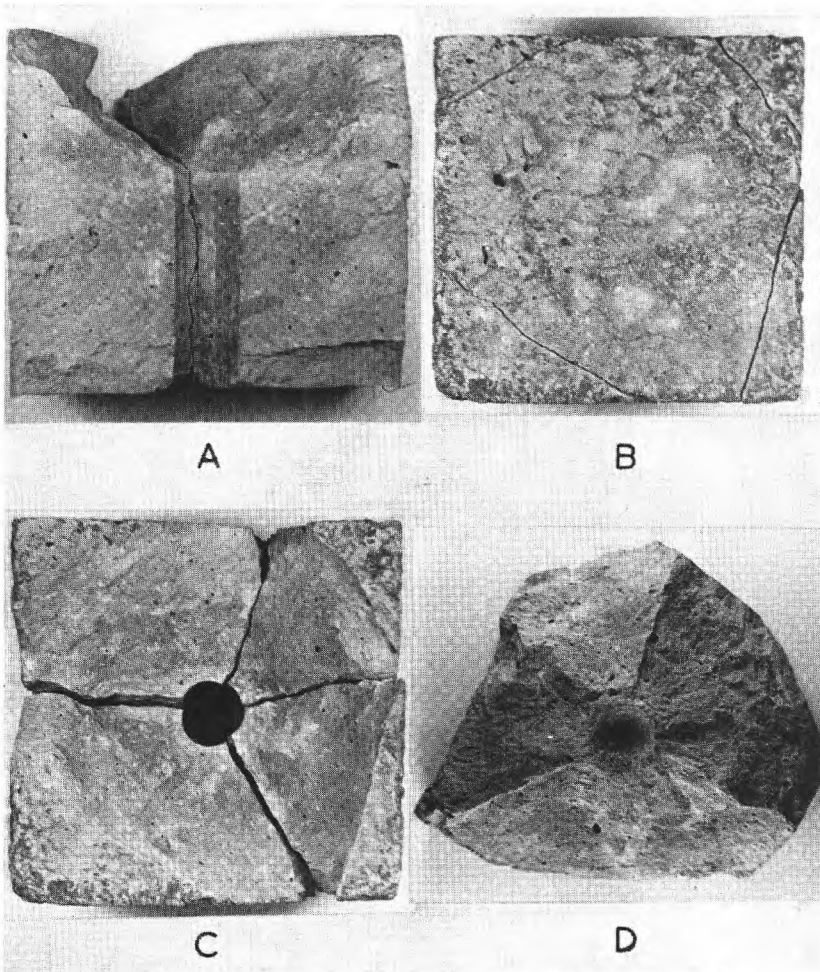
Fig. 19   Rock blasting modelled by an electrohydraulic spark

specimen. The exploding wire created a channel of about 1 mm diameter along its length. This is the nearest approach to a crush zone that was found and it was observed only when the wire was

exploded in air. It seems then, that the "crush zone" damage might have been caused by a combination of heat flash and rock to air reflections at the load face. Presumably the gases are cooled and absorbed more rapidly in the underwater explosion than in the air explosion. However, the interpretation of the crush-zone is still open to discussion.

b) Multiple bore-hole blasting:

It was found that as many as 3 separate wires could be exploded simultaneously with one capacitor. This phenomenon suggested some experiments to observe the result of interacting cylindrical shock waves.

Rectangular prisms of synthetic rock with two symmetric holes parallel to the axis were fractured by placing two exploding wires in the holes (Fig. 20A, B).
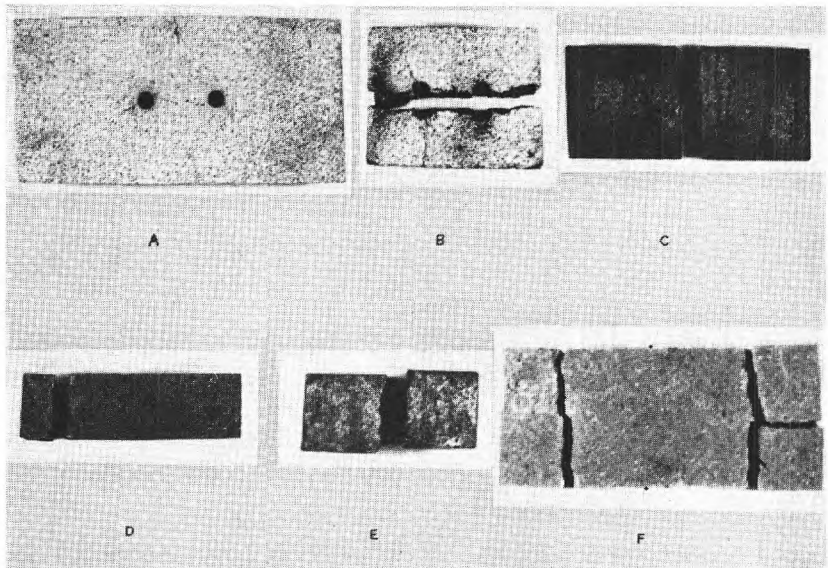
Fig. 20   Effect of two simultaneous cylindrical pulses with internal loading (A, B) and external loading (C, F). The right-hand face of F in air.

From the fracture patterns it seems that the main fractures occur along the lines of concentration of hoop stresses due to two cylindrical shock wave fronts. The resultant fracture is exactly analogous to the practice of cutting a rock face by simultaneous blasts with so-called "perimeter holes".

E. Electrohydraulic crushing by multiple sparks

From the theoretical considerations and the above observations, it would seem to be advantageous to use simultaneous multiple sparks, because of the reinforcement of the stresses of the individual spark.

To investigate this, some rectangular prisms of synthetic rock were fractured by placing two exploding wires on their external faces. Arrangements are shown in Fig. 21 (a, b).
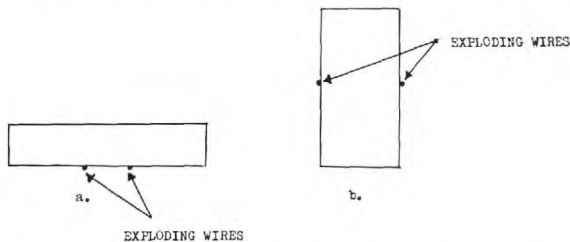

Fig. 21   Experimental arrangements using two exploding wires.

The specimen in Fig. 20C was fractured as in Fig. 21A. The fracture is through the plane of symmetry between the two exploding wires, which corresponds to the line reinforcement of the hoop stresses.

A similar specimen, when loaded by only one exploding wire with half of the energy of two exploding wires (corresponding roughly to the same pressure at the shock wave front) did not fracture.

The specimens in Fig. 20D, E, F were fractured as in Fig. 21B. In Fig. 20D, E the fractures are due to reinforcement of hoop stresses. In Fig. 20F the specimen was chosen fairly thick, so that fracture due to the reinforcement of hoop stresses has not occurred. Instead, two Hopkinson spalls were produced. The upper spall was again fractured into two because this face was kept in contact with air. In this experiment it seems that two cylindrical shock wave fronts have created, by reinforcement, a fairly planar wave front after reflection at the opposite faces, favourable to Hopkinson spalling.

From a single wire with half energy, as above, no fracture resulted.

More significantly, another specimen, this time with a single wire of the same energy (i.e. 1.4 x the pressure [9]) fractured by hoop stress only, (i.e. similarly to Fig. 20E), but did not spall.

Another similar specimen was loaded by putting one exploding wire of double energy along the small face of the prism (as in Fig. 15D, in order to produce a fairly planar wave front. No fracture at all was observed in this case.

575

It seems from the above observations that both the hoop and Hopkinson stresses due to the two separate cylindrical shock wave fronts can reinforce each other, to produce fractures which might not otherwise have occurred. Thus the use of multiple sparks in electro-hydraulic crushing experiments might increase the efficiency, because those particles which with one spark would only be deformed elastically might, with simultaneous multiple sparks, be fractured by reinforcement for stresses. However, continuous crushing experiments using multiple sparks have not been performed as yet.

Conclusions

1. Experiments were performed on the electrohydraulic crushing of centimeter size squat particles, completely immersed in water. The chief cause of fracture in this case was ascribed to hoop stresses, on both theoretical and experimental grounds. These hoop stresses are dynamic hoop stresses and are caused by the cylindrical shape of the expanding wave front. There are some similarities between the static hoop stresses produced in a pressure vessel and the present dynamic hoop stresses, mainly in that the highest tensile stress distribution is across the shortest radial section. Also, the dynamic hoop stresses have their peak at the inner surface of the specimen.

There is, however, one significant difference. In the static case, the hoop stresses rapidly disappear when the first crack develops in the pressure vessel, because of the release of pressure. In the dynamic case, the pressure is not released after production of the first crack, which simply halves the length of arc subject to hoop stress by the wave front (see Fig. 5). Therefore, if there is still a sufficient length of arc remaining for the front to produce large enough dynamic hoop stresses, further cracks will develop.

However, there is as yet no satisfactory quantitative explanation of the remarkable symmetry of the radial cracks. Rinehart's [13] explanation of angular symmetry, based on the critical impact velocity, is for infinite bodies, and does not take into account the shape of the specimen. From the observed fracture patterns, it seems that angular symmetry depends largely on the geometry of the specimen, and the angle between radial fractures on the intensity of the shock wave front.

2. The geometry of the specimen and type of loading are important parameters. For example, it was very easy to produce pure Hopkinson spalling in long, flat rectangular prisms, where the length of specimen was greather than half the wave length, provided that the

specimens were loaded along the axis of one of their smallest faces. On the other hand, when the type of loading was changed, in the same shape of specimen, so that they were now loaded along the axis of their largest faces, it was very easy to produce pure hoop stress fracture.

3. For Hopkinson spalling and for other fractures due to concentrations of reflected tensile stresses, the size of the specimen should be greater than half the wave length, in order to get efficient crushing.

4. The reflection coefficient for the waves outgoing from the specimen should be increased in order to increase the efficiency of electrohydraulic comminution through the agency of Hopkinson spalling and of fractures due to concentrations of reflected tensile stresses. This was achieved by starting the pulse in a dense medium, e.g. water, while keeping all the opposite faces of specimen in contact with air, so that the reflection coefficient was practically unity. Since the reflection coefficient of the solid-water interface was only 0.5, it is of possible theoretical significance that a net doubling of the crushing efficiency was observed.

5. Using two sparks, produced simultaneously by two exploding wires, reinforcement of dynamic hoop stresses, and also reinforcement of reflected tensile stresses, were observed. From the above observation, it is suggested that the use of multiple sparks in electrohydraulic crushing might increase comminution efficiency.

6. The electroacoustic spark is suggested as a scientific research tool in rock mechanics.

a) To model bore-hole blasting:
   Burden to wave-length ratio can be reproduced in small scale models by electroacoustic sparks. Moreover, in electroacoustic pulses the wave-front can be made more cylindrical (i.e. less conical) than the wave-front from explosive sticks.

b) To investigate some properties of explosions:
   In electroacoustic sparks, the energy and shape of wave front can be regulated closely. Foil can be used instead of wire, to obtain a planar wave-front.

c) To investigate dynamic stress and strain problems on models.
   A geometric shape would be loaded accurately because of the very small volume of the exploding wire or foil, and by several sparks simultaneously. Also very high repetition rates can be used, e.g. for vibration studies.

However, because of the electrical interference caused by the spark, instrumentation of electroacoustic apparatus is difficult, since, for example, conventional wire strain gauges tend to pick up electrical noise. However, the remarkable symmetry and precision of fracture obtained with the present very primitive apparatus suggests that more refined experimental techniques should yield quantitative answers to some of the problems of rock behaviour under dynamic loading.

List of symbols

a	=	Diameter of cylindrical wave front, size of specimen of cubic shape.
C	=	Propagation velocity of longitudinal wave.
C_L	=	Velocity of longitudinal (dilatational) wave.
C_S	=	Velocity of distortional (shear) wave.
G	=	Rigidity modulus.
K	=	Bulk modulus.
l	=	Thickness of Hopkinson spall.
L	=	Wave length
N	=	Number of the spalls.
P	=	Pressure at the wave front. Total compressive force at the wave front. Resultant stress of the wave after reflection.
P'	=	Intensity of the resultant tensile stress after reflection.
P'_a	=	Average resultant stress of the wave front.
T	=	Dynamic tensile strength of material.
T_{hoop}	=	Total hoop tensile force.
$T_{Hopkinson}$	=	Total Hopkinson tensile force.
ϱ	=	Density
ν	=	Poisson ratio
σ_I	=	Intensity of Incident longitudinal wave.
σ_R	=	Intensity of Reflected longitudinal wave.
σ_{Tr}	=	Intensity of Transmitted longitudinal wave.

Discussion

A. S. J o y , Stevenage:

In earlier work by Dr. Maroudas, he used a system in which the pulp was through a chamber where a plasma discharge achieved the fine comminution. That method seemed to show promise, and recent

reports, including patents applications, from UKAEA suggest they have a machine on this basis operating at a considerable number of cycles/sec.

Was this system ever developed and if not can the author suggest the reasons why it was not a success?

N. G. M a r o u d a s :

The first E.H.C. patent application by the UKAEA was for a machine designed by Dr. Maroudas. We have not been informed about their subsequent developments.

However, we have every confidence in the eventual success of E.H.C., provided machines are designed on a scientific basis, and are properly optimised. We have for some years now been trying to obtain support for the development of E.H.C. technology. We hope that our latest scientific findings, as outlined in the present paper, will stimulate interest in the technology, and would be glad to co-operate with anybody in this field.

T. P. M e l o y , Milwaukee:

Continuing work in electrohydraulic comminution indicates no for-seeable commercial use for this process. The shock mechanism is efficient in energy use for crushing. Your values are surprisingly low. The work needed to effectively place the electrodes on the specimen will be expensive. Tensile comminution is not more effective than compression comminution.

N. G. M a r o u d a s :

Dr. Meloy has made a prediction about the future of E.H.C. So have we. Time alone will give the answer.

As to his remark that our values of 20 kWh/ton for Bond's Index are "surprisingly low", we find it amusing, for the following reason. Dr. Meloy represents Allis-Chalmers, who were one of the two pioneers in E.H.C., but who have since abandoned it. The other pioneer was Prof. Yutkin in Leningrad. Now it so happens that three years ago Dr. Maroudas sent Prof. Yutkin the first report of the UKAEA work, with a Bond's Index of 70 kWh/ton. Yutkin's reply was that these figures were "exaggerated".

As to Dr. Meloy's views on the relative efficiency of tensile and compressive comminution, we can only refer him to the work of Mr. Hiorns and coworkers (this symposium) who have conducted experiments on this subject.

K. M e y e r , Berlin-Adlershof:

Wir befassen uns u. a. mit der Einwirkung von Schockwellen auf die Versetzungsstruktur und Bruchvorgänge an Einkristallen. Beobachten Sie bei Ihren Untersuchungen bestimmte Eigenschaftsänderungen des Materials als Folge einer durchlaufenden Schockwelle, z. B. der Härte? Liegen mikroskopische Untersuchungen über den Rißverlauf vor? Ist damit eine Auflockerung des Materials verbunden?

N. G. M a r o u d a s :

This is a very interesting question on the scientific basis of comminution. Apart from the technology, we regard E.H.C. as a promising tool for this type of investigation. We have no views at present on the answers to these questions, but one of the first priorities in our basic research will be to set up experiments on the initiation and propagation of cracks by high-velocity stress waves in perfect single crystals.

J. E. E n g l i s h , London:

I would like to ask the authors if they consider that it is possible that the holes through the specimens tested so complicate the shock wave and stress distribution patterns, in the specimens, that any reasonably simple theory of the mechanism of electrohydraulic crushing is rendered invalid?

In this connection, it would appear possible that in Sample F of Fig. 14 the crack could be due to the stress generated by the shock wave from the top hole with the lower holes merely acting as stress raisers. Furthermore, would it be expected that a theory of crushing based upon the generation of shock waves i n s i d e the particle can be validly applied to the case of crushing by shock waves generated o u t s i d e the particle?

It would be of interest if the authors could indicate the extent to which these questions constitute objections to the techniques and conclusions treated in their paper.

N. G. M a r o u d a s :

The answer to the first question is no. The answer to the criticism in the second sentence is that the effect of 3 holes is mainly to reinforce the stresses of the 3 exploding wires, according to stress geometry. In general, the extreme precision and symmetry of our high-speed fracture-patterns would seem to bring into question the importance or even the necessity of "stress raisers" for crack propagation.

The answer to the third question is that it depends on the effect of the boundary conditions on the Hopkinson and the hoop stresses, and also on the shear stresses. Our paper presents analogous results for both internal and external loadings. However, our present experimental set-up did not appear to have produced a very high level of shear stress. Our latest views are that high shear stress level will influence the formation of "crush-zones" near the wire; however, these crush-zones should then appear regardless of whether loading is internal or external.

References

[1] T. Svedberg: Berichte der Deutschen Chemischen Gesellschaft **38** (1905) 3616

[2] A. Michel-Levy, H. Marour: Comptes Rendus **18** (1934) 9 1760

[3] C. G. Suits: Notes on high intensity sound waves. Gen. Elec. Rev. **39** (1939) 430

[4] L. Yutkin: The electrohydraulic effect. Mashgiz, Moscow (1955)

[5] F. Früngel, H. Keller: Zeit. für Angewandte Phy. **9** (1957) 3 145

[6] B. H. Bergstrom: The electrohydraulic crusher. Eng. & Min. Jour. **162** (1961) Feb. 134

[7] E. A. Martin: The underwater spark an example of gaseous conduction at about 100,000 atmospheres. Jour. App. Phys. **31** (1960) 2, 255

[8] N. G. Maroudas, R. F. Taylor: A.E.R.E. M 1261 (1963)

[9] N. G. Maroudas: Electrohydraulic Crushing. A.E.R.E. R 4550 (1964)

[10] N. G. Maroudas: Apparatus for Electrohydraulic Crushing. British Patent App. No. P 5070/64

[11] K. W. Carley-Macauly, J. W. Hitchon, N. G. Maroudas: Energy consumption in electrohydraulic crushing. Trans. Instn. Chem. Engrs. (London). To be published.

[12] U.S. Patent   No. 3207447. Eng. & Min. Jour. **167** (1966) 1 98/99

[13] J. S. Rinehart: The role of stress waves in the comminution of brittle rock-like materials. Inter. Symp. on stress wave propagation in materials (1960) 247/269

[14] J. S. Rinehart: Fracturing under explosive loading. Chem. Eng. Prog. **55** (1959) 2 59/64

[15] J. S. Rinehart: Transient stress wave Boundary Interactions. Symp. on stress waves in anelastic solids. Academic Press (1963) 193/206

[16] J. S. Rinehart: Fracturing by spalling. WEAR **7** (1964) 315—329

[17] J. H. Charles and J. S. Rinehart: Coupling between unconfined cylindrical explosive charges and rock. Int. Jour. of Rock Mechanics and Mining Sciences. **2** (1965) 13/24

[18] J. S. Rinehart and J. Pearson: Behaviour of metals under impulsive loads. Dover Publ. Inc. New York (1965)

[19] D. G. Christie and H. Kolsky: The fracture produced in glass and plastics by the passage of stress waves. Jour. Soc. Glass Technology. **36** (1952) 65/73

[20] D. G. Christie: An investigation of cracks and stress waves in glass and plastics, by high speed photography. Jour. Soc. Glass Technology. **36** (1952) 74/89

[21] H. Kolsky and Y. Y. Shi: Fracture produced by stress pulses in glass-like solids. Proc. Phys. Soc. **72** (1958) 447/453

[22] F. C. Bond: Bond indexes tabulated. A.I.M.E. Mining Engineering (1953) March 315/316

[23] R. H. Cole: Underwater explosions. Princeton University Press (1948)

[24] K. Hino: Theory and practice of blasting. Nippon Kayaku Co. Ltd. (1959)

[25] T. H. Hueter and R. H. Bolt: Sonics. John Wiley & Sons Inc.

[26] U. Langefors and B. Kihlström: Rock blasting. John Wiley & Sons Inc. (1963)

[27] M. A. Cook: The Science of High Explosives. Reinhold Publ. Corp.

[28] F. Früngel: High speed pulse technology. Academic Press (1965)

ERRATA

Page	Line	Wrong	Right
21	Last	solid particle.	solid particle,but can be generated by longitudinal stress wave
23	9	the total hoop ...	a hoop ...
23	11	compressive wave front as in pressure vessel is:	compressive wave,is shown.As a rough analogy, this may be compared with the static cas of a pressure vessel where,
23	13	diameter of wave front	diameter
23	14	compressive pressure of the wave front at the distance a/2 from the source	compressive pressure in the vessel shell
23	16	The hoop stress...	This analogy is a first approximation in the case of dynamic compression.The actual hoop stress...
40	14	expected, since...	considerable, since ....
40	15	not possible for...	reduced for...

ERRATA

Page	Line	Wrong	Right
40	20	shear waves are transmitted	shear waves are possibly transmitted....
40	21	the necessary condition which	the important condition for their formation, which ....
40	22	a plane surface for produced longitudinal waves, was not present.	a plane surface was not present
87	17	The total hoop tensile force....	Referring to the previous analogy, the total hoop tensile force....
91	18	(i)The metal wear...	(i) It is assumed that the metal wear ...
92	6	is not a function...	is not a direct function...
94	6	hoop stress by the wave front....	hoop stress by the wave...
94	9	enough hoop stresses ($T_\varphi = 2.R.\sin^2(\frac{\varphi}{2}).p$) further	enough hoop stresses, further..